Doctoral Thesis reviewed
by Ritsumeikan University

Ultrashort Optical Pulse Generation Using Actively Mode-Locked and FM Fiber Ring Lasers

(アクティブモード同期と FM ファイバリングレーザを用いた超短パルスの発生)

September, 2014
2014 年 9 月

Doctoral Program in Integrated Science and Engineering

Graduate School of Science and Engineering

Ritsumeikan University

立命館大学大学院理工学研究科

総合理工学専攻博士課程後期課程

NGUYEN Dang Trang
グエンダントラン

Supervisor: Professor TAGUCHI Kozo
Professor MORIMOTO Akihiro
指導教員：田口耕造教授
森本朗裕教授

Declaration of Authorship

I, NGUYEN Dang Trang, declare that this thesis titled, "Ultrashort Optical Pulse Generation Using Actively Mode-Locked and FM Fiber Ring Lasers" and the work presented in it are my own. I confirm that:

- This work was done wholly or mainly while in candidature for a research degree at Ritsumeikan University.
- Where any part of this thesis has previously been submitted for a degree or any other qualification at this University or any other institution, this has been clearly stated.
- Where I have consulted the published work of others, this is always clearly attributed.
- Where I have quoted from the work of others, the source is always given. With the exception of such quotations, this thesis is entirely my own work.
- I have acknowledged all main sources of help.

Signed: _____

Date: _____

"Imagination is more important than knowledge. For knowledge is limited to all we now know and understand, while imagination embraces the entire world, and all there ever will be to know and understand."

Albert Einstein

Abstract

Ultrashort Optical Pulse Generation Using Actively Mode-Locked and FM Fiber Ring Lasers

by NGUYEN Dang Trang

Fiber lasers with ultrashort pulse generation and high beam quality have been becoming significant in various fields of applications, such as optical communication, high-precision material processing, and bio-medicine. This thesis works on developing new technologies for generation of ultrashort optical pulses using fiber lasers. A picosecond frequency modulation (FM) fiber laser and an actively mode-locked femtosecond fiber laser have been investigated and developed.

Picosecond optical pulse generation using the FM fiber ring laser was analyzed in detail. FM fiber laser operation was realized by using a fiber ring with an internal phase modulator and an erbium-doped fiber amplifier. To generate picosecond pulses from the FM fiber laser, an external dispersive single-mode fiber was employed. By external intensity modulation, the background of the output optical pulse chain was removed. The background ratio of the generated ultrashort pulses was calculated and compared with the experimental results. The experimental results showed an output optical pulse width of 1.77 ps and a spectral bandwidth of 0.5 THz. The pulse train had the repetition rate of about 10 GHz. With short pulse width, wide and flat bandwidth, and high repetition rate, this laser can be used for many applications, such as optical communication.

In addition, an actively mode-locked erbium-doped fiber ring laser was developed to generate femtosecond pulses. Instead of using conventional sinusoidal modulation, impulse modulation was utilized to modulate the fiber ring cavity losses. The impulse modulation was realized by a dual-electrode Mach-Zehnder intensity modulator, which was driven by a fabricated electrical impulse generator. The principles of femtosecond optical pulse generation by the proposed laser was analyzed in detail. The active mode-locking directly generated optical pulses with duration of 300 fs and a repetition rate of 9.188 MHz, the same as the fundamental frequency of the cavity. With such short pulse width and fundamental repetition rate, the generated pulses contain very high peak power, which is promising for applications in biology such as cell fusion and cell killing.

Acknowledgements

The work presented in this thesis has been carried out at the Ultrashort Optoelectronics Laboratory and the Biophotonics Laboratory, Ritsumeikan University, during the years 2011-2014. I would like to acknowledge all people who have helped me both in academic and non-academic fields.

I gratefully acknowledge my first supervisor Prof. Morimoto Akihiro for his invaluable assistance, support, and guidance. I would like to express deep regret over his serious stroke. Deepest gratitude is also to my second supervisor Prof. Taguchi Kozo for giving me a chance to join his lab and to work under his guidance as well as his support. I would also like to thank Dr. Takahiro Teramoto for his assistance and support.

I gratefully thank my current and former labmates for sharing their friendship and helpful assistance, including Mr. Mizuta Yoshihiro, Mr. Nishimoto Kyohei, Mr. Nakakita Hideki, Mr. Iwamoto Syuya, and Mr. Yasunaga Takanori. Especially, Mr. Wada Taisuke, Mr. Junji Abou and Mr. Akio Muramatsu who have helped me very much in my research for the beginning time of my doctoral program. Without their knowledge and assistance, my study would not have been successful.

I would like to convey thanks to Japanese Government for the grant of Monbukagakusho (MEXT) scholarship. Special thanks are also to Ritsumeikan University for exempting me from academic tuition fee of my doctoral program.

Last but not least, I warmly thank my beloved family for supporting my studies. Big thanks also to my friends. Best of all, I would like to thank my dear wife Dung for all the support and love.

Kusatsu, August 2014
NGUYEN Dang Trang

List of Publications

Journal Publications

1. NGUYEN Dang Trang and Akihiro Morimoto, "Generation of ultra-wideband picosecond impulses with fast fall-time," Microwave and Optical Technology Letters, WILEY, vol. 56, no. 9, pp. 2165-2167, September 2014.

2. NGUYEN Dang Trang, Akio Muramatsu, and Akihiro Morimoto, "Femtosecond pulse generation by actively modelocked fibre ring laser," Electronics Letters, IET, vol. 49, no. 8, pp. 556-557, April, 2013.

3. NGUYEN Dang Trang, Junji Abou, and Akihiro Morimoto, "Ultrashort pulse generation using fiber FM laser," Optical Review, vol. 19, no. 5, pp. 337-340, September, 2012.

Presentations

1. NGUYEN Dang Trang, Yoshihiro Mizuta, and Kozo Taguchi, "Femtosecond fiber laser applying for cell fusion," Asia-Pacific Symposium on Applied Electromagnetics and Mechanics, Taichung, Taiwan, Jul. 2014.

2. NGUYEN Dang Trang and Akihiro Morimoto,"Actively Mode-Locked Fiber Laser Using Impulse Modulation," JSAP-OSA Joint Symp., Kyoto, Japan, Sep. 2013.

3. NGUYEN Dang Trang, Akio Muramatsu, and Akihiro Morimoto, "Generation of femtosecond pulses using actively mode-locked fiber ring laser," Photonics Global Conf. (PGC 2012), Singapore, Dec. 13-16, 2012.

4. NGUYEN Dang Trang, Akio Muramatsu, and Akihiro Morimoto, "Femtosecond pulse generation by actively mode-locked fiber ring laser," JSAP-OSA Joint Symp., Ehime, Japan, Sep. 2012.

5. NGUYEN Dang Trang, Junji Abou, and Akihiro Morimoto,"Ultrashort pulse generation of fiber FM laser," The 1st Advanced Lasers and Photon Sources Conf. (ALPS'12), Yokohama, Japan, Apr. 26-27, 2012.

Contents

To my parents and my wife.

List of Figures

List of Tables

Abbreviations

AM	**A**mplitude **M**odulator (Modulation)
Att	**Att**enuator
CW	**C**ontinuous **W**ave
DC	**D**irect **C**urrent
EDFA	**E**rbium **D**oped **F**iber **A**mplifier
EIG	**E**lectrical **I**mpulse **G**enerator
Er	**Er**bium
ESA	**E**xcited **S**tate **A**bsorption
FM	**F**requency **M**odulator (Modulation)
FWHM	**F**ull **W**idth at **H**alf **M**aximum
GD	**G**roup **D**elay
GDD	**G**roup **D**elay **D**ispersion
Ho	**Ho**lmium
Nd	**N**eodymium
NLTL	**N**onlinear **T**ransmission **L**ine
PC	**P**olarization **C**ontroller
PM	**P**olarization **M**aintaining
PMF	**P**olarization **M**aintaining **F**iber
PS	**P**hase **S**hifter
SA	**S**aturable **A**bsorber
SMF	**S**ingle **M**ode **F**iber
SRD	**S**tep **R**ecovery **D**iodes
Tm	**T**hulium
UWB	**U**ltra-**W**ide**B**and
Yb	**Y**tter**b**ium

Chapter 1

Introduction

1.1 Overview

Let's begin with the meaning of 'ultrashort' term used in ultrafast optics. First, we consider the relevant time units:
1 nanosecond (ns) = 10^{-9} second (s),
1 picosecond (ps) = 10^{-12} s,
1 femtosecond (fs) = 10^{-15} s.
The word 'ultrashort' is usually used for the picosecond time scale and below. The spatial equivalent of these short time units is very useful to put them in perspective. For example, one second light pulse can travel over a distance of 300,000 km, equal to the speed of light multiplied by 1 s. "This is roughly three-fourths of the distance from the Earth to the moon, a distance we will consider very slow!" [24] Meanwhile, a picosecond pulse has a spatial extent of only 0.3 mm and that of a femtosecond pulse is only 0.3 μm.

Since the first laser was reported in 1960 [25], laser has been applying in every aspect of our modern life. In recent decades, with the development of various doped fibers, fiber lasers have been increasingly investigated. The fiber lasers have many advantages over solid-state glass lasers, such as high beam quality, high laser efficiency, compact volume, good thermal management, and low noise floor. In addition, the fiber itself is the waveguide so it minimizes the need for bulk optics and alignment mechanism. With

fibers and fiber couplers, many cavity configurations can be built. Among them, the fiber ring cavity have been widely utilized [26–30] because of its simplicity.

In this thesis, we specifically focus on generating ultrashort optical pulses in picosecond and femtosecond time scales with wavelength in 1550 nm band using erbium-doped fiber ring cavities.

1.1.1 Ultrashort pulse generation using FM fiber ring laser

Phase modulation of light inside the laser cavity is a more efficient method to generate modulated continuous wave (CW) or chirped light compared with modulating a single mode laser output externally with a phase or frequency modulator. Through mode coupling, this method can perform FM modulation with higher modulation index. The first demonstration of FM laser was in He-Ne gas laser [31], which was produced by detuning the phase modulation frequency slightly further from the axial mode spacing.

Thanks to its broad, flat, and tunable spectral bandwidth characteristics, fiber ring FM lasers have been recently investigated [26, 32, 33]. The output of the FM laser is a widely chirped CW with a modulation frequency equal to the applied frequency and an FM index that is much larger than the single-pass modulation index of the intracavity phase modulator. In addition, the spectral bandwidth of the FM laser can be easily tuned by the modulation index and detuning frequency of the internal phase modulator. Therefore, the FM laser operation is a promising technique for optical frequency comb generation [26].

In the time domain, the output waveform of the FM laser is a frequency-modulated constant-amplitude signal [33]. This property limits the applications of the FM laser. Short pulses can be generated by active FM mode-locking [34–36]. Yet, the output spectrum of the FM mode-locked operation exhibits a bell-shaped pattern. It was also observed that for a given gain medium, the spectrum width of the FM laser output can be much larger than that achievable from a conventional active mode-locking [33]. Therefore, to generate ultrashort FM laser pulses while maintaining the broad and flat spectrum characteristics, an external compression scheme added at the output of the FM laser should be employed. There are various methods for compressing optical pulses, such as the use of a dispersive single-mode fiber (SMF) [37] and diffraction gratings[38].

Compared with the use of diffraction gratings, the use of a dispersive SMF has the advantage of low insertion loss.

This thesis uses the method based on chirp compensation using an external dispersive SMF to generate high-repetition-rate picosecond pulses by fiber ring FM lasers. The FM laser operation is realized by detuning the modulation frequency of a phase modulator in a fiber ring cavity with an erbium-doped fiber amplifier (EDFA). The compression scheme utilizes a dispersive SMF for pulse compression and an intensity modulator for pulse background removal.

1.1.2 Ultrashort pulse generation using actively mode-locked fiber ring laser

Mode-locking is the most common way to generate ultrafast optical pulses. The fiber lasers can be mode-locked to generate single or multiple pulses per a cavity round-trip. Passively mode-locked fiber lasers can generate short pulses in the femtosecond range [28, 29]. However, the passive mode-locking is sensitive and almost uncontrollable as the stable mode-locking is achieved. By slightly changing in surrounding conditions, the passively mode-locked lasers can generate multiple optical pulses per a round-trip at random times [10, 30].

In contrast, actively mode-locked fiber lasers are stable and controllable because active elements (acousto-optic or electro-optic modulators) are used inside the laser cavity. However, the active mode-locking often generates relatively long pulse duration in the picosecond range [35, 39–42] because the modulation speed of active modulators is limited. To generate pico-subpicosecond optical pulses, the active mode-locking using the conventional sinusoidal modulation needs to operate at a high repetition rate of 10 GHz or higher [35, 36, 39]. With such a high repetition rate, multiple pulses are simultaneously oscillated inside the cavity per a round-trip. They share the same cavity power so that the peak power per a single pulse is low compared with the case where only a single pulse is oscillated per a round-trip. Recently, an actively mode-locked fiber laser that can generate femtosecond optical pulses at the fundamental repetition rate has been reported [43]. It used an electro-optic phase modulator in a Sagnac loop.

In this thesis, we introduce an actively mode-locked mechanism that utilizes impulse modulation inside an erbium-doped fiber ring cavity to generate optical pulses at the fundamental repetition rate with pulse duration in the sub-500 fs range. The impulse modulation is studied and developed to obtain fast and large modulation of the cavity losses. As a result, femtosecond pulses can be generated by the proposed actively mode-locked fiber laser.

1.2 Thesis Aim

This thesis concentrates on investigating new technologies to generate ultrashort optical pulses using an FM fiber laser and an actively mode-locked fiber laser. A pulse compression technique based on a dispersive single mode fiber is investigated to obtain picosecond pulses from the FM fiber laser while remaining the interesting properties of the FM fiber laser. Beside, impulse intensity modulation is studied and introduced to use in a fiber ring cavity in order to achieve the actively mode-locked fiber laser, which can generate sub-500 fs optical pulses.

1.3 Outlines of Thesis

Coming after this introduction, the thesis is organized by other five chapters as follows:

- Chapter 2 gives an overview of fiber laser technology including various gain fibers covering the whole infrared spectral region from 1μm to 2 μm.
- Chapter 3 describes the mathematical description of ultrashort laser pulses. In addition, the most common method for generation of ultrashort laser pulses, which is mode-locking, is described.
- Chapter 4 demonstrates one of the main achievements and findings of this thesis: Ultrashort pulse generation using FM fiber ring laser. The basic principles of FM laser are described. The theoretical analysis of chirping compression using a dispersive optical fiber is also included. Finally, theoretical analysis and experimental results of the proposed mechanism are covered.

- Chapter 5 describes the other main achievements and findings of this thesis: Femtosecond pulse generation by actively mode-locked fiber ring laser. In this chapter, an introduction of impulse modulation is included first and then several setups are developed. Operation principles and experimental results are also described.

- Finally, chapter 6 concludes this thesis and suggests some future promising research related to the contents.

Chapter 2

Fiber Laser

In general, a fiber laser consists of a gain medium made of rare-earth-ion doped fibers. Sometimes, this definition covers those lasers where most of the laser resonator is made of fibers. This chapter pays attention on the rare-earth-ion doped fibers which are used in high power and ultrashort pulse fiber lasers such as erbium (Er), ytterbium (Yb), thulium (Tm), and holmium (Ho). In this thesis, we use fiber lasers with the gain medium made of Er-ion doped fiber, which emits optical wavelength in 1.5-1.6 μm band. This chapter also provides a brief review of fiber laser technologies.

2.1 Rare-Earth-Ion Doped Fibers

Table 2.1 shows the most common laser-active rare-earth ions and their characteristics. Among these ions, erbium-doped fibers and ytterbium-doped fibers are the technologically most important. They are used to make erbium-doped fiber amplifiers and high-power fiber lasers and amplifiers.

The chemical composition of the host glass affects the possible performance and practical use of an active doped fiber. The core composition of rare-earth-doped fibers is normally modified by additional dopants to increase doping concentrations or to have effects on the refractive index, on the spectral shape of the optical transitions, or on the rate of energy transfers. Pure silicate is rarely used, but aluminosilicate, germanosilicate, or phosphosilicate glass is used instead [22].

TABLE 2.1: Common laser-active rare-earth ions and host glasses and important emission wavelength [22].

Ion	**Common host glasses**	**Important emission wavelengths**
Ytterbium (Yb^{3+})	Silicate glass	1.0 - 1.1 μm
Erbium (Er^{3+})	Silicate and phosphate glasses, fluoride glasses	1.5 - 1.6 μm, 2.7 μm, 0.55 μm
Thulium (Tm^{3+})	Silicate and germanate glasses, fluoride glasses	1.7 - 2.1 μm, 1.45 - 1.53 μm, 0.48 μm, 0.8 μm
Holmium (Ho^{3+})	Silicate glasses, fluorozirconate glasses	2.1 μm, 2.9 μm

Erbium, ytterbium, and thulium doped fibers are the most well-known active gain media. As described in table 2.1, the emission wavelength of Yb-doped fibers is around 1.0μm, the main emission wavelength of Er-doped fibers around 1.55 μm, and that of Tm-doped fibers around 2.0 μm. Some fibers are intentionally doped with two different kinds of ions to obtain interesting properties. Er and Yb can be doped together to increase pump absorption per unit length. Tm-ions can be combined with Ho-ions to extend the emission wavelength band.

2.1.1 Erbium-doped fibers

The technically most important rare-earth metal ions are Er^{3+}. Er-ions provide gain in a main broad wavelength range around 1.55 μm. This band lies in the low-loss transmission window of optical fibers so it is particularly interesting and important for optical communication. The first Er-doped fibers were reported in 1985 [44]. Er-doped fiber amplifiers and lasers were demonstrated after two years in 1987 [45, 46].

Host glasses for Er-ions are mostly silicate and phosphate types. They are used both for bulk lasers and fiber lasers and amplifiers. Fig. 2.1 shows the energy level diagram of the Er-ion and some common optical transitions. The most common optical pumping bands of Er-ions are 980 nm (the transition ${}^4I_{15/2} \rightarrow {}^4 I_{11/2}$) and 1450 nm (the transition ${}^4I_{15/2} \rightarrow {}^4 I_{13/2}$). These wavelength bands can be generated by commercial semiconductor laser diodes. Due to high phonon energies, silicate glasses exhibit a relatively fast multi-phonon transition leading from ${}^4I_{11/2}$ to ${}^4I_{13/2}$. The upper-state

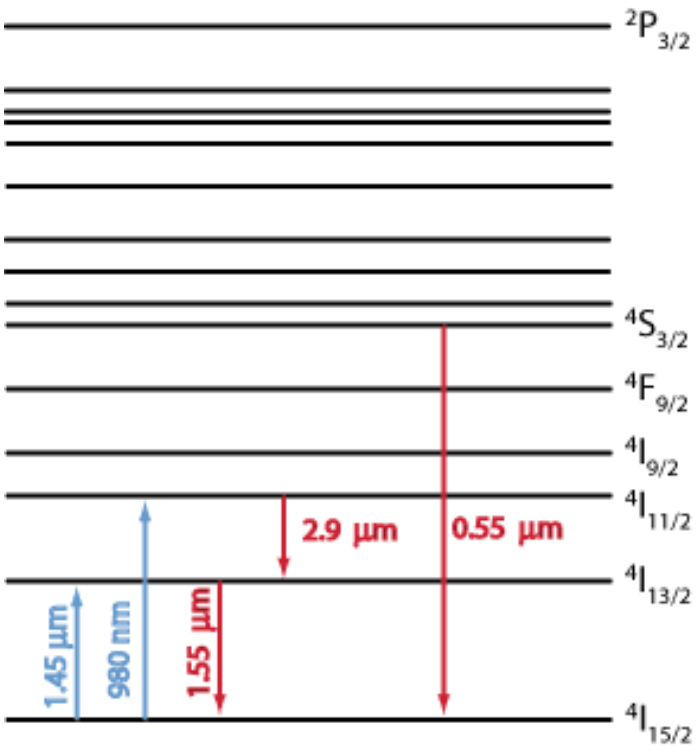

FIGURE 2.1: Energy level structure of the erbium ions, and some common optical transitions [1]

lifetime of $^4I_{13/2}$ manifold is of the order of 8 - 10 ms. Meanwhile, due to fast multi-phonon decay, all higher levels have lifetimes of at most a few microseconds.

In lasers and amplifiers, the Er behaves as a quasi-three-level transition system as confirmed by experimental relaxation oscillation measurement [47]. Therefore, Er-doped lasers and amplifiers require a significant excitation density of the Er-ions, and Er-lasers typically exhibit a high threshold pump power. The most common laser transition (widely used in erbium-doped fiber amplifiers) is from $^4I_{13/2}$ manifold to the ground-state manifold $^4I_{15/2}$. The transition wavelength is usually around 1.53 - 1.6 μm.

Fig. 2.2 shows the absorption and emission cross-sections for Er-ions in Er:Yb-doped phosphate glass. Er-fibers are often co-doped with Yb^{3+} sensitizer ions to achieve efficient pump absorption on the $^4I_{15/2} \rightarrow ^4 I_{11/2}$ transition. The Yb-ions can efficiently absorb pump radiation e.g. at 980 nm, and then transfer the energy to Er-ions in the ground-state manifold, bring them into $^4I_{11/2}$ manifold. The ions are quickly transfered from that level to the laser level $^4I_{13/2}$.

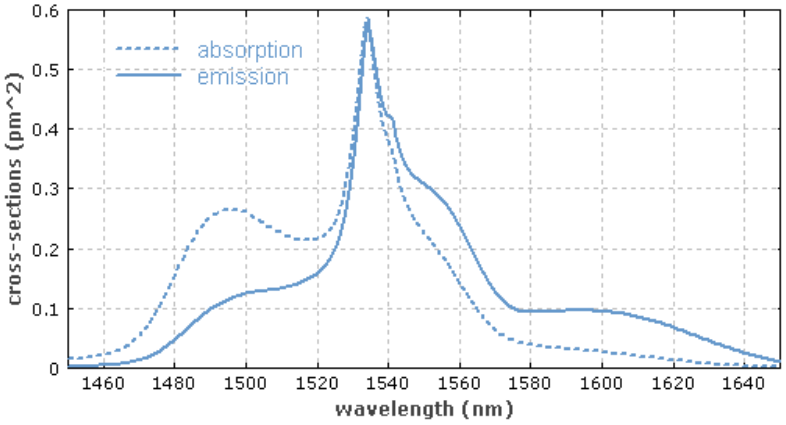

FIGURE 2.2: Absorption and emission cross-sections of Er^{3+}-ions in Er:Yb-doped phosphate glass [2]

Er-fibers are also beneficial gain medium for ultrashort mode-locked fiber laser because the gain spectrum of Er-fibers is broad [35, 36]. In addition, the fiber dispersion at 1550 nm is anomalous, which supports mode-locked fiber lasers operating in the soliton regime [10, 43].

In this thesis, we use an Er^{3+}-doped fiber amplifier (EDFA) as a gain medium for proposed ultrafast fiber lasers. The EDFA provides gain in a broad wavelength band of 1530 - 1560 nm.

2.1.2 Ytterbium-doped fibers

Yb is a chemical element that belongs to the group of rare-earth metals. In laser technology, Yb provides optical amplification and gain around 1000 nm wavelength. It has obtained a remarkable role in the form of the trivalent ion Yb^{3+}, which is used as a laser-active dopant in a variety of host materials, including both crystals and glasses. Yb-activated glass was initially reported for laser material in 1962 [48]. However, the first Yb-based silicate gain fiber was proposed in 1988 [49], 26 years later. Since then, Yb-doped fibers have been intensively investigated during the last two decades. It is often used for high-power lasers and for wavelength-tunable solid-state lasers.

Fig. 2.3 displays the energy level diagram of the Yb^{3+}-ions in Yb:YAG. Yb is a quasi-three level laser medium. Yb-doped lasers have a number of interesting properties. They have a very simple electronic level structure with only one excited state at ${}^2F_{5/2}$ manifold.

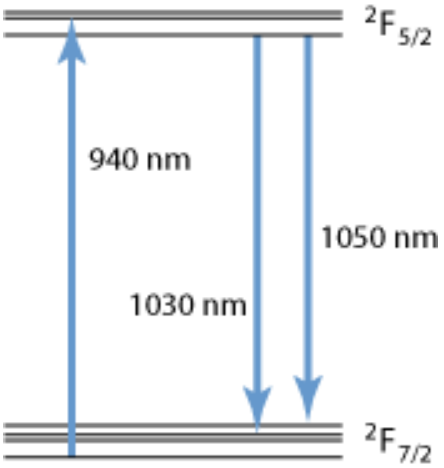

FIGURE 2.3: Energy level structure of the ytterbium ions in Yb:YAG, and the usual pump and laser transitions [3]

Pumping and amplification involve transitions between the ground-state manifold $^2F_{7/2}$ and the excited-state. The small quantum defect allows for very high power efficiencies of lasers and reduces the thermal effects in Yb-lasers and amplifiers. The fairly large gain bandwidth of the laser transitions allows for generating ultrashort pulses in mode-locked Yb-lasers.

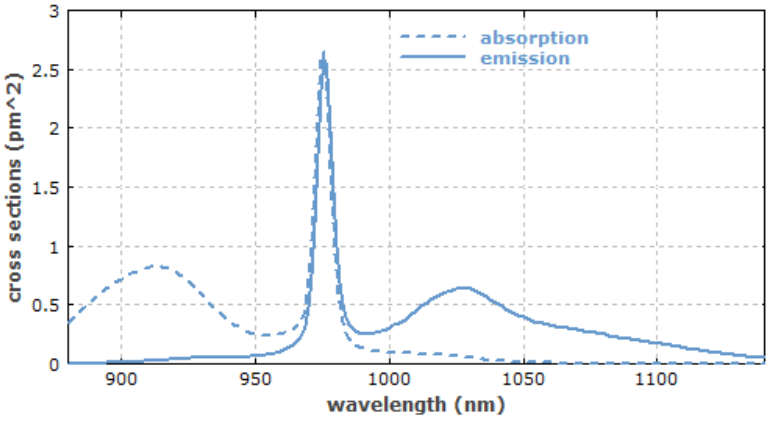

FIGURE 2.4: Absorption and emission cross-sections of Yb^{3+}-ions doped in the cores of germanosilicate glass fibers [3]

The absorption and emission spectra of Yb-ions in the cores of germanosilicate glass fibers are shown in Fig. 2.4. It can be seen that efficient pumping is possible around a wavelength of 910 nm or near 975 nm. In the 975 nm pumping case, the pump linewidth

must be small and about 50 % excitation level can be obtained due to stimulated emission. However, the absorption length and the quantum defect are smaller compared with 910 nm pumping case. Yb-ions generates strong fluorescence bands at 980 nm and at 1030 nm.

Although the Yb-ion has the simple electronic level structure, strong quenching effects can occur in Yb-doped fibers [50]. With quenching effects, some fraction of the Yb-ions (from a few percents to more than 50 %, depending strongly on the fabrication conditions) has an extremely short upper-state lifetime, whereas the other Yb-ions are basically unaffected. Quenching effects are severe because even a small fraction is sufficient for strongly reducing the laser or amplifier performance. Some high doping concentration Yb-doped fibers have been demonstrated to suffer another detrimental effect that is photodarkening [51]. This effect results in a broadband loss centered at the visible wavelengths and decreases the output power efficiency and long-term reliability of a high-power laser. To avoid photodarkening, fiber doping concentration and core structure design should be carefully considered.

2.1.3 Thulium-doped fibers

Tm^{3+}-ions provide gain in a broad wavelength range from 1700 to 2100 nm. This wavelength range is beneficial for some applications operating in the mid infrared range e.g. spectroscopy and biomedical and military applications [52, 53]. The first Tm-doped fiber laser was pumped at 800 nm by a dye laser, providing gain at 1900 nm [54]. Common Tm^{3+}-based glasses are silicate, germanate, and fluoride glasses.

Fig. 2.5 shows the energy level structure of Tm^{3+} and important transitions. Tm^{3+} is a quasi-three level medium. Tm-ions allow for several pumping wavelengths including 800 nm, 1150 nm, and 1600 nm. The most common pumping wavelength is 800 nm but at this wavelength Tm^{3+}-doped fibers suffer large quantum defect, leading to the increase of temperature and cooling problems. Commercial semiconductor-based lasers can be used for pumping at 1150 nm. For the sake of low quantum defect, an Er-fiber amplifier operating at 1560 nm can be used to pump Tm-doped fibers. In this case, quantum defect is significantly decreased by directly pumping into the core of Tm-doped fibers.

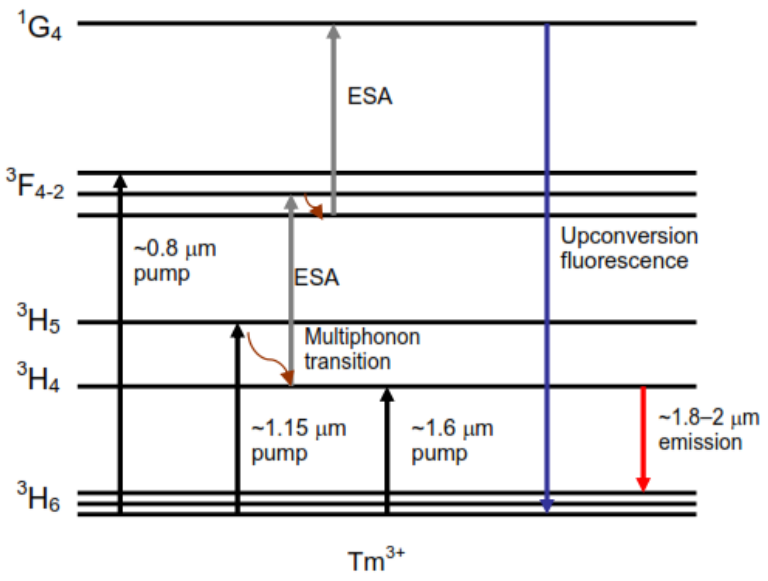

FIGURE 2.5: Energy level structure of Tm^{3+}, and the usual pump and laser transitions [4]

The main absorption bands of Tm-ions are shown in Fig. 2.6 (a). The main emission band is broad, from 1700 nm to 2100 nm (Fig. 2.6 (b)). Tm^{3+}-doped fibers can also be used to emit 480 nm (visible blue) via upconversion process (Fig. 2.5) [55]. By using the pumping wavelength of 1150 nm and excited state absorption (ESA), upconversion lasers can produce hundreds of mW output power at 480 nm [55]. These effects are harmful as Tm^{3+}-doped fibers are used for 2000 nm laser emission.

The emission wavelength band of Tm^{3+}-doped fibers is up to 2100 nm but the long wavelength tail beyond 2000 nm is weak. This wavelength tail is able to enhance by adding Ho^{3+}-ions as sensitizers.

2.1.4 Holmium-doped fibers

Ho^{3+}-doped fiber lasers have emission wavelength band centered at 2100 nm [8]. There is another emission band centered at mid-infrared 2900 nm [56] which was pumped at the visible absorption peak located at 640 nm. Fig. 2.7 displays the simplified energy level diagram of Ho^{3+}-ions and the important pumping and lasing transitions. It can be seen that there are three main pumping wavelength of 640 nm, 1150 nm, and 1900 nm. Therefore, Ho-doped fibers can be used in-band pumping with Tm-doped fiber lasers

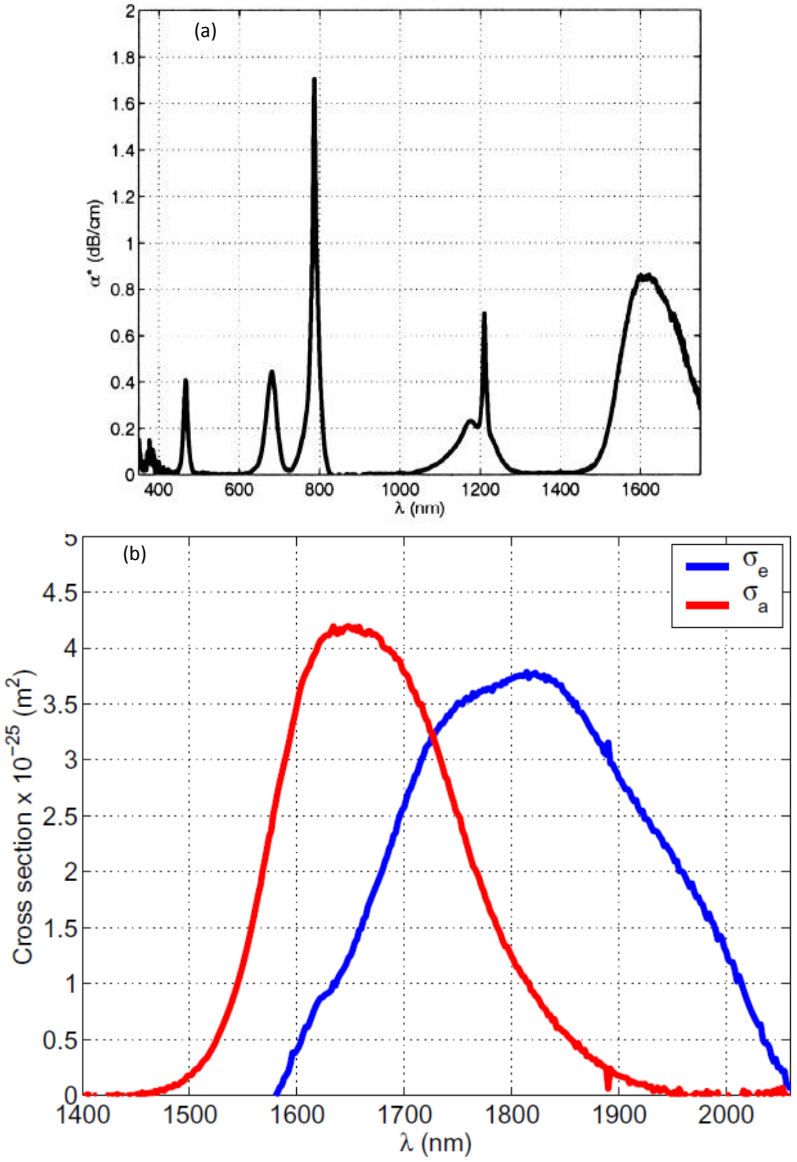

FIGURE 2.6: (a) Absorption spectrum [5] and (b) absorption and emission cross-sections of Tm^{3+}-ions doped in the cores of silica fibers [6]

operating at 1900 nm. Typical host materials for Ho^{3+}-doped fibers are silicate and fluoride glasses.

Fig. 2.8 shows the room-temperature absorption and emission spectra of Ho^{3+}-ions doped in the cores of scandium silica fibers (Ho:SSO). The absorption spectrum is from 1750 nm to 2200 nm with the maximum peak located at 1940nm. Emission spectrum is from 1800 nm to 2200 nm with broad emission waveband centered at 1943 nm, 2028 nm, and 2087 nm. The full width at half maximum (FWHM) of the spectrum is about 193 nm.

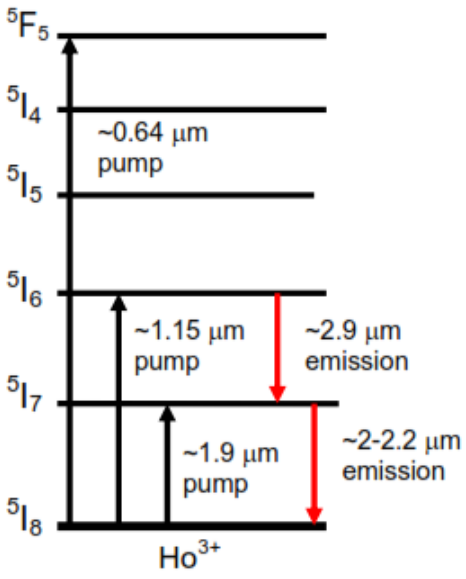

FIGURE 2.7: Simplified energy level structure of Ho^{3+}, and the usual pump and laser transitions [7]

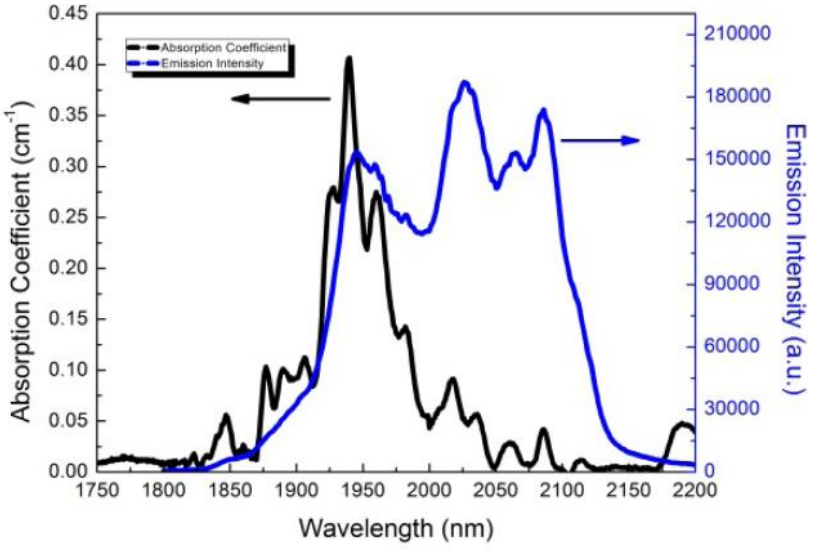

FIGURE 2.8: Absorption and emission cross-sections of Ho^{3+}-ions doped in the cores of scandium silica fibers (Ho:SSO) [8]

2.2 Review of Fiber Lasers

2.2.1 Review

Fiber lasers are usually meant to be lasers with a gain medium made of a rare-earth-doped fiber. The previous section reviews some common rare-earth-ions doped in fiber lasers. The first reported experiments with gain fibers and amplification in a fiber laser were conducted in the beginning of the 1960s using Nd^{3+}-doped fiber pumped with a flash lamp [57, 58]. Since then, fiber lasers have been widely investigated and become practical systems with many advantages.

One of the most important steps in the development of fiber lasers was the manufacturing and using of low loss silica (SiO_2) host glass fibers in 1973 [59]. However, it took 12 years for the first single mode CW fiber lasers were developed in 1985 [60]. After the development of a novel manufacturing technology for rare-earth-ion-doped fibers based on the modified chemical vapor deposition method [61], new lasers and gain fibers doped with various rare-earth-ions were fabricated with precise and controllable doping concentrations.

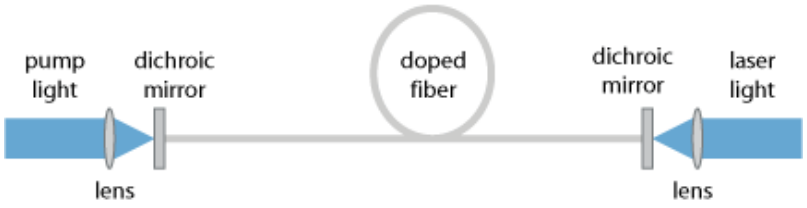

FIGURE 2.9: Typical setup of a simple fiber laser [9]

The most important part in fiber lasers is the fiber resonator. There are various types of fiber resonators including fiber ring resonators and linear resonators using reflectors (mirrors). Fig. 2.9 shows a simple laboratory setup of a fiber laser. In this setup, pump light is launched from the left-hand side with a lens through a dichroic mirror into the core of the doped fiber. The generated laser light is extracted on the right-hand side through another dichroic mirror. Other types of reflectors are also used to form linear fiber laser resonators including Fresnel reflection from a bare fiber end face (Fig. 2.10), fiber Bragg grating (Fig. 2.11), and fiber coupler.

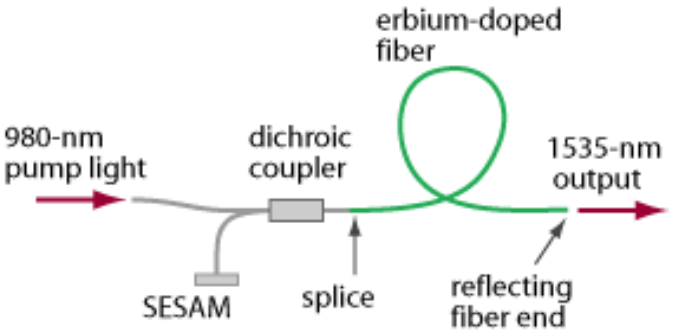

FIGURE 2.10: A simple erbium-doped laser, where the Fresnel reflection from a fiber end is used for output coupling [9]

FIGURE 2.11: Short distributed Bragg reflector fiber laser for narrow-linewidth emission [9]

The first Q-switched fiber lasers were proposed in 1986 [62], using an acousto-optic modulator to initiate pulse. Experimental results showed that the Q-switched fiber laser could generate 200 ns pulses. The first mode-locked single mode CW fiber laser was also reported in 1986 [63] with 1 ns pulse generation. In 1989, the first mode-locked Er-doped fiber laser with soliton pulse shaping was demonstrated with 4 ps pulse generation [64]. Sub-picosecond pulses were generated for the first time in the beginning of the 1990s by using a Nd-doped fiber laser [65, 66]. Compact all-fiber lasers without bulk elements such as gratings and prims was developed during this period by Duling with an all-fiber Er-laser mode-locked using a nonlinear loop mirror [10, 67]. This setup is shown in Fig. 2.12, which is so-called figure-eight cavity configuration.

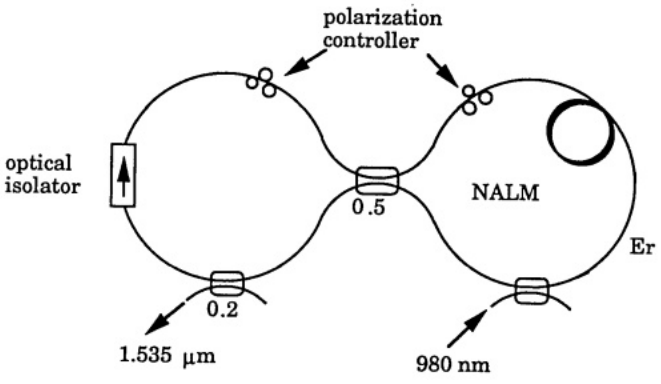

FIGURE 2.12: Configuration of the figure-eight laser. The loop of fiber in the nonlinear mirror was varied from 90 to 2 m [10]

So far, a countless number of development in ultrafast fiber lasers has been demonstrated. Consequently, the pulse duration has been reduced to the femtosecond regime and the pulse energy has been increased up to μJ levels. There are a lot kinds of ultrafast fiber lasers those can emit at different wavelengths and with different pulse durations and pulse energies. Sub-30 fs pulses were obtained from passively mode-locked Yb-fiber lasers [68].

Both actively and passively Q-switched fiber lasers can be used for generating pulses with durations in the range of tens and hundreds of nanoseconds. The pulse energy generated by Q-switched fiber laser with large mode area fibers can be mJ scales [69]. Output pulses as short as 8 ns were generated by a stable passively Q-switched Yb-doped fiber laser [70].

High-power fiber lasers have been intensively studied and developed. Whereas the first fiber lasers could generate only a few milliwatts of output power, there are now high-power fiber lasers which can provide output power up to hundreds of watts or even higher. This results from a very high surface-to-volume ratio of fibers (avoiding heat issues) and the guiding effect. With the development of double-clad fiber structure [71], high-power fiber lasers were much improved. Nowadays, double-clad fiber laser structures have a core for signal propagation together with a larger second clad for the multimode pumping light. This mechanism allows to pump with low-brightness and low-cost multimode emitters while maintaining the desired single mode beam-quality for the signal. In addition, the development of high-power low-brightness semiconductor pump diodes also contributes to the development of the high-power fiber laser.

2.2.2 Fiber lasers versus bulk lasers

It is natural to make a comparison between fiber lasers and bulk lasers (solid-state lasers) because they are used in overlapping application areas. Recently, there have been claims that fiber lasers will gradually replace most bulk lasers because they could reach the same or even better performance but at low price. However, they still have a bunch of challenges. The comparison outcome thus depends on various details of the specific requirements. In the following, the most important aspects of technical challenges of fiber lasers and bulk lasers are briefly described to obtain a fair comparison [72].

Rare-earth-doped fibers are limited by the doping concentration in glasses. As a result, their gain and pump absorption per unit length are moderate. They require the use of relatively long gain media, which has various consequences. It leads to strong effects of the Kerr nonlinearity, though the relatively small nonlinear index of fused silica. Consequently, the pulse duration or output power of fiber lasers is limited.

Fiber lasers often operate with high gain and high resonator losses. In contrast, many bulk lasers operate with the small resonator losses, which make them interesting for intra-cavity frequency doubling and can lead to lower phase noise. Uncontrollable birefringence occurs in many fiber devices, which changes the polarization state from linear to elliptical and these changes are dependent on surrounding temperature and fiber bending. Therefore, many fiber lasers require the use of polarization controllers as the temperature changes. This problem can be eliminated by using polarization-maintaining fibers.

Fiber laser setups can be made with fibers only, without any air space components. Compared with bulk lasers, the fiber laser setups need fewer mechanical components. The output of fiber lasers can be delivered to a fiber connector allowing convenient connection to external devices without any alignment procedures. In addition, fiber devices do not often require maintenance. However, if there is a defect, it is relatively difficult to locate the defect part.

Both fiber and bulk lasers can generate high-power up to kilowatts. Compared with bulk lasers, the power conversion efficiency of fiber lasers are often higher but fiber lasers require pump sources with higher beam quality and brightness. Fiber lasers can eliminate disturbing thermal effects so make it possible to achieve an excellent beam quality. Bulk lasers are generally more difficult to obtain this.

In high-power fiber devices, nonlinearities such as Raman effect and stimulated Brillouin scattering can limit the performance. All these nonlinearities are generally less severe in bulk laser devices.

Q-switching and mode-locking can be obtained by both fiber and bulk lasers to generate short and ultrashort pulses. With Q-switching, the shortest pulses is usually achieved with bulk lasers because the gain per unit length is smaller compared with fiber devices. Because rare-earth-doped glass fibers offer a broad amplification bandwidth,

fiber lasers can generate very short pulses using passive mode-locking and have very broad wavelength tunability.

An effective technique for mode-locked fiber lasers is nonlinear polarization rotation, which is less critical than additive-pulse mode-locking of bulk lasers. Harmonic mode-locking is used in fiber lasers for generating high pulse repetition rates (multi-gigahertz). However, this makes the laser setup more complex than that of a compact bulk laser.

Optical feedback is a very critical difficulty in high-power fiber lasers used for material processing. Because they often use master oscillator power amplifiers, which amplifies the back-reflected light. The fiber ends are also easily damaged due to the fairly small effective mode are. At high-power level the use of an isolator at the fiber ends to cancel back-reflected light is not always practical.

To determine in which applications fiber lasers or bulk lasers are more applicable, some general guidelines are as follows:

- "Fiber lasers are suitable for generating very high average powers with high beam quality. This holds particularly for unusual wavelengths, where no good bulk crystals or glasses are available. Fiber lasers are clearly superior for difficult lasing schemes such as low-gain transitions or upconversion. However, bulk lasers are required for some other spectral regions; for example, there is no fiber laser to replace a broadly tunable Ti:sapphire laser in the region of 700–1000 nm." [72]
- "Bulk lasers have a higher potential for high pulse energies and peak powers either with Q switching or with mode locking." [72]
- "Bulk lasers can utilize pump sources with very poor beam quality. In the most extreme case, a side-pumped rod laser can be pumped with discharge lamps. This can be advantageous e.g. when very high peak powers in pulses with moderate repetition rates are required." [72]
- "Bulk lasers are often preferable when a stable linear polarization is required (and polarization-maintaining fibers can not be used for some reason)." [72]
- "For ultrashort pulse generation, bulk lasers make it easier to achieve a high peak power and a high pulse quality in terms of smooth spectral shape, low chirp and low background." [72]

- "In terms of fabrication cost, fiber lasers will often be superior for devices with low demands on peak power, polarization, emission bandwidth, pulse quality, etc. However, more stringent demands of such type can often favor a bulk laser, as a fiber device would require complicated additional measures or very special parts. Also, the often higher development cost of fiber-based devices can be a problem in cases with small sales numbers." [72]

From the above guidelines, one can see that depending on the particular demands, fiber lasers or bulk lasers can be utilized based on their own advantages and disadvantages.

Chapter 3

Ultrashort Laser Pulses

Since the first laser was reported in 1960 [25], scientists have been continually interested in finding new methods to generate ultrashort laser pulses in the picosecond (ps) and femtosecond (fs) regime. The generation of ultrashort pulses opens up fascinating applications based on their unique properties [23]: the pulse energy can be concentrated in a temporal interval as short as several fs, which corresponds to only a few optical cycles in the visible range; the pulse peak power can be extremely high even at moderate pulse energies. This chapter starts with mathematical description of laser pulses and then pays attention on the most common methods for generation of ultrashort laser pulses.

3.1 Mathematical Description of Laser Pulses

This description is essentially referred from [11, 24, 73]. Generally, we write an optical pulse in terms of a slowly varying envelope function $A(t)$ times an optical carrier term:

$$\varepsilon(t) = Re[A(t)e^{j\omega_0 t}] = \frac{1}{2}[A(t)e^{j\omega_0 t} + A^*(t)e^{-j\omega_0 t}], \tag{3.1}$$

where $A^*(t)e^{-i\omega_0 t}$ is the complex conjugate of $A(t)e^{i\omega_0 t}$, and ω_0 is a carrier frequency. The average power over an optical cycle is given by

$$P(t) = |A(t)|^2. \tag{3.2}$$

The spectrum $\tilde{E}(\omega)$ is then given by

$$\tilde{E}(\omega) = \frac{1}{2}[\tilde{A}(\omega - \omega_0) + \tilde{A}^*(-\omega - \omega_0)], \tag{3.3}$$

where

$$\tilde{A}(\omega) = \int_{-\infty}^{\infty} A(t)e^{-j\omega t}dt \tag{3.4}$$

is the Fourier transform of the envelop function $A(t)$. The power spectrum is given by $|\tilde{E}(\omega)|^2$.

We can derive the optical pulse $\varepsilon(t)$ directly from performing the inverse Fourier transform of the double-sided spectrum described in Eq. 3.3 or from the single-sided spectrum as follows

$$\varepsilon(t) = Re[\frac{1}{2\pi}\int \tilde{A}(\omega - \omega_0)e^{j\omega t}d\omega]. \tag{3.5}$$

Table 3.1 lists mathematical description of three common pulse shapes e.g. Gaussian, secant hyperbolic ($sech^2$), and Lorentzian. These pulse shapes are standard for theoretically analyzing and often used to approximate experimental results. Temporal amplitude and intensity distributions as well as spectral amplitude and intensity distributions are shown. Gaussian pulse shape has quickly falling wings, which are proportional to e^{-t^2}. Gaussian pulse shape is not always true in a real experiment.

The $sech^2$ pulse shape has slower falling wings proportional to e^{-t}. Finally, Lorentzian pulses with large wings proportional to $1/t$. These later shapes are more appropriate to represent experimental situations.

To measure an event in time a shorter event is required. Therefore, for pulses of an ultrashort duration, the pulse is used to measure itself and using the autocorrelation function is a solution. The operation principles of this method is to divide the desired measuring pulse using a beam splitter into two copies with one is delayed with respect to the other. These copies are superimposed in a nonlinear crystal, where they interact on the basis of some nonlinearity, provided that they overlap temporarily.

The intensity autocorrelation function plays an important role in temporal pulse characterization techniques. It is determined as the time integral of temporal pulse

TABLE 3.1: The mathematical description of some common pulse shapes in the time and frequency domains [23], respectively. τ and ω_0 are temporal FWHM and carrier frequency, respectively.

Shape	**Temporal amplitude**	**Temporal intensity**
Gaussian	$\exp[-2ln2(\frac{t}{\tau})^2]$	$\exp[-4ln2(\frac{t}{\tau})^2]$
$sech^2$	$sech[2ln(1+\sqrt{2})\frac{t}{\tau}]$	$sech^2[2ln(1+\sqrt{2})\frac{t}{\tau}]$
Lorentzian	$[1+\frac{4}{1+\sqrt{2}}(\frac{t}{\tau})^2]^{-1}$	$[1+\frac{4}{1+\sqrt{2}}(\frac{t}{\tau})^2]^{-2}$
Shape	**Spectral amplitude**	**Spectral intensity**
Gaussian	$\sqrt{\frac{\pi}{2ln2}}\tau\exp[-\frac{\tau^2(\omega-\omega_0)^2}{8ln2}]$	$\frac{\pi}{2ln2}\tau^2\exp[-\frac{\tau^2(\omega-\omega_0)^2}{4ln2}]$
$sech^2$	$\frac{\pi}{2ln(1+\sqrt{2})}\tau sech[\frac{\pi\tau(\omega-\omega_0)}{4ln(1+\sqrt{2})}]$	$(\frac{\pi}{2ln(1+\sqrt{2})})^2\tau^2 sech^2[\frac{\pi\tau(\omega-\omega_0)}{4ln(1+\sqrt{2})}]$
Lorentzian	$\frac{\pi\sqrt{1+\sqrt{2}}}{2}\tau\exp[-\frac{\sqrt{1+\sqrt{2}}\tau\lvert\omega-\omega_0\rvert}{2}]$	$\frac{\pi^2 1+\sqrt{2}}{4}\tau^2 exp[-\sqrt{1+\sqrt{2}}\tau\lvert\omega-\omega_0\rvert]$

intensity function $I(t)$ multiplies with its shifted replica $I(t-\delta)$, as follows

$$S(\delta)=\int_{-\infty}^{\infty}I(t)I(t-\delta)dt. \tag{3.6}$$

The shifted replica is used as a gate to scan the same pulse. The autocorrelation function has a property that is always symmetric and centered around $\delta=0$. Autocorrelation width τ_{AC} is determined by the pulse width τ as follows

$$\tau_{AC}=\frac{1}{D_{AC}}\tau, \tag{3.7}$$

where D_{AC} is the deconvolution factor. D_{AC} depends on the assumed pulse shape.

Fig. 3.1 (a) and (b) show calculated optical pulses and intensity autocorrelation traces in different assumed pulse shapes (Lozentzian, Gaussian, and $sech^2$). Even though all three pulses have the same 100 fs FWHM pulsewidth, the width of the autocorrelation traces differs according to the value of D_{AC} for each kind of pulse shape. The values of D_{AC} for different commonly used pulse shapes are listed in Table 3.2.

In characterizing ultrashort pulses, the information about phase variations in either the frequency or time domains is also important. The temporal phase $\phi(t)$ and the spectral phase $\varphi(\omega)$ are defined, as follows

$$A(t)=|A(t)|e^{j\phi(t)} \tag{3.8}$$

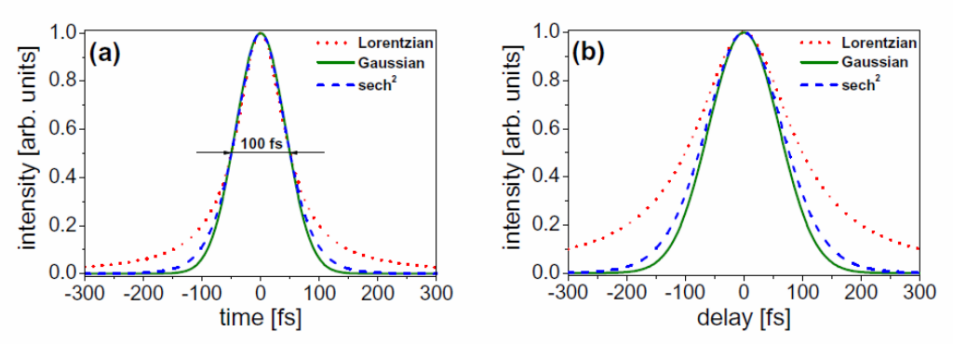

FIGURE 3.1: (a) Calculated optical pulses of different assumed shapes with the same FWHM. (b) Their correspondingly calculated autocorrelation traces [11]

TABLE 3.2: Deconvolution factors D_{AC} and time-bandwidth products K_{TB} for common pulse shapes.

Pulse shape	D_{AC}	K_{TB}
Gaussian	$1/\sqrt{2}$	0.441
$sech^2$	0.6482	0.315
Lorentzian	0.5	0.142

and

$$\tilde{A}(\omega) = |A(\omega)|e^{j\varphi(\omega)}. \tag{3.9}$$

The temporal phase $\phi(t)$ can also be expanded into the Taylor series around time zero for small derivations

$$\phi(t) = \sum_{k=0}^{\infty} \frac{\phi^{(k)}(0)}{k!}(t)^k, \tag{3.10}$$

where

$$\phi^{(k)}(0) = \left.\frac{\partial^k \phi(t)}{\partial t^k}\right|_{t=0}. \tag{3.11}$$

Instantaneous frequency $\omega(t)$ is defined from the time derivative of the temporal phase as follows

$$\omega(t) = \omega_0 - \frac{d\phi(t)}{dt}. \tag{3.12}$$

The first term of the Taylor series of the temporal phase $\phi(0)$ is the absolute phase of the pulse. The first order derivative $\phi'(0)$ in the second term of the series is linear with time and describes a shift of the carrier frequency ω_0. While the second order derivative in the third term corresponds to the linear motion of the instantaneous frequency; this term is called a linear chirp. The up-chirp and down-chirp correspond to the frequency

increasing and decreasing versus time, respectively. The next terms are the quadratic chirp, cubic chirp, and so on.

Similarly, the spectral phase $\varphi(\omega)$ can be expanded into the Taylor series around the carrier frequency ω_0, as follows

$$\varphi(\omega) = \sum_{k=0}^{\infty} \frac{\varphi^{(k)}(\omega_0)}{k!}(\omega - \omega_0)^k, \tag{3.13}$$

where

$$\varphi^{(k)}(\omega_0) = \left.\frac{\partial^k \varphi(\omega)}{\partial \omega^k}\right|_{\omega=\omega_0}. \tag{3.14}$$

The first term $\varphi(\omega_0)$ in Eq. 3.13 is the absolute phase of the pulse in the time domain. The first order derivative $\varphi'(\omega_0) = T_g(\omega_0)$ is the so-called group delay (GD), which leads to a shift of the pulse envelope in the time domain. While the second order derivative

$$D_2(\omega_0) = \varphi''(\omega_0) = \left.\frac{\partial T_g(\omega)}{\partial \omega}\right|_{\omega=\omega_0} \tag{3.15}$$

is so-called group delay dispersion (GDD), as call as second order dispersion. The higher order derivatives (GDD and higher) describe the frequency dependence of the GD. These higher order derivatives are responsible for dispersive effects and changes in temporal structure of the optical pulse envelope.

A pulse is called a Fourier transform limited pulse if the phase variation of such pulse has a linear time dependence; in other words, the instantaneous frequency of the pulse is time-independent. In such case, the pulse width is determined by its spectral width as given by

$$\tau \Delta\omega = 2\pi K_{TB}. \tag{3.16}$$

τ and $\Delta\omega$ are FWHM of intensity profile in the time domain and frequency domain, respectively. K_{TB} is a constant, its value depends on the pulse shape as shown in Table 3.2. Eq. 3.16 is called time-bandwidth product, which means that the shorter pulse width, the wider frequency bandwidth. For a given spectrum, there is only one shortest possible pulse duration. Therefore, this equation provides the lower limit for the estimation of the real laser pulse duration.

3.2 Methods for Generation of Ultrashort Laser Pulses: Mode-Locking

Mode-locking is a technique referred to a locking of the phase relationship between longitudinal modes of the laser resonator. This technique was first proposed in 1964 [74]. Mode-locking is a group of methods to obtain ultrashort pulses from lasers, which are then so-called mode-locked lasers. When a laser operates, it oscillates simultaneously over all the resonance frequencies of the laser cavity as long as the gain is greater than the cavity losses. These resonance frequencies make up the set of longitudinal modes of the laser [75]. As longitudinal modes are locked together, the laser output intensity is no longer constant with time. Fig. 3.2 illustrates the temporal evolution of the intracavity field in a laser. The top blue curve shows a pulse train with a fixed phase relationship, so that at periodic temporal positions the electric fields of all longitudinal modes add up to a maximum. In the case of random phases, the time distribution of the intensity shows a random distribution of maxima.

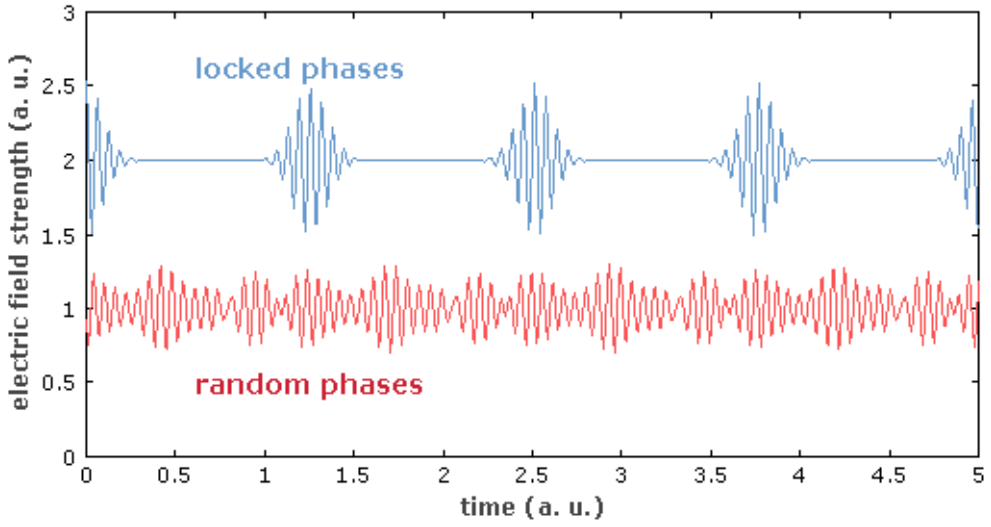

FIGURE 3.2: Illustration of the influence of the phase relation when mode-locking. The longitudinal modes have a fixed phase relationship and random phases [12]

To achieve mode-locking, the laser cavity contains either an active element (an optical modulator) or a nonlinear passive element (a saturable absorber). The main role of these active and passive elements is to form an initial ultrashort pulse circulating in the laser resonator. In the stable state, the circulating pulse is affected by various effects. As an equilibrium reached, the pulse parameters are stable after each round-trip. In the case of single circulating pulse, the pulse repetition rate is the same as the the

resonator round-trip time (typically several nanoseconds), whereas the pulse duration is much lower (typically between 30 fs and 30 ps). Therefore, the peak power of an output pulse can be orders of magnitude higher than the average power. In the following parts, principle of the mode-locking will be briefly discussed.

Let's consider the longitudinal modes that can self-oscillate in the free multi-mode regime of the laser, where the unsaturated gain is greater than the cavity losses, as shown in Fig. 3.3. the number of these modes, so-called N, can vary from just a few (e.g. He-Ne lasers) to tens of thousands (e.g. Ti:sapphire lasers). If the modes have constant phase differences, the laser output will have a periodic pulse train with each pulse lasting $\Delta\tau$ and the pulse repetition rate being $T = 2L/c$, where L is the cavity length and c is the speed of light. The larger the number of resonance modes, the shorter the circulating pulse is [75]. The laser working under this conditions is said to operate in the mode-locked regime.

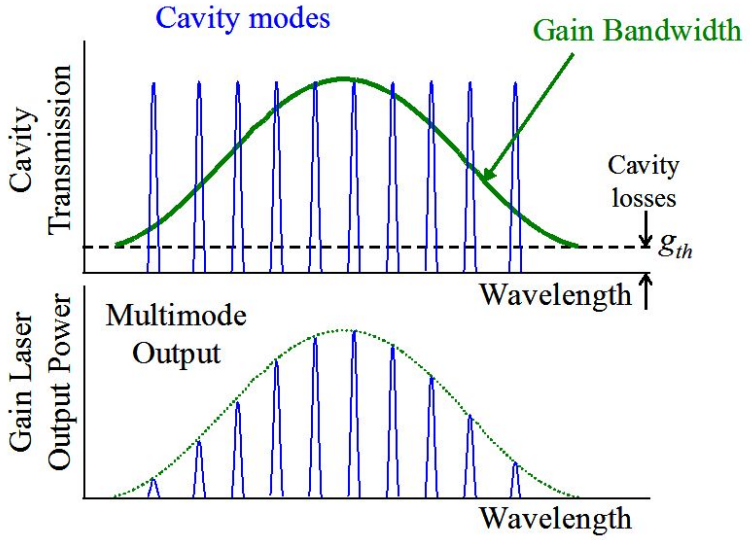

FIGURE 3.3: Cavity resonance modes and gain bandwidth [13]

The circulating signal inside an oscillating laser cavity can be described either in the time domain or in the frequency domain. Recirculating pulse concepts are used in the time domain, and multiple axial-mode concepts are used in the frequency domain. Before introducing any of the mode-locking techniques, let me describe briefly these time and frequency approaches (detail description can be referred in [14]).

- **Time-domain description of laser signals**

The optical field inside the laser cavity with two mirrors M_1 and M_2 can be illustrated as Fig. 3.4. M_2 is the output mirror. After being weakened by reflection from the output coupling mirror, the fields will circulate again inside the cavity and be restrengthened by the amplification medium. The laser amplification process is basically linear and coherent so that the signal's shape will stay unchanged and thus it will look essentially the same one round-trip transit time later. The repetition rate (axial mode spacing frequency) will be described as follows

$$\omega_{ax} = \omega_{q+1} - \omega_q = \frac{2\pi}{T}, (q = 1, 2, ...), \tag{3.17}$$

where ω_q is the $q - th$ axial mode and T is period given by $T = 2L/c$ for a cavity of length L, c is the speed of light.

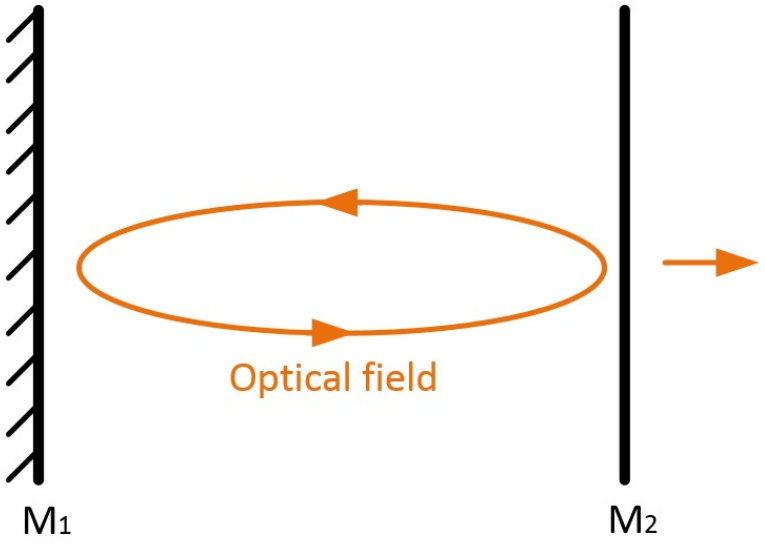

FIGURE 3.4: Optical field pattern circulating inside a laser cavity

Let's consider the real laser signal $\varepsilon(t)$ that may come out of a laser cavity during a single round-trip i.e. $0 \leq t \leq T$, with $\varepsilon(t) = 0$ outside that range, as shown in Fig. 3.5. $\tilde{E}(\omega)$ is the Fourier transform of this time-limited signal. If $\varepsilon(t)$ has time fluctuations in either amplitude or phase that are rapid compared to the cavity round-trip time, its spectrum $\tilde{E}(\omega)$ will have a spread in radian frequency that is wide compared to $2\pi/T$ and compared to the axial-mode interval ω_{ax}.

Now, let's consider a signal $\varepsilon^{(2)}(t) = \varepsilon(t) + \varepsilon(t - T)$, which consists of the same signal $\varepsilon(t)$ repeated for two round trips. The signal $\varepsilon(t - T)$ is delayed by an amount T in the time domain and its Fourier transform is given by $e^{(-jT\omega)} \times \tilde{E}(\omega)$. Hence, the Fourier

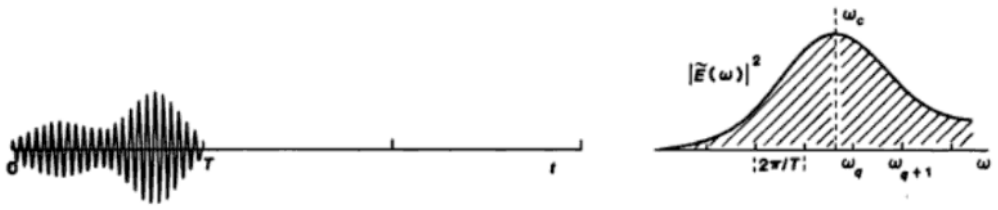

FIGURE 3.5: One period of signal $\varepsilon(t)$ (left) and its power spectrum $|\tilde{E}(\omega)|^2$ (right) [14]

transform of $\varepsilon^{(2)}(t)$ is given by

$$\tilde{E}^{(2)}(\omega) = \frac{1}{2}[1 + e^{-jT\omega}] \times \tilde{E}(\omega) = \tilde{E}(\omega)\cos(T\omega/2)e^{-jT\omega/2}. \tag{3.18}$$

Its intensity (power spectrum) is

$$I^{(2)}(\omega) = |\tilde{E}^{(2)}(\omega)|^2 = \frac{1}{2}[1 + \cos(T\omega)] \times I(\omega) = I(\omega)\cos^2(T\omega/2). \tag{3.19}$$

Fig. 3.6 illustrates two-period time signal $\varepsilon^{(2)}(t)$ and its power spectrum $|\tilde{E}\ (2)(\omega)|^2$. It can be seen that the two-period signal has the same spectrum as the one-period signal.

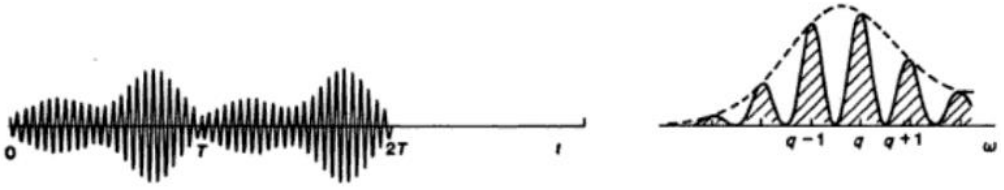

FIGURE 3.6: A time signal $\varepsilon^{(2)}(t)$ (left) and its power spectrum $|\tilde{E}\ (2)(\omega)|^2$ (right) for the same signal repeated two times in a series [14]

If we combine N round trips of the the same time signal $\varepsilon(t)$ such that

$$\varepsilon^{(N)}(t) = \sum_{n=0}^{N-1} \varepsilon(t - nT), \tag{3.20}$$

and the Fourier transform of Eq. 3.20 is

$$\tilde{E}^{(N)}(\omega) = \sum_{n=0}^{N-1} e^{-jnT\omega} \times \tilde{E}(\omega) = \frac{1 - e^{-jNT\omega}}{1 - e^{-jT\omega}}\tilde{E}(\omega). \tag{3.21}$$

Hence, the power spectrum is

$$I^{(N)}(\omega) = |\tilde{E}^{(N)}(\omega)|^2 = \frac{1-\cos(NT\omega)}{1-\cos(T\omega)} I(\omega). \tag{3.22}$$

An illustration of the power spectrum described in Eq. 3.22 for the case of N = 10 is displayed in Fig. 3.7.

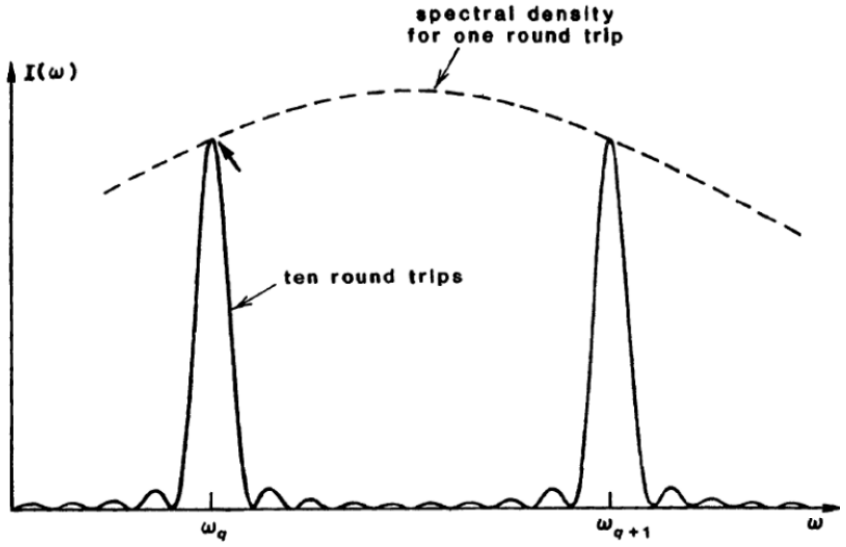

FIGURE 3.7: Power spectrum density $|\tilde{E}\ (10)(\omega)|^2$ for the same signal repeated 10 times in succession [14]

These equations describe the circulating signal inside an oscillating laser cavity in the time-domain, established by recirculating pulse concepts. Next part discusses this problem in the frequency domain.

- **Frequency-domain description**

Now, we will consider this laser signal again but focusing on the frequency domain. A laser operating in a single axial mode is the simplest situation. That means the signal amplitude, phase, and frequency are all constant in time. Such characteristics never happen in a real laser. In the case of two oscillating axial modes, the output field as a function of time can be written as

$$\varepsilon(t) = Re[E_1 e^{j(\omega_1 t+\phi_1)} + E_2 e^{j(\omega_2 t+\phi_2)}]. \tag{3.23}$$

The output intensity then becomes

$$I(t) = |\varepsilon(t)|^2 = E_1^2 + E_2^2 + 2E_1E_2\cos[(\omega_2 - \omega_1)t + \phi_2 - \phi_1], \tag{3.24}$$

where ϕ_1 and ϕ_2 are the phase of the two phaser amplitudes $\tilde{E}_1$ and $\tilde{E}_2$, respectively. From Eq. 3.24 shows that the output intensity is a sinusoidal function with a frequency $(\omega_2 - \omega_1)$. In the case of equal amplitude $E_1 = E_2$, the depth of modulation of this sinusoidal beating is 100%. With two axial modes only, the concept of mode locking is not so meaningful because any two sinusoidal signals are always mode-locked.

The situation turns more interesting when a laser oscillates three or more equally spaced axial modes. Supposed that we have three sinusoidal wave with equally spaced frequencies ω_q, ω_{q+1}, and ω_{q+2} as shown in the top three parts of Fig. 3.8. If they are exactly in phase, the amplitude of the sum signal will appear as in the bottom part of Fig. 3.8.

Consider the case of having N equally spaced axial-mode frequencies, where for the sake of simplicity, assuming that these sidebands have the same amplitude. Again, if they are all exactly in phase, we can write the total wave amplitude in the form

$$\varepsilon(t) = \sum_{n=0}^{N-1} e^{j(\omega_0 + n\omega_{ax})t} = \frac{e^{jN\omega_{ax}t} - 1}{e^{j\omega_{ax}t} - 1} e^{j\omega_0 t}, \tag{3.25}$$

and the signal intensity is

$$I(t) = |\varepsilon(t)|^2 = \frac{1 - \cos(N\omega_{ax}t)}{1 - \cos(\omega_{ax}t)} = \frac{\sin^2(N\omega_{ax}t/2)}{\sin^2(\omega_{ax}t/2)}. \tag{3.26}$$

Fig. 3.9 (a), (b), and (d) displays the periodic time envelopes that derive from Eq. 3.25 for the case N = 8. From the phasor viewpoint, adding together N equal-amplitude sinusoidal waves, if all in phase at $t = 0$, a peak will arise at $t = 0, \pm T, \pm 2T$.... The peak amplitude is N times the amplitude of each sine wave. "After a time $\Delta t = \pm T/N$ on either side of these peaks, however, the phasor amplitudes rotate by enough relative to each other to become uniformly distributed in angle, so that the total field amplitude and intensity fall to exactly zero" [16]. Fig. 3.9 (c) displays a Gaussian spectrum (Gaussian sideband amplitude distribution) with all modes in phase at $t = 0$. It also shows an output pulse train but the pulses now have the Gaussian shapes in time with almost no subsidiary peaks.

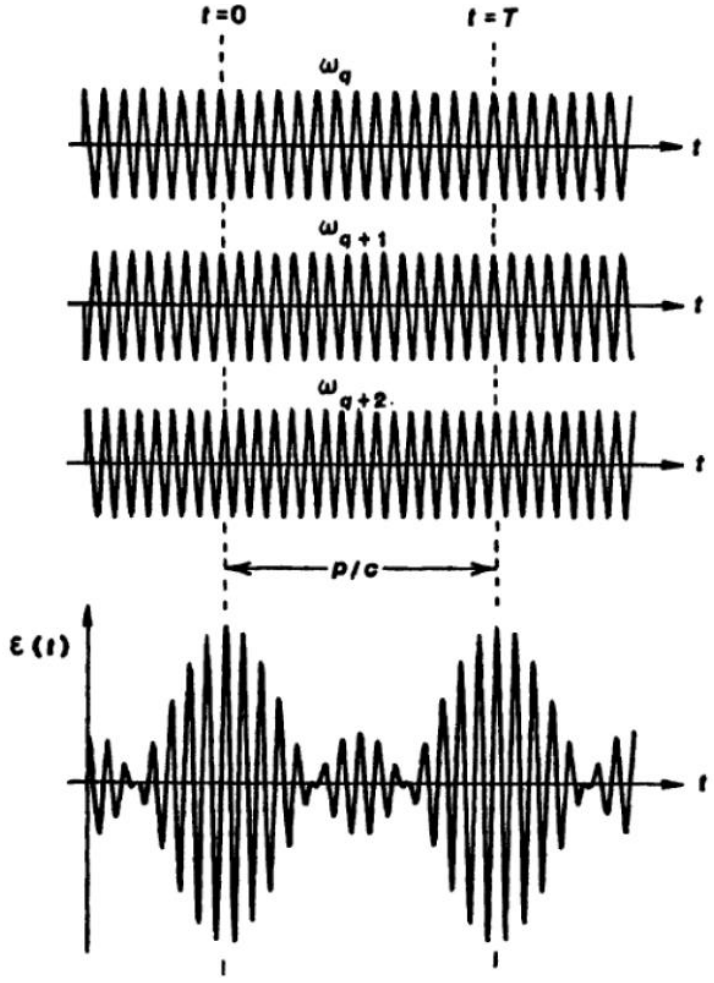

FIGURE 3.8: Superposition of three equally spaced frequency components [15]

In general, equally spaced axial modes create a periodic signal in time domain. Mode coupling is the situation when the amplitude and phase of modes are arbitrary but fixed. Meanwhile, mode locking is the situation when all modes are in phase so there are $t = nT$ where all relative phases are zero. Some remarks to remember are the broader the spectrum, the shorter the pulse and vice versa. Repeated signal creates mode-structured spectrum and vice versa. Spectrum's envelope is exact single pulse spectrum. Modes in phase create periodic signal with one dominant short pulse per a period.

3.2.1 Active mode-locking

Let's insert an active element, e.g. an intensity (or amplitude) modulator (AM) or a phase (or frequency) modulator (FM), inside the cavity which modulates its losses,

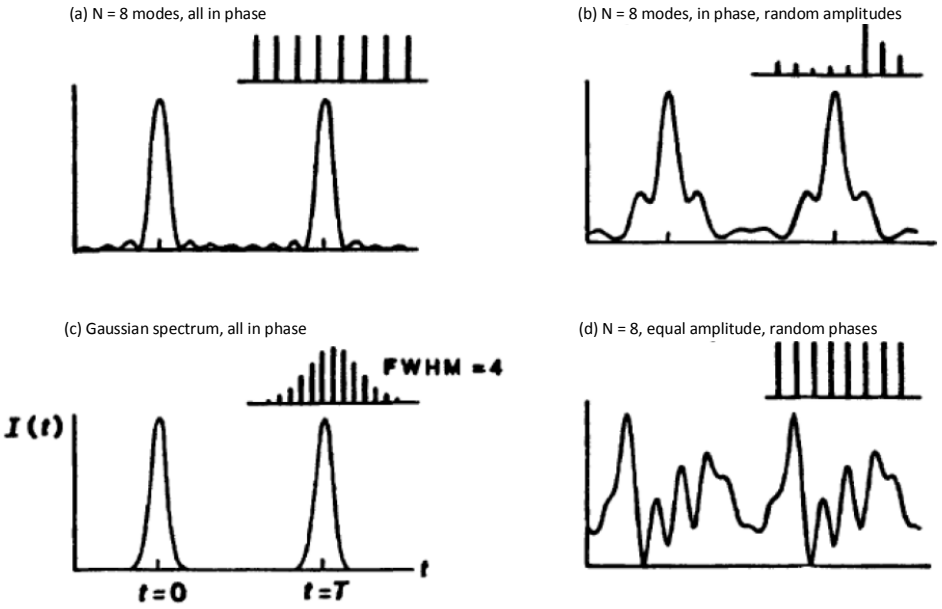

FIGURE 3.9: Examples of the different intensity patterns in time [16]

as shown in Fig. 3.10. So that we can have what is referred to as either "AM mode locking" or "FM mode locking". The modulator will induce modulation of the amplitude of each longitudinal mode. If the modulation frequency ω_m is synchronized with the cavity round-trip frequency, this leads to the generation of ultrashort pulses. Fig. 3.11 illustrates mode-locked time domain behavior. From a time-domain viewpoint, the laser begins to oscillate in the form of a short pulse which circulates inside the cavity, passing through the modulator on each round trip exactly at the moment when the modulator transmission is at its maximum.

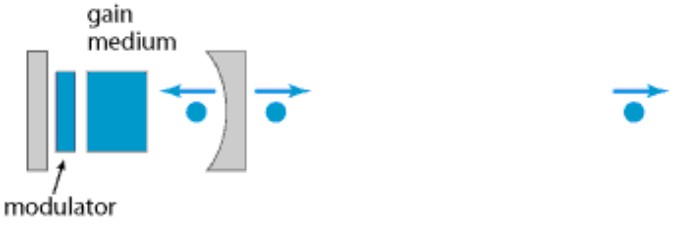

FIGURE 3.10: Schematic setup of an actively mode-locked laser [17]

From a frequency-domain viewpoint, we can say that each of the oscillating axial modes present in the laser cavity at frequency ω_q will acquire modulation sidebands at frequencies $\omega_q \pm n \times \omega_m$ as a result of the active modulator. If the modulator is driven at a modulation frequency ω_m equal or very close to the axial-mode spacing, or one of its integer multiples, the modulation sidebands from each axial mode will fall on top of, or very close to, one of the other axial modes in the cavity. As shown in Fig. 3.12, each

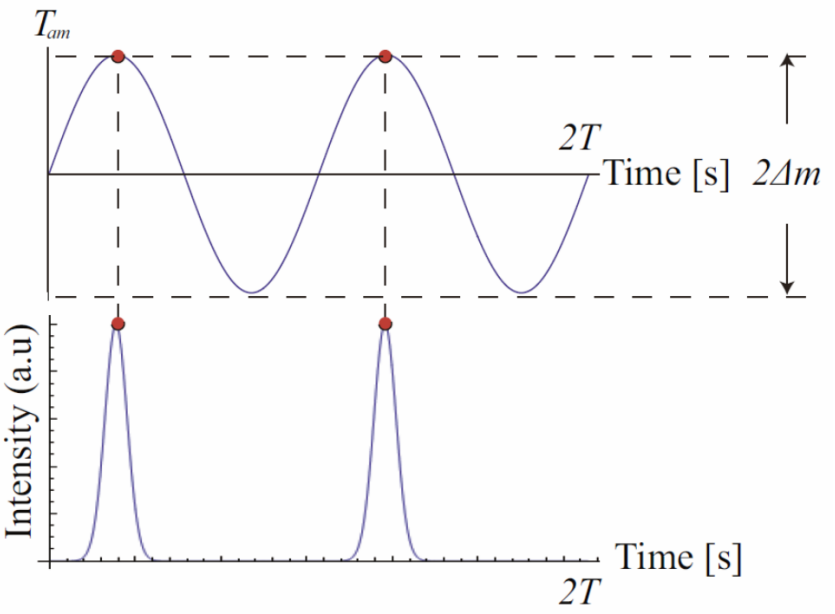

FIGURE 3.11: Illustration of mode-locked time-domain behavior

of these side bands will injection lock the axial mode with which it is in resonance. The modulator will then tend to couple together, so-called mode-lock, each axial mode to one or more of its neighboring modes.

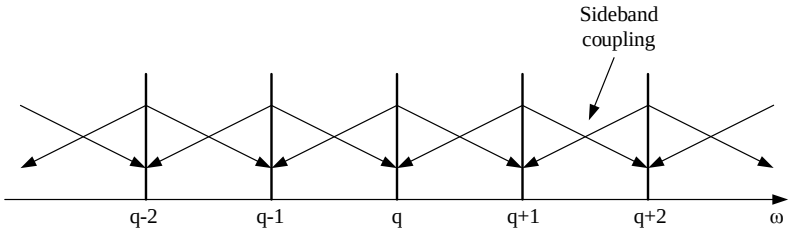

FIGURE 3.12: Illustration of mode-locked frequency-domain behavior [16]

This form of intracavity modulation represents the most common form of active mode locking. The modulation frequency must be tuned very close to the fundamental round-trip frequency ω_{ax} of the laser cavity. The pulse formation process is controlled and synchronized by the applied modulation frequency.

As the circulating pulse becomes shorter, it has less loss when passing through the modulator. The pulse spectrum becomes wider with more axial modes. However, when the spectral width begins to approach the amplification bandwidth of the laser medium, the gain will decrease. Therefore, the pulsewidth limitation results from a compromise

between the pulsewidth shortening effects of the modulator and the spectral narrowing effects of the laser gain medium.

Assume that the pulse circulating inside the laser cavity is described by a Gaussian pulse envelope with the general form as follows

$$\varepsilon(t) = \exp[-\Gamma t^2 + j\omega_0 t], \tag{3.27}$$

The spectral spectrum of this Gaussian pulse is given by

$$E(\omega) = \exp[-\frac{(\omega - \omega_0)^2}{4\Gamma}]. \tag{3.28}$$

Here, ω_0 and $\Gamma = \alpha - j\beta$ are carrier angular frequency and the complex Gaussian pulse coefficient, respectively. α is proportional to $\sqrt{1/\tau}$ and β is chirp.

This pulse propagates through the laser gain medium (with gain function $g(\omega)$) in one complete round trip. It can be written in the frequency domain as

$$E'(\omega) = g(\omega)E(\omega). \tag{3.29}$$

The transfer function $g(\omega)$) can be written in the form

$$g(\omega) = \exp[\frac{\alpha_m p_m}{1 + 2j(\omega - \omega_a)/\Delta\omega_a} - j\frac{\omega p}{c}], \tag{3.30}$$

where $\alpha_m p_m$ is the round-trip voltage gain coefficient, ω_a is the atomic transition frequency, and $\frac{\omega p}{c}$ is the round-trip phase shift in the empty cavity. The frequency spectrum $E(\omega)$ of the mode-locked pulse remains narrow compared to the full atomic linewidth $\Delta\omega_a$ of the laser gain medium. Therefore, the Taylor series expansion of Eq. 3.30 will be a valid approximation, as written by

$$g(\omega) \approx \exp[\alpha_m p_m(1 - 2j\frac{\omega - \omega_a}{\Delta\omega_a} - \frac{4}{\Delta\omega_a^2}(\omega - \omega_a)^2) - j\frac{\omega p}{c}]. \tag{3.31}$$

As the pulse propagates through the laser gain medium, we multiply the Gaussian pulse spectrum with pulse coefficient Γ by the atomic gain function $g(\omega)$ using the quadratic expansion (the second-order term in Eq. 3.31). We will achieve a new Gaussian pulse

with a modified $\Gamma^{'}$ given by

$$\exp[-\frac{(\omega-\omega_a)^2}{4\Gamma}] \times \exp[-\frac{4\alpha_m p_m}{\Delta\omega_a^2}(\omega-\omega_a)^2)] = \exp[-\frac{(\omega-\omega_a)^2)}{4\Gamma'}]. \tag{3.32}$$

After passing through the gain medium, the Gaussian pulse parameter has a net change given by

$$\frac{1}{\Gamma'} = \frac{1}{\Gamma} + \frac{16\alpha_m p_m}{\Delta\omega_a^2}. \tag{3.33}$$

Eq. 3.33 has small $\alpha_m p_m$ compared to unity and the pulse spectrum is also usually small compared to the atomic line width $\Delta\omega_a$. So that it can be well approximated by

$$\Gamma^{'} - \Gamma \approx -\frac{16\alpha_m p_m}{\Delta\omega_a^2}\Gamma^2. \tag{3.34}$$

This approximation summarizes the spectral narrowing of the pulse envelop in the frequency domain, or the pulse broadening in the time domain, produced by one round-trip transit through the laser gain medium.

As the pulse propagates through an AM modulator, the net amplitude or voltage transmission as a function of time can be given by

$$\varepsilon^{''}(t) = T_{am}(t)\varepsilon^{'}(t), \tag{3.35}$$

where $T_{am}(t)$ is the time-varying transmission function of the modulator. For a simple AM, it is given by

$$T_{am}(t) = \exp[-\Delta_m(1-\cos\omega_m t)], \tag{3.36}$$

where ω_m is some integer multiple of cavity axial frequency ω_{ax}. $2\Delta_m$ gives the peak-to-peak voltage modulation index as shown in Fig. 3.11.

The transmission function can be approximated by its quadratic variation about the peak transmission point, as given by

$$T_{am}(t) \approx \exp[-\frac{\Delta_m\omega_m^2}{2}t^2], |t| \ll T. \tag{3.37}$$

Therefore, the change in the Gaussian pulse parameter $\Gamma^{'}$ when passing through the modulator is given by

$$\Gamma^{''} - \Gamma^{'} \approx +\frac{\Delta_m\omega_m^2}{2}. \tag{3.38}$$

The expression in Eq. 3.38 implies that the pulse narrowing, or the spectral broadening, of the pulse produced by passing through the amplitude modulator.

As the pulse propagates through an FM modulator, we can write a formally similar expression in which the phase modulation effects of the FM modulator, given by the following transmission function

$$T_{fm}(t) = \exp[j\Delta_m \cos(\omega_m t)]. \tag{3.39}$$

In this case, the modulation index $2\Delta_m$ corresponds to the peak-to-peak phase deviation in passing through the modulator. A single round trip through the modulator imposes on a CW signal $2\Delta_m\omega_m$ peak-to-peak frequency deviation.

The circulating pulse in an FM mode-locked laser always passes through the modulator very near one or the other of the two peaks of the phase modulation cycle [76]. The transmission function can be approximated by its quadratic in the form

$$T_{fm}(t) \approx \exp[\pm j\Delta_m(1 - \omega_m^2 t^2/2)]. \tag{3.40}$$

The static portion of this phase shift can be absorbed into a very small net change in the total effective length of the laser cavity. Meanwhile, the quadratic portion imposes a small chirp on the pulse on each cavity round trip [76].

As passing through the FM, the Gaussian pulse changes parameter as given by

$$\Gamma'' - \Gamma' \approx \pm j\frac{\Delta_m\omega_m^2}{2}. \tag{3.41}$$

From Eq. 3.38 and Eq. 3.41 we can see that the net change in Γ is purely real for AM modulation, but purely imaginary for FM modulation.

Thus, we can calculate the total change in the Gaussian pulse parameter after one complete round trip around the laser cavity, which is given by

$$\Gamma'' - \Gamma \approx -\frac{16\alpha_m p_m}{\Delta\omega_a^2}\Gamma^2 + \left\{\begin{array}{c} 1 \\ \pm j \end{array}\right\}\frac{\Delta_m\omega_m^2}{2}. \tag{3.42}$$

The modulation term on the right-hand side has the front value of 1 as the intracavity modulator is an AM modulator, whereas it is $\pm j$ as the intracavity modulator is an FM

modulator. Eq. 3.42 is equal to zero for steady-state mode-locking. In steady state mode-locking, the spectral narrowing causing by the gain medium is compensated by spectral broadening in the modulator. It can be found more detail discussion given in [76].

3.2.2 Passive mode-locking

Passive mode locking is a technique of mode locking which provides an alternative approach to generate ultrashort pulses. Passive mode locking is useful for high-power flash-pumped lasers and for generating the shortest possible pulses in CW mode-locked lasers. Passive mode locking is, however, also generally more difficult to control, especially if we wish to obtain stable and reliable mode-locked operation.

This type of mode locking is an inherently nonlinear process so it is also rather more complex to describe and less amenable to simple analytical approaches than active mode locking.

In nearly all passive mode locking, the basic mechanism is pulse shortening during propagating through a saturable absorber (SA) placed inside the laser cavity as generally shown in Fig. 3.13. The time-variation of the mode-locked pulse is slow compared to the dephasing time T_2 in the SA. The pulse-shape change as passing through the absorber will depends strongly on whether the absorbing medium is a fast or slow saturable absorber. In fast saturable absorber, the recovery time T_1 is much shorter than the pulse width τ_p, so that the absorber saturates in essence on the instantaneous intensity $I(t)$ of the optical pulse. By contrast, in slow saturable absorber, $T_1 \gg \tau_p$ and the absorption saturates primarily on the integrated intensity in the optical pulse [19].

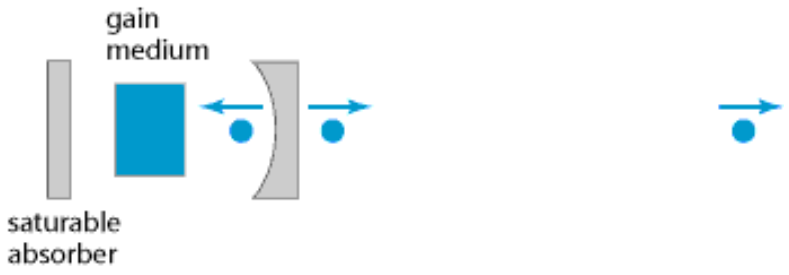

FIGURE 3.13: Schematic setup of a passively mode-locked laser with a saturable absorber mirror [18]

For the simplest case of using a fast, homogeneously saturable, two-level absorber, the instantaneous input and output intensities can be described by

$$ln\frac{I_2(t)}{I_1(t)} + \frac{I_2(t) - I_1(t)}{I_{sat}} = lnT_0, \tag{3.43}$$

where $T_0 = \exp(-2\alpha_0 L)$ is the small signal or unsaturated intensity transmission through the absorbing medium. With Eq. 3.43, if we have a given input pulse-shape $I_1(t)$ passing through this medium, then we can obtain the output pulse-shape $I_2(t)$.

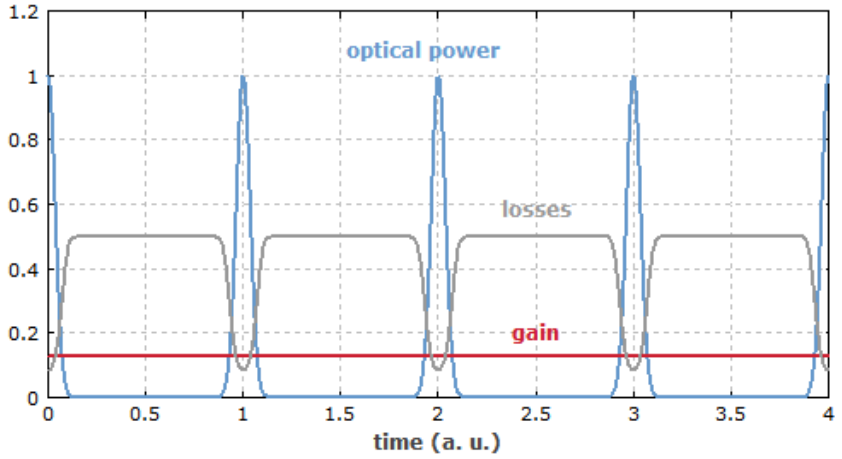

FIGURE 3.14: Temporal evolution of optical power and losses in a passively mode-locked laser with a fast saturable absorber [18]

Fig. 3.14 shows schematic of temporal evolution of optical power and losses in a passively mode-locked laser with a fast saturable absorber. For each time the pulse hits the saturable absorber, the absorption is saturated, and thus temporarily reducing the losses.

Fig. 3.15 shows peak pulse intensity transmission and pulsewidth reduction for a Gaussian input pulse after one round trip through a fast saturable absorber, plotted versus the peak input intensity of the input pulse. The initial intensity transmission $T_0 = 0.01$. It can be seen that for input peak intensities near or a few times larger than the saturation intensity I_{sat}, the transmission of the pulse increases quite rapidly from T_0 up toward unity. At the same time, the pulse width of the output pulse is reduced by a maximum ratio of nearly 0.6 per transit.

The pulsewidth reduction occurs because the stronger central part of the pulse partially saturates the absorber and is transmitted with less absorption. Whereas, the weaker leading and trailing edges of the pulse are strongly absorbed and will experience high

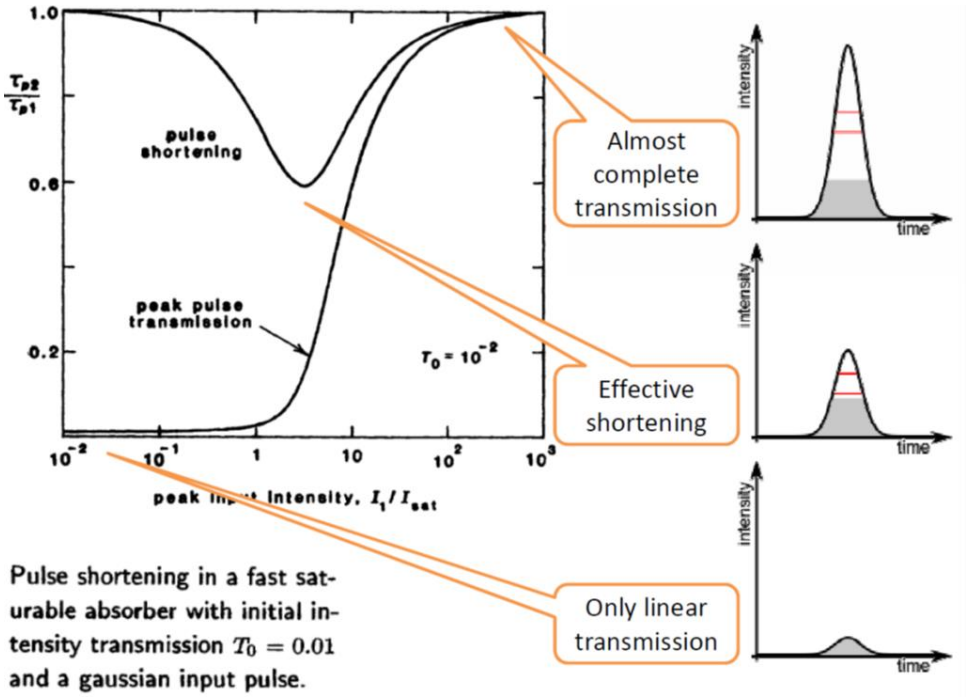

FIGURE 3.15: Illustration of the resulting peak pulse intensity transmission and pulsewidth reduction for a Gaussian input pulse after one round trip through a fast saturable absorber, plotted versus the peak input intensity of the input pulse [19, 20]

losses. The absorber can thus suppress any additional weaker pulses and any continuous background light.

Now, let's consider a passively mode-locked laser with the use of a slow saturable absorber. The instantaneous input and output intensities can be described by

$$ln\frac{I_2(t)}{I_1(t)} = \frac{T_0 \exp[U_1(t)/U_{sat}]}{1 + T_0[\exp(U_1(t)/U_{sat}) - 1]}, \tag{3.44}$$

where $U_{sat} = I_{sat}T_1$ is the saturation energy and $U_1(t) = \int_{-\infty}^{t} I_1(t)dt$ is the integrated energy up to time t in the input pulse. Typical results from calculation of this Eq. 3.44 are not shown because in nearly all cases they turn out to be very similar to the results of fast absorber cases already shown in Fig. 3.15.

For the slow absorber, the actual pulsewidth reduction mechanism is, however, significantly different from the fast absorber. In this situation, the slow saturable medium absorbs the leading edge of the input pulse, but then the medium is saturated so that the trailing edge of the pulse is transmitted nearly unchanged, as shown in Fig. 3.16.

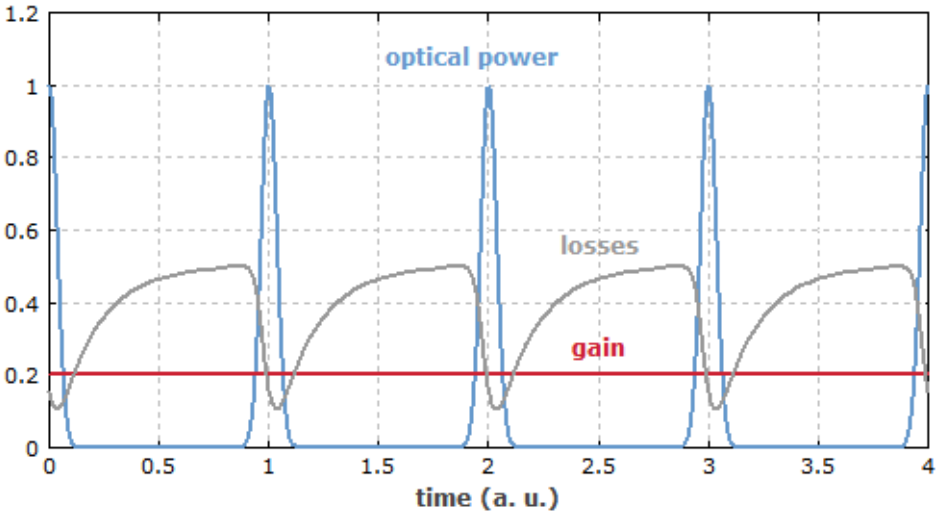

FIGURE 3.16: Temporal evolution of optical power and losses in a passively mode-locked laser with a slow saturable absorber [18]

Therefore, the output pulse in this situation expects to acquire an asymmetry in the time domain, with a faster leading edge and a more or less unchanged trailing edge.

Chapter 4

Ultrashort Pulse Generation Using FM Fiber Ring Laser

In this chapter, I will describe the idea of using an external dispersive single-mode fiber to compress the constant output of a FM fiber ring laser to picosecond pulse chain output. The issue has been studied theoretically through computer simulation and then experimentally through in-lab experiments. I will first start with the theoretical operation of FM laser. After that, the theoretical analysis of chirping compression technique using a dispersive medium will be included. Finally, the experimental setup and results will be discussed.

4.1 FM Laser

First, I would like to describe briefly the theory of FM laser in this section; it is essentially referred from [21]. It was described in the "active mode locking" section that an intracavity phase or FM modulator which is synchronized to the round-trip frequency (axial mode spacing frequency, ω_{ax}) of a laser cavity can lead to mode locking in the laser. This is generally called "FM mode-locked" laser operation. In addition to this short-pulse operation, a laser containing an intracavity FM can also exhibit an interesting frequency-swept mode of operation. This frequency-swept mode is called "FM laser", which occurs when the FM modulation frequency ω_m is detuned by a modest amount from the FM mode-locked frequency ($k\omega_{ax}, k = 1, 2, ...$).

By using FM coupled-mode analysis, we have the basic coupled-mode equations for an FM-modulated laser cavity given by [21]

$$\frac{d\tilde{E}_n(t)}{dt} + [(\frac{\gamma - \omega\chi_n''}{2}) + j(n\omega_d)]\tilde{E}_n = j\frac{\Delta_m}{2T}(\tilde{E}_{n+1} + \tilde{E}_{n-1}), \tag{4.1}$$

where $\tilde{E}_n$ is the complex phasor amplitude of the n-th sideband, γ is the total cavity decay rate for the n-th mode, χ_n'' is the imaginary part of the linear susceptibility of the laser medium evaluated at the mode frequency ω, and $\gamma - \omega\chi_n$ is called the net loss minus gain. ω_d is a significant amount of detuning frequency between the modulation frequency ω_m and the FM mode-locked frequency $(k\omega_{ax}, k = 1, 2, ...)$.

Now, assume steady-state operation so it is unchanging in time and thus $\frac{d\tilde{E}_n(t)}{dt} = 0$. FM laser operation can take place in either homogeneously or inhomogeneously broadened lasers. For either reasonably wide homogeneous lines or inhomogeneous lines, it is possible to have the approximation below even for rather small values of the detuning frequency ω_d

$$|\gamma - \omega\chi_n''| \ll n\omega_d. \tag{4.2}$$

With this approximation in Eq. 4.2, Eq. 4.1 can reduce to the steady-state relationship

$$jn\omega_d\tilde{E}_n \approx j\frac{\Delta_m}{2T}(\tilde{E}_{n+1} + \tilde{E}_{n-1}), \tag{4.3}$$

or

$$\frac{2n\omega_d T}{\Delta_m}\tilde{E}_n \approx \tilde{E}_{n+1} + \tilde{E}_{n-1}. \tag{4.4}$$

Compare Eq. 4.4 with a standard recursion relationship for Bessel function $J_n(\Gamma)$ of argument Γ as given by

$$\frac{2n}{\Gamma}J_n(\Gamma) = J_{n+1}(\Gamma) + J_{n-1}(\Gamma). \tag{4.5}$$

They are similar. Therefore, a steady-state mode-coupled solution for the FM laser with ω_d is given by

$$\varepsilon(t) = E_0 \sum_{n=-\infty}^{\infty} J_n(\Gamma)\exp[j(\omega_0 + n\omega_m)t], \tag{4.6}$$

where E_0 is the amplitude, ω_0 is the carrier angular frequency, and Γ is defined by

$$\Gamma = \frac{\Delta_m}{\omega_d T} = \frac{\omega_{ax}}{\omega_d} \times \frac{\Delta_m}{2\pi}. \tag{4.7}$$

There is another standard Bessel function identity as follows

$$\exp(j\Gamma \sin \omega_m t) = \sum_{n=-\infty}^{\infty} J_n(\Gamma) \exp(jn\omega_m t). \tag{4.8}$$

Hence, the general form of laser signal at any arbitrary reference plane inside the laser cavity is given by

$$\varepsilon(t) = E_0 e^{j\omega_0 t} \sum_{n=-\infty}^{\infty} J_n(\Gamma) e^{(jn\omega_m t)} = E_0 \exp[j(\omega_0 t + \Gamma \sin \omega_m t)]. \tag{4.9}$$

Obviously, this FM laser signal has the form of a constant-amplitude oscillation (without pulse).

The instantaneous phase $\phi(t)$ of the output signal can be derived from Eq. 4.9 as follows

$$\phi(t) = \omega_0 t + \Gamma \sin \omega_m t, \tag{4.10}$$

where Γ is the modulation index or the peak phase deviation (in radians) of the output signal. The instantaneous frequency is then given by

$$\omega_i(t) = \frac{d\phi(t)}{dt} = \omega_0 + \Gamma\omega_m \cos \omega_m t. \tag{4.11}$$

From Eq. 4.11 viewpoint, the instantaneous frequency swing back and forth in sinusoidal function about the modulation frequency ω_m with a frequency range of $\pm\Gamma\omega_m$. From Eq. 4.7, the modulation index Γ can increase up to ≈ 100 as the detuning frequency $\omega_d \ll \omega_m$. Therefore, the frequency deviation of the FM laser output can be very much larger than the intracavity modulation frequency ω_m [21]. The maximum spectral bandwidth is $2\Gamma\omega_m$.

At small detuning frequency ($\approx 1\%$ of ω_{ax}) from the FM mode-locked operation, the FM laser operation will begin as shown in Fig. 4.1. The intermediate detuning region between the two mode-locked and FM laser operations is unstable operation.

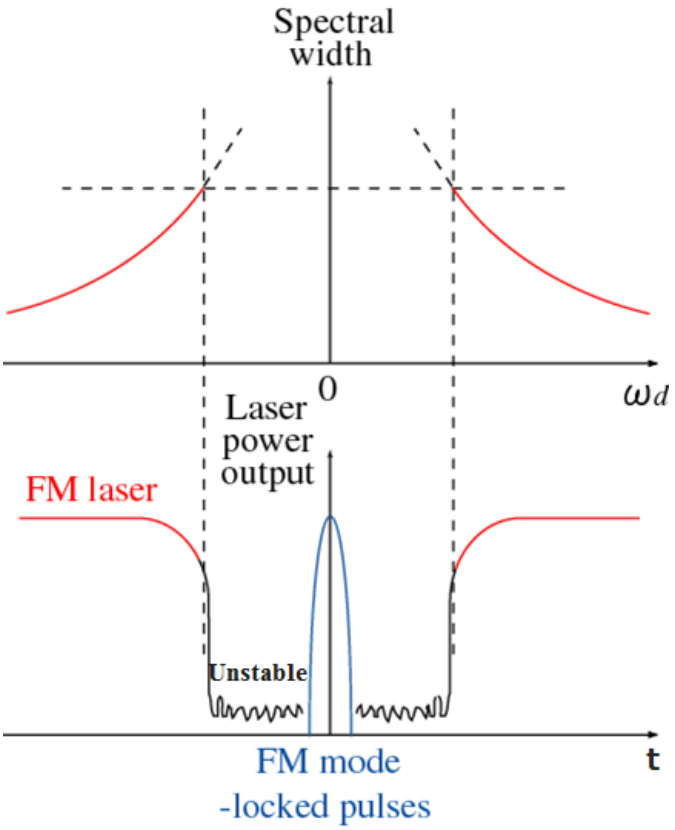

FIGURE 4.1: The transition from FM-laser or frequency -swept operation to FM mode-locked operation [21]

4.2 Pulse Compression Using a Dispersive Optical Fiber

In this section, the theoretical analysis of the pulse compression technique using a dispersive optical fiber will be discribed. it is essentially referred from [37]. Assume that we have the phase-modulated CW light passing through a frequency dispersive optical fiber e.g. SMF-28.

From Eq. 4.11, the instantaneous frequency of the modulated light is given by

$$f_i(t) = f_0 + \Gamma f_m \cos 2\pi f_m t. \tag{4.12}$$

This light has a nearly linear frequency chirp, and the optical frequency chirping rate is expressed by

$$\frac{df_i}{dt} = \pm\frac{1}{2\pi}\Gamma\omega_m^2 = \pm 2\pi f_m^2\Gamma. \tag{4.13}$$

The phase retardation $\varphi(f)$ of a dispersive medium can generally be approxiamted using Taylor series expansion around $f = f_0$ as

$$\varphi(f) \approx \varphi(f_0) + \frac{d\varphi(f)}{df}\bigg|_{f=f_0} \times (f - f_0) + \frac{d^2\varphi(f)}{2df^2}\bigg|_{f=f_0} \times (f - f_0)^2. \tag{4.14}$$

From Eq. 4.6, the output field becomes

$$\varepsilon(t) = E_0 \sum_{n=-\infty}^{\infty} J_n(\Gamma) \exp[j2\pi(f_0 + nf_m)t - j2\pi\varphi(f_0 - nf_m)], \tag{4.15}$$

which can be approximated by

$$\varepsilon(t) \approx E_0 \exp[j(2\pi f_0 t - \varphi(f_0))] \sum_{n=-\infty}^{\infty} J_n(\Gamma) \exp[-j2\pi n f_m(t - \tau_0) - j\pi n^2 f_m^2(\frac{d\tau}{df})], \tag{4.16}$$

where $\tau_0 = \tau(f_0) = \frac{d\varphi(f_0)}{2\pi df}$. The term $\frac{d\tau}{df}$ corresponds to the frequency dispersion of the group delay τ (GDD).

The signs "$\pm$" in Eq. 4.13 shows that both possitive and negative group delay dispersions can be used for chirping compression, as a result, generating ultrashort optical pulses.

The bunching coefficient (B) of the light output of the dispersive medium is defined as

$$B = -(\frac{df}{dt})(\frac{d\tau}{df}) = \mp 2\pi f_m^2 \Gamma(\frac{d\tau}{df}). \tag{4.17}$$

As $B = 0$, pure frequency modulation with ($\frac{d\tau}{df} = 0$) takes place. As $B = 1$ ($\frac{d\tau}{df} = -(\frac{df}{dt})^{-1}$), this is the situation in which the tail of the linear frequency chirp region of the optical field just catches up with the head after passing through the dispersive medium. Finally, for $B > 1$, the tail becomes faster than the head, and hence the pulse begins to break.

In fact, the B value that yields the highest peak is slightly different from the one that yields the narrowest pulse duration. It has been proved in [77] the optimumly compressed pulse duration is obtained by overbunching of $B \approx 1.2$. The pulse width (FWHM) is given by

$$\Delta t \approx \frac{a}{2\Gamma f_m}, \tag{4.18}$$

where $a = 0.6 - 0.7$.

4.3 Picosecond Pulse Generation Using FM Fiber Ring Laser

4.3.1 FM fiber laser oscillation

The fiber FM laser oscillation setup is shown in Fig. 4.2(a). It consists of a LiNbO3 optical phase modulator (see Appendix A) and an erbium-doped fiber ring laser. The FM laser oscillation is realized by detuning the modulation frequency f_m of the internal phase modulator. The frequency-sweeping mode of operation or FM laser operation occurs as the modulation frequency f_m is purposely detuned by approximately 1% or so from the axial mode spacing or one of its harmonics. In this setup, the axial mode spacing f_{ax} of the fiber ring laser is about 9.5 MHz, and the initial RF modulation frequency f_m is set at 10 GHz. The output electric field of the FM laser is expressed by Eq. 4.9. It can be rewritten as

$$\epsilon(t) = E_0 \exp[j(2\pi f_0 t + \Gamma \sin 2\pi f_m t)]. \tag{4.19}$$

And the instantaneous frequency is derived from Eq. 4.11

$$\nu_i(t) = f_0 + \Gamma f_m \cos(2\pi f_m t), \tag{4.20}$$

with the FM modulation index Γ given by Eq. 4.7

$$\Gamma = \frac{\theta_0}{2\pi}\frac{f_{ax}}{f_d}, \tag{4.21}$$

where E_0 is the electric field amplitude and f_0 is the optical frequency. Γ correlates with the single-pass modulation index $\theta_0 = \Delta_m$, axial mode spacing f_{ax}, and detuning frequency f_d. The FM laser operation with $f_d/f_{ax} \ll 1$ produces an output FM modulation index Γ much larger than the single-pass modulation index θ_0. From Eq. 4.20 and 4.21, the spectral bandwidth given by $2\Gamma f_m$ can be easily tuned by adjusting f_d.

4.3.2 Optical pulse compression

The optical pulse compression setup is shown in Fig. 4.2(b) including a SMF-28 fiber with the dispersion of 18 ps/(nm.km) and a guided-wave dual-electrode Mach-Zehnder

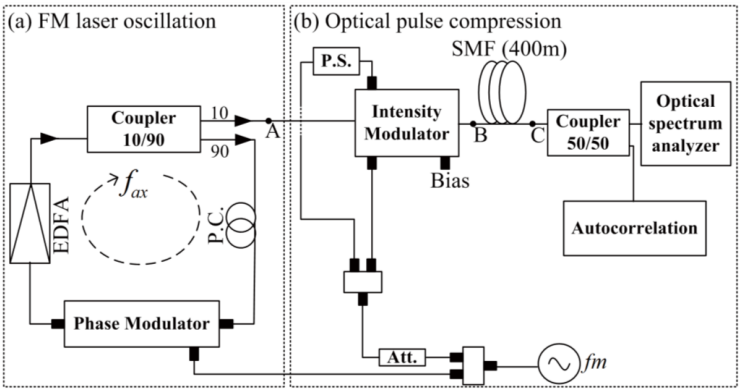

FIGURE 4.2: Experimental setup: (a) FM laser oscillation and (b) optical pulse compression. Here, P.C., P.S., and Att. denote the polarization controller, phase shifter, and attenuator, respectively

intensity modulator (see Appendix B). Using Eq. 4.17 to calculate the required fiber length for chirping compression of the output FM-modulated light, the fiber length is about 400 m. The modulator has two RF modulation ports and one DC bias port. The transmission function of the intensity modulator is given by

$$T(t) = \frac{1}{2}(e^{[-j(\theta_1 \sin(2\pi f_m t + \phi_m) + \Delta\phi_0)]} + e^{[-j\theta_2 \sin(2\pi f_m t)]}), \tag{4.22}$$

where θ_1 and θ_2 are the modulation indices of the two electrodes, ϕ_m is the phase difference between two RF signals, and $\Delta\phi_0$ is the optical bias. ϕ_m is fixed at π for chirp-free intensity modulation. θ_1 and θ_2 are fixed at 0.6 rad. $\Delta\phi_0$ is used as an adjusted parameter.

First, we consider the setup (Fig. 4.2) without the intensity modulation (points A and B are unified). The chromatic dispersion characteristic of the SMF is applied for chirping compression of the output FM-modulated light, and consequently compressing temporally to a pulse train. The instantaneous frequencies at points A and C are shown in Figs. 4.3(a) and 4.3(b), respectively. Because of the dispersion characteristic of the SMF, the instantaneous frequency changes from the sinusoidal pattern (Fig. 4.3(a)) to the saw pattern (Fig. 4.3(b)). The saw pattern shows an edge with a fast transition of frequency versus time; as a result, the intensity is higher around this edge. Moreover, Figs. 4.3(c) and 4.3(d) show the instantaneous intensities at points A and C, respectively. Note that, the optical pulse has been formed from the flat intensity after the impact of the SMF. However, as shown in Fig. 4.3(d), there exists the background of the generated optical pulse, because the energy in the half period does not contribute to the pulse

formation. To remove this background, we further employ an intensity modulator as detailed below.

Second, we consider the setup (Fig. 4.2) with the intensity modulation. To remove the background, the intensity of the output signal in the range of the background is reduced before going through the SMF. Therefore, the intensity modulator is added between points A and B in Fig. 4.2(b). The intensity modulator is adjusted to obtain a response similar to Fig. 4.3(e). The intensity of the output signal at point B is reduced to be in the range of the background while maintaining the maximum intensity in the pulse range. As a result, the output signal at point C (Fig. 4.3(f)) shows that the background has been removed while maintaining the expected ultrashort pulse.

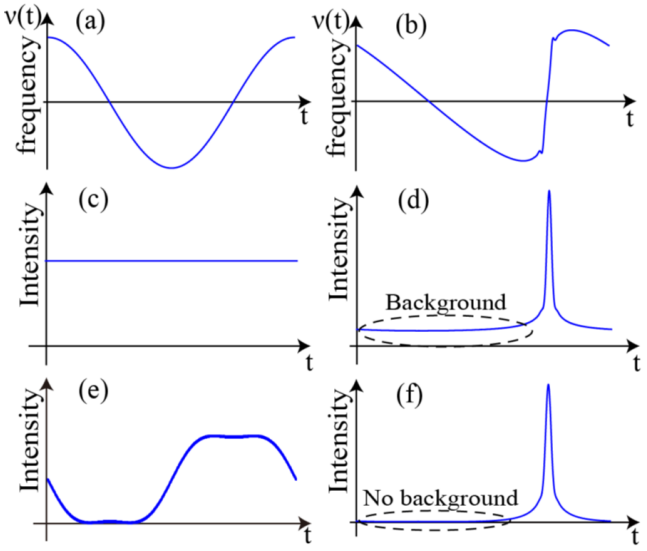

FIGURE 4.3: Simulation results of the setup in Fig. 4.2: (a) instantaneous frequency at point A, (b) instantaneous frequency at point C, (c) instantaneous intensity at point A, (d) ultrashort pulse shape at point C after compression without the intensity modulation, (e) temporal intensity at point B after the intensity modulation, and (f) compressed pulse shape at point C with the intensity modulation

4.3.3 Results and discussion

4.3.3.1 Experimental results

The experiment was carried out using the setup shown in Fig. 4.2 with various parameters: $\theta_0 = 3.2$ rad, $f_d = 200$ kHz, $\theta = \theta_1 = \theta_2 = 0.6$ rad, $\phi_m = \pi$, and $\Delta\phi_0 = 2$ rad. Figs. 4.4(a) and 4.4(b) show the experimental autocorrelation traces of

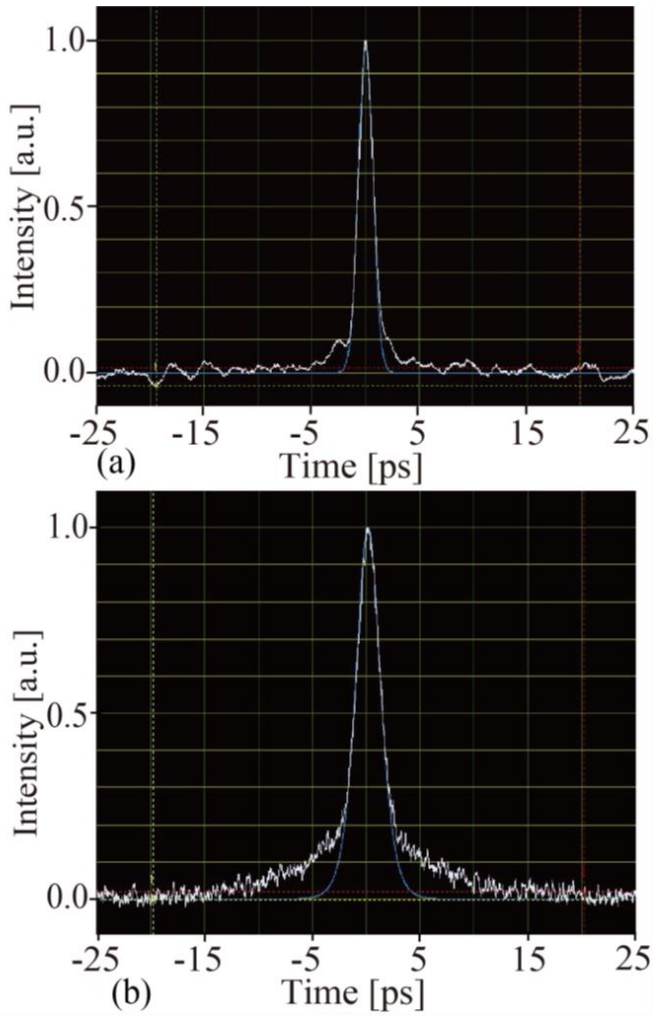

FIGURE 4.4: Experimental results. (a) Autocorrelation trace of the setup without the intensity modulation (autocorrelation trace width of 1.6 ps). (b) Autocorrelation trace of the setup with the intensity modulation (autocorrelation trace width of 2.68 ps)

the setup without and with the intensity modulation, respectively. At this stage, the autocorrelation traces are normalized and automatically set the intensity in the zero-one scale; thus, we cannot see the background of the output pulses but the pulse width. The real scale of the autocorrelation trace of the output signal will be discussed in the next section. It can be seen in Fig. 4.4(a) and 4.4(b) that the experimental autocorrelation trace widths are 1.6 and 2.68 ps, respectively. The intensity modulator might have increased the frequency chirp of the output FM laser. Therefore, the output optical pulse increased its pulse width and thus autocorrelation trace width increased from 1.6 ps to 2.68 ps.

To estimate the experimental pulse widths, we carried out theoretical calculation and obtained the ratios of theoretical autocorrelation trace width to theoretical pulse width

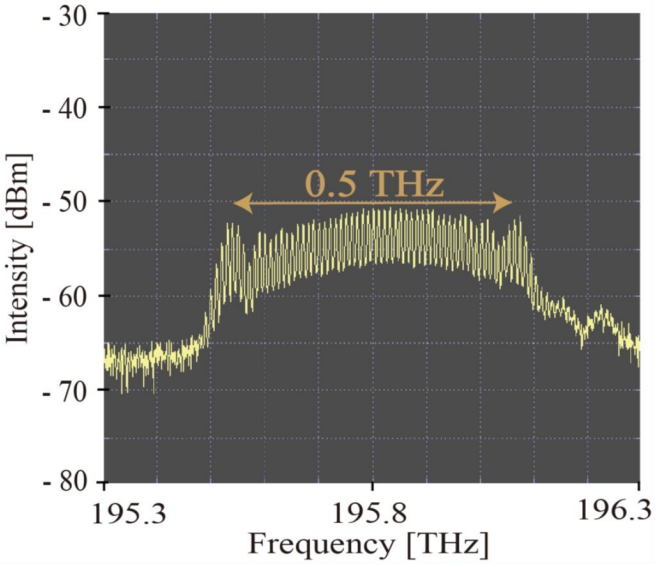

FIGURE 4.5: Output spectrum of FM laser with the external intensity modulation

in two cases without and with the intensity modulation, which were about 1.63 and 1.51, respectively. From these ratios and the experimental autocorrelation trace widths, the experimental pulse widths were estimated to be 0.98 and 1.77 ps for the setups without and with the intensity modulation, respectively. Obviously, the ultrashort pulse of the fiber FM laser was generated by the compression scheme utilizing the dispersive 400 m SMF and intensity modulator. The output FM laser spectrum with 10 GHz

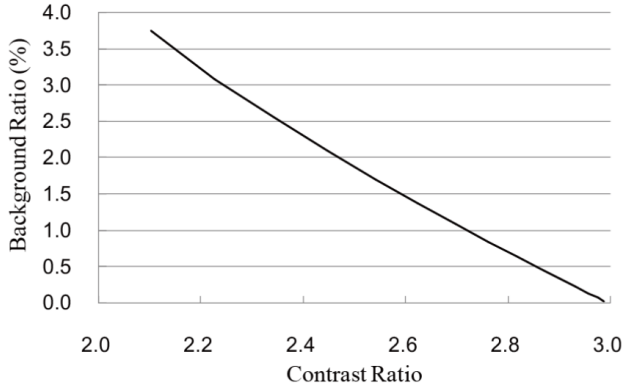

FIGURE 4.6: Calculated relationship between background ratio of output pulse and contrast ratio of autocorrelation trace

carrier frequency spacing, which corresponds to the modulation frequency f_m, is shown in Fig. 4.5. The output spectral bandwidth of the FM laser is about 0.5 THz, which is in good agreement with the theoretical calculation, $2\Gamma f_m$. The time-bandwidth products are 0.49 and 0.885 for the setups without and with the intensity modulation, respectively.

These values are different because of the effects of the intensity modulation. There exists a small chirp in the output pulses; therefore, they may be further compressed.

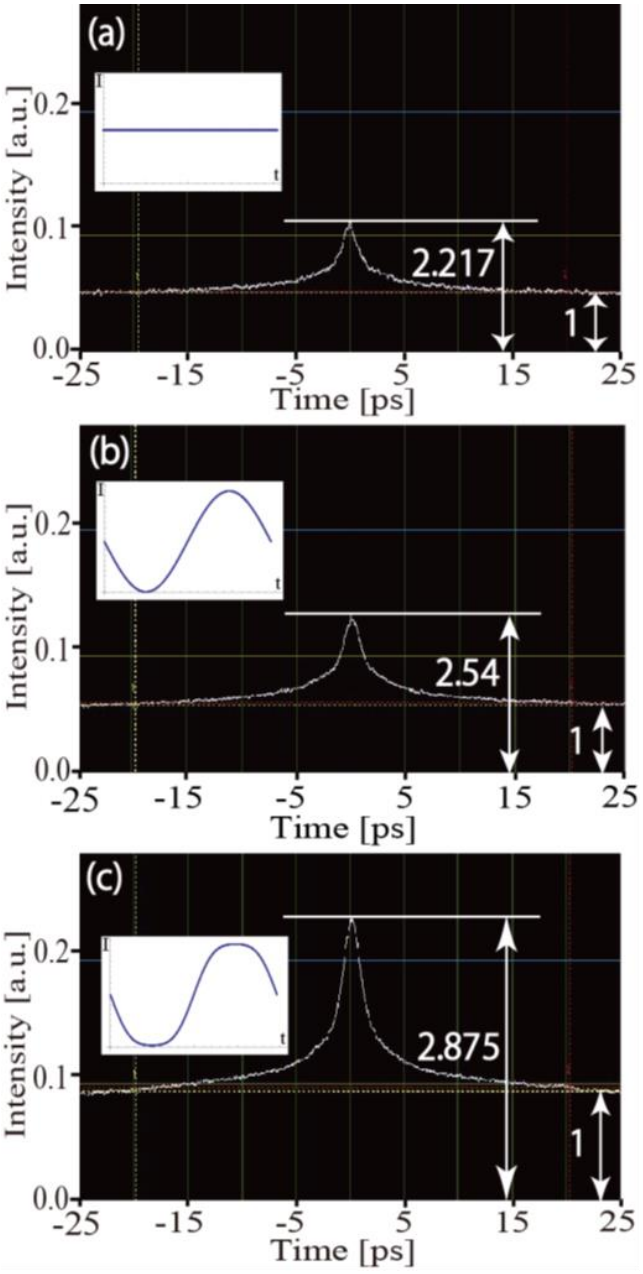

FIGURE 4.7: Experimental autocorrelation traces. The insets show the instantaneous intensity output of the intensity modulation at the respective modulation index: (a) $\theta = 0$ rad, contrast ratio of 2.217:1, (b) $\theta = 0.12$ rad, contrast ratio of 2.54:1, and (c) $\theta = 0.6$ rad, contrast ratio of 2.875:1

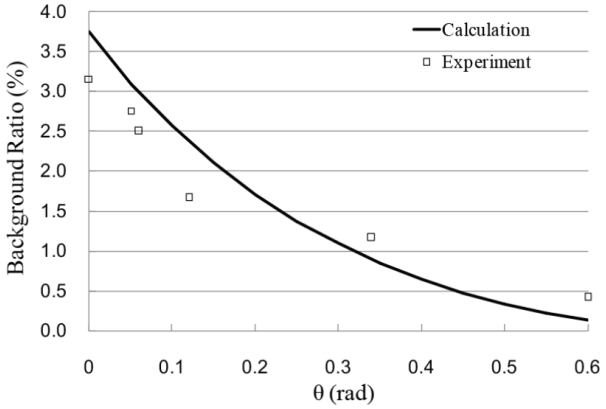

FIGURE 4.8: Calculated and experimental background ratio versus the intensity modulation index

4.3.3.2 Background determination

By determining the contrast ratio of the output autocorrelation trace, we can determine the background ratio of the output pulse. The operation principle of autocorrelation is based on the phenomenon of optical second harmonic generation. An autocorrelation trace consists of a peak of height of 3 atop a base of unity height; [78] thus, the ideal contrast ratio is 3:1, which means that the pulse has no background (background ratio of 0%). The background ratio and the contrast ratio are simulated with the same intensity modulation indices. The background ratio is calculated using the amplitude of the base of the pulse over the amplitude of the peak of the pulse. In addition, the contrast ratio is the ratio of the amplitude of the peak of the autocorrelation trace to the amplitude of the base of the autocorrelation trace. Using the same intensity modulation index, the relationship between the background ratio and the contrast ratio is drawn, as shown in Fig. 4.6. Moreover, on the basis of the linear relationship in Fig. 4.6, once the experimental contrast ratio is determined, the equivalent experimental background ratio is also determined.

Fig. 4.7 shows the experimental results of the autocorrelation traces at different intensity modulation index θ values. The insets show the output signal of the intensity modulation at the respective intensity modulation index. As shown in Fig. 4.7, the contrast ratio increases from 2.217:1 to 2.875:1 as θ increases from 0 to 0.6 rad. Obviously, the experimental result is in good agreement with the theoretical analysis result.

As shown in the inset of Fig. 4.7(a), the intensity modulation has no effects on the output signal since $\theta = 0$ rad. Therefore, there exists the background of the ultrashort pulse; as a result, the contrast ratio is 2.217:1, which is low compared with the ideal value of 3:1. As $\theta = 0.6$ rad, with the effect of the intensity modulation (Fig. 4.7(c)), the contrast ratio increases to 2.875:1, which is close to 3:1. On the basis of the results in Fig. 4.6, we can transform the experimental contrast ratio to the background ratio. Fig. 4.8 shows the calculated and experimental background ratios versus the intensity modulation index. It can be seen that the background ratio decreases from about 3.1% to about 0.4% as the intensity modulation index increases from 0 to 0.6 rad. Therefore, we conclude that by external intensity modulation, the background has been almost removed.

Chapter 5

Actively Mode-Locked Femtosecond Fiber Ring Laser

In this chapter, I will introduce the use of impulse modulation inside an actively mode-locked erbium-doped fiber laser to generate femtosecond (fs) pulses. As the operating frequency of the modulator is synchronized with the fundamental round-trip frequency of the ring cavity, active mode-locking will take place. Although the impulse modulation operates in the MHz region, it produces the gating window as fast as that of the conventional sinusoidal modulation operating in the GHz region. With fast and lange modulation characteristics, the impulse modulation creates an ultrashort pulse inside the laser cavity that is amplified and further compressed after each round-trip to the femtosecond range.

This chapter will start with an introduction of impulse modulation. After that two experimental setups which can generate 500 fs and 300 fs optical pulses will be described in detail.

5.1 Impulse modulation

In this thesis, I used an erbium doped fiber ring laser with an intracavity dual-electrode Mach-Zhender intensity modulator. The intracavity modulator has two RF electrodes with 180^o phase difference that were driven by impulse signal instead of conventional sine signal. Therefore, it is called impulse modulation. The illustration of this proposed

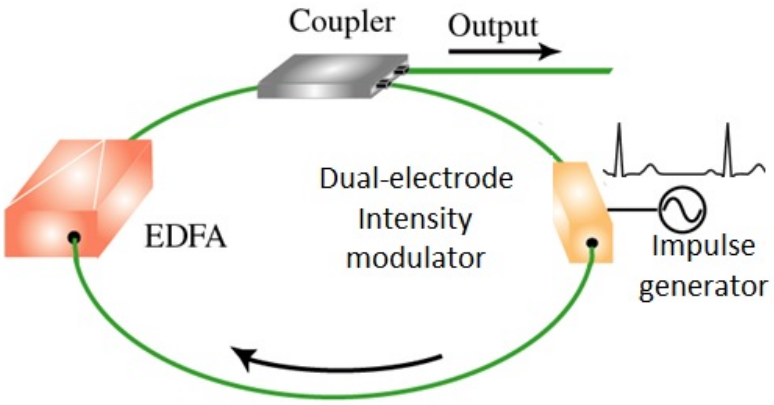

FIGURE 5.1: Erbium-doped fiber ring cavity with impulse modulation

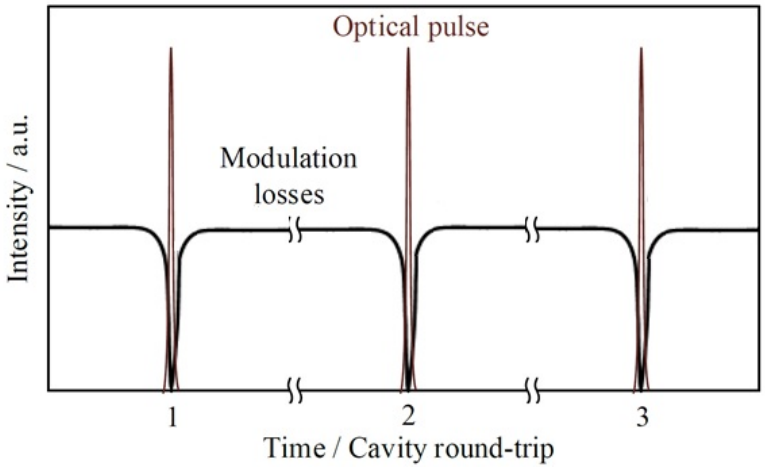

FIGURE 5.2: Time domain illustration of the active mode-locking using the impulse modulation

laser setup is shown in Fig. 5.1. With the impulse modulation, we can obtain very high modulation speed at relatively low frequency if compared with the sinusoidal modulation. The modulation speed depends on the speed (pulse width and transition time) of driving impulses. Therefore, if we can achieve the shorter driving impulses, we can achieve faster impulse modulation, and thus shorter optical pulses can be generated after the impulse modulation.

Now, let's see the optical pulse shortening mechanism of active mode-locking using impulse modulation. In general, mode-locking occurs as the modulation frequency is synchronized with the fundamental round-trip frequency. Due to fast impulse modulation, ultrashort optical pulse is generated and travel around the cavity. After each round-trip it undergoes impulse modulation again and be further compressed, because the wings of the pulse experience more attenuation than the peak. Fig. 5.2 illustrates this shortening processes in the time domain.

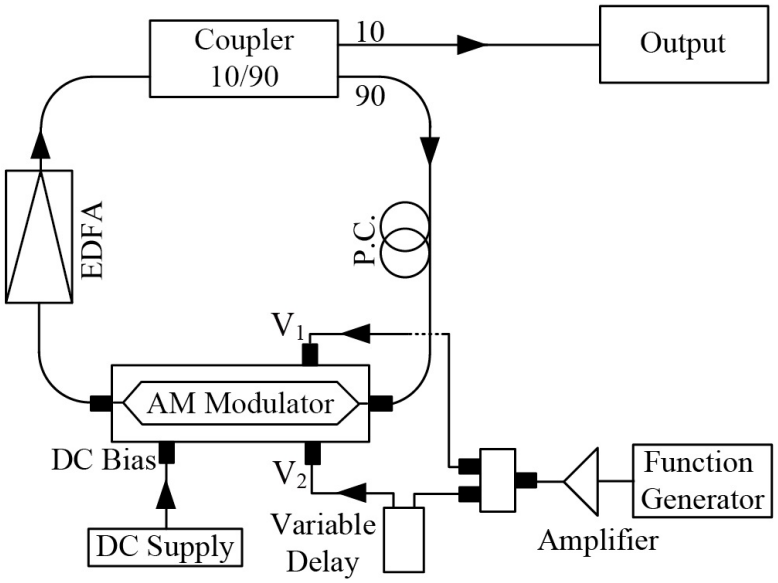

FIGURE 5.3: Experimental setup of the proposed actively mode-locked fiber ring laser

5.2 500-Femtosecond Pulse Generation

5.2.1 Experimental setup

The experimental setup of the actively mode-locked fiber ring laser is shown in Fig. 5.3. The fiber ring cavity consists of a dual-electrode Mach-Zehnder intensity modulator (see Appendix B), an EDFA (see Appendix C), a polarization controller (P.C.), and a 10/90 output coupler. The output is characterized by an autocorrelator, a spectrum analyzer, and an oscilloscope.

5.2.2 Impulse modulation and mode locking

In actively mode-locked fiber lasers, to shorten optical pulses, fast and large modulation is required. Here, I employed impulse modulation to achieve femtosecond optical pulses. The impulse modulation operates based on driving two electrodes of the Mach-Zehnder intensity modulator by two electrical impulse trains generated by an electrical pulse generator.

The electrical pulse generator consists of a function generator (Agilent 33250A) and a power amplifier (R & K AA180-RS) working in saturation mode. By using a broadband power splitter, the output of the amplifier is divided into two arms with one delayed by a variable delay (Fig. 5.3). Because the two electrodes are made with 180^o phase

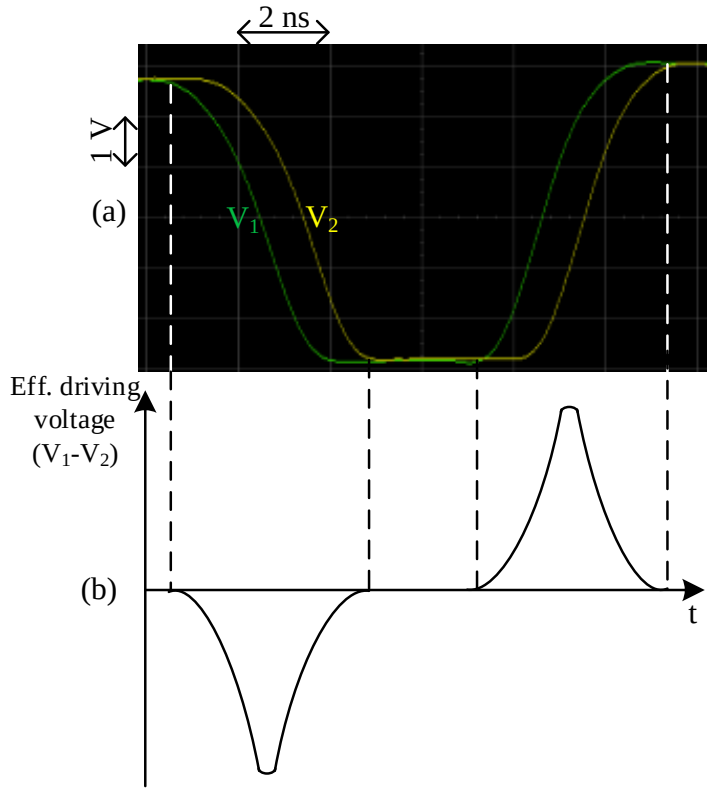

FIGURE 5.4: (a) Measured result of two driving signals fed into two electrodes of the intensity modulator. (b) Modelled effective driving pulses

difference, the short delay between the two driving signals creates a short in-phase window for the output signal.

In our experiment, we used the shortest electrical pulses generated by the function generator, which have a pulsewidth of 8 ns and a risetime of 5 ns. Fig. 5.4 (a) shows the measured result of two driving signals fed into two electrodes of the intensity modulator, where the delay-time was 1 ns. After the amplifier, electrical pulses from the function generator are amplified and shaped to sharper driving pulses with a risetime of about 2 ns (calculated from 10% to 90% of pulse amplitude).

To explain the operation of the employed impulse modulation, the impacts of two individual driving pulses on two electrodes can be modelled by single effective driving pulses as shown in Fig. 5.4 (b). This is the difference between the two driving signals. In other words, the effective driving voltage is the combined modulation signal.

Fig. 5.5 shows measured transmission factor of the intensity modulator as a function of applied DC bias. The effective driving pulses modulate the transmitted intensity about the bias point. The inset of Fig. 5.5 shows the output temporal transmission profile after the impulse modulation with two ultrafast optical pulses. These pulses will be amplified by the EDFA then go around the fiber ring cavity. After the mode-locking, only the greater pulse (in two generated pulses) survives in the ring cavity. In case, two generated pulses are same amplitude by tuning the optical bias, after the mode-locking, both pulses exist in the laser cavity. These analyses will be experimentally demonstrated in the next section.

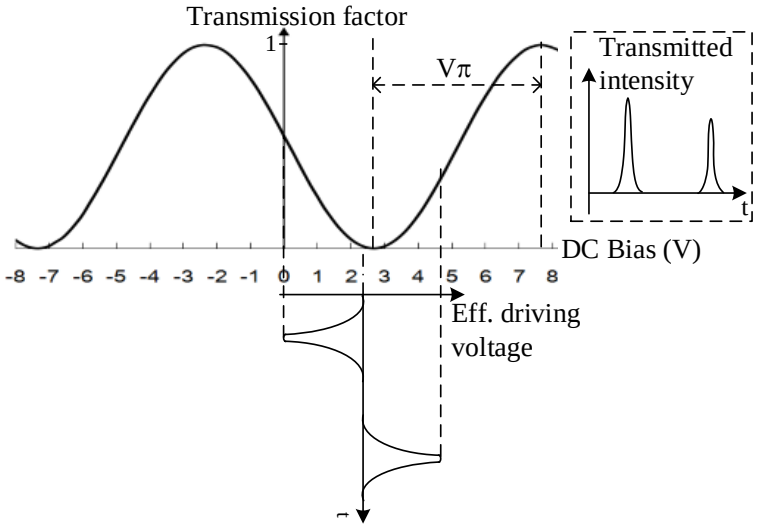

FIGURE 5.5: Measured transmission factor of the intensity modulator as a function of applied DC bias; the applied effective driving voltage modulates the transmitted intensity about the bias point. The inset shows the output temporal transmission profile after the impulse modulation

5.2.3 Experimental results

The round-trip frequency of the employed fiber ring cavity is $f_m = 9.188$ MHz. In our experiment, the impulse modulation carried out at this fundamental frequency. The variable delay was set at 1 ns. The DC bias of the intensity modulator was set at 2.5 V. The output power of the internal EDFA was about 20 mW.

The output ultrafast optical pulses were measured by an autocorrelator (Alnair HAC-150). Fig. 5.6 shows the experimental autocorrelation trace. The autocorrelation trace

width is about 770 fs (FWHM). By assuming $sech^2$ pulse profile, the pulsewidth is about 500 fs. The output spectrum is displayed in Fig. 5.7 with 3 dB spectral bandwidth of about 0.39 THz. The time-bandwidth product is 0.195, which is smaller than the transform limited time-bandwidth product of 0.315 for $sech^2$ pulse shape. Therefore, the generated optical pulses have real pulse shape which is different from the assumed $sech^2$ shape.

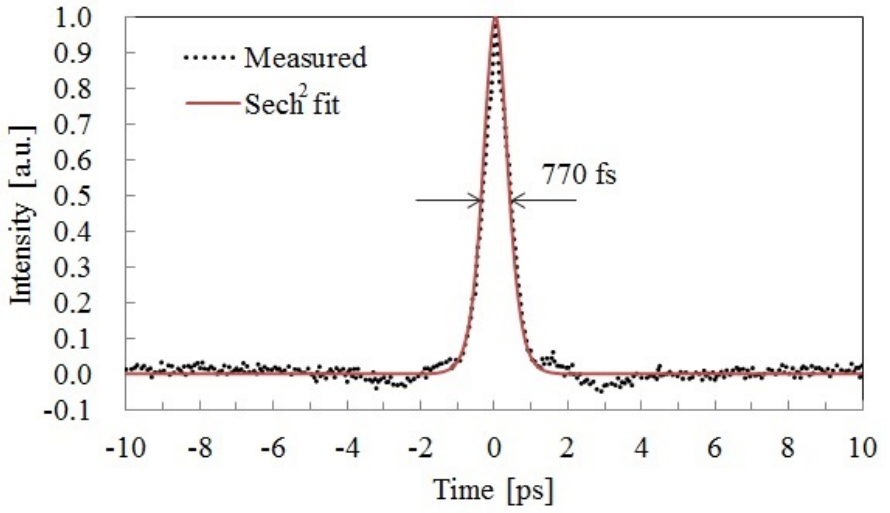

FIGURE 5.6: Experimental normalized autocorrelation trace (dotted line) and corresponding sech^2 fit (solid line)

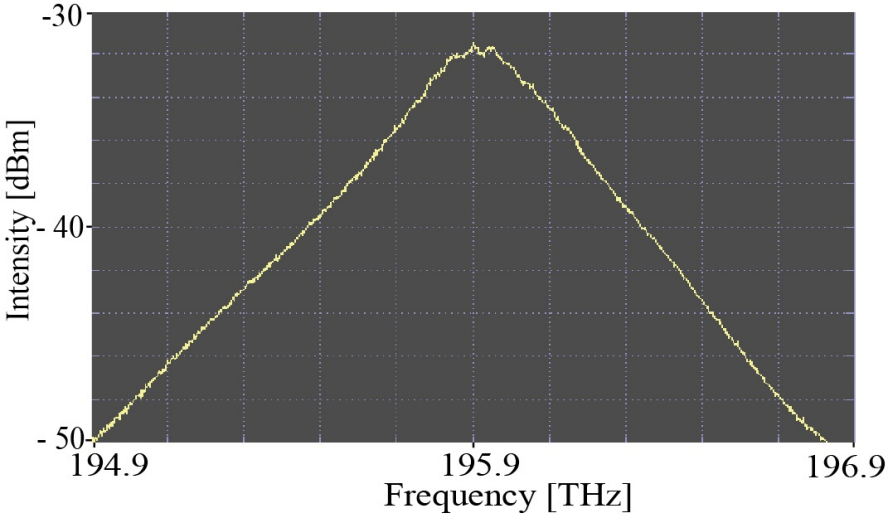

FIGURE 5.7: Output spectrum; the FWHM spectral bandwidth is about 0.39 THz

A fast photodiode connected to an oscilloscope was used to characterize the output optical pulse trains. Fig. 5.8 shows the output optical pulse trains at different bias points of the impulse modulation. As analyzed in the last section, after impulse modulation two optical pulses with different amplitude were generated when DC bias set at 2.5 and 2.9

V. Therefore, after mode-locking only one optical pulse exists in each round-trip of the laser cavity as shown in Fig. 5.8 (a) and (c), respectively. Meanwhile, two optical pulses with the same amplitude were generated as DC bias set at the minimum transmission point of 2.7 V. As a result, after mode-locking both optical pulses still survive as shown in Fig. 5.8 (b).

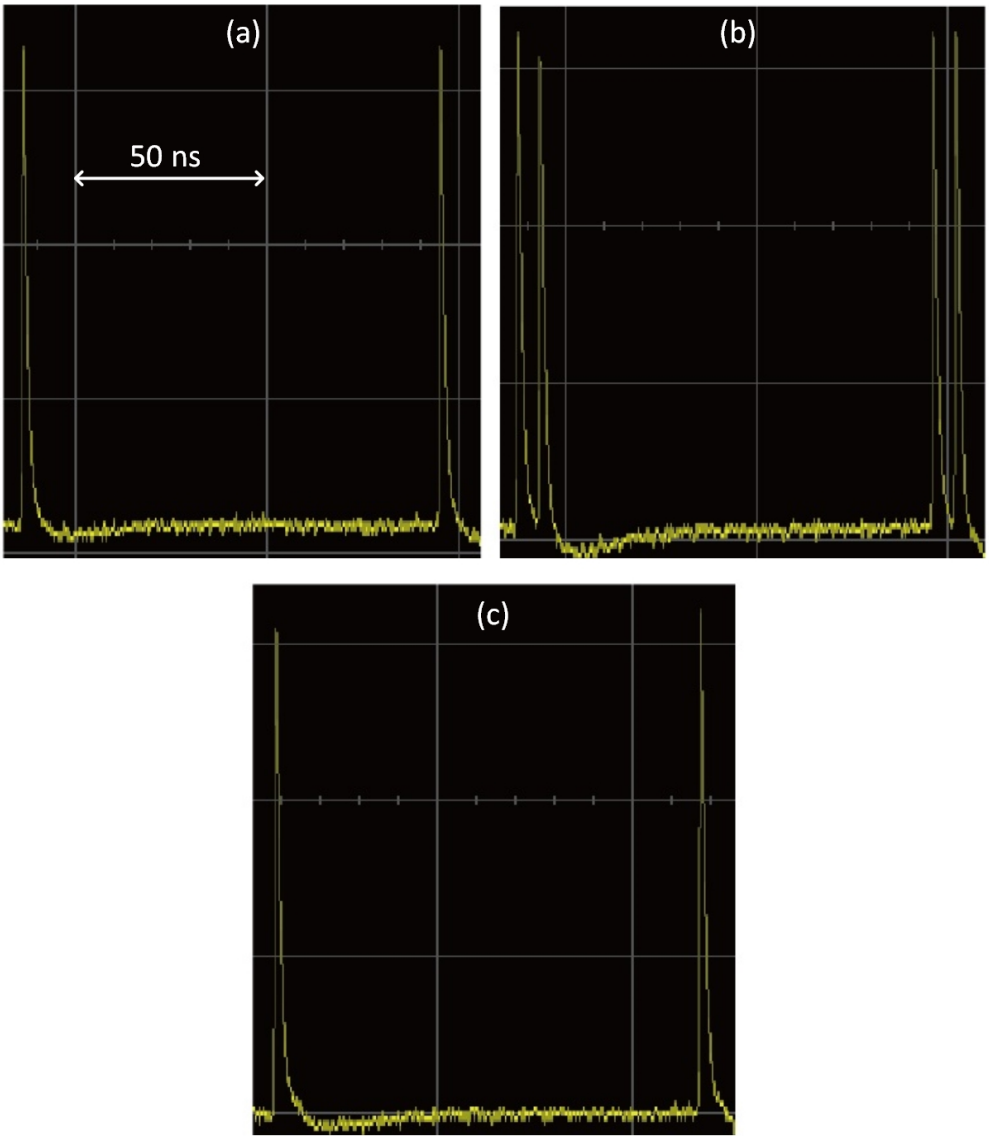

FIGURE 5.8: Output optical pulse trains with DC bias was set at (a) 2.5 V, (b) 2.7 V, and (c) 2.9 V, respectively

Furthermore, the influence of the delay-time of the variable delay on the output optical pulses was studied. Fig. 5.9 shows the relationship between the delay-time and the pulsewidth of the output optical pulses. As the delay-time increases from 1 to 4 ns, the pulsewidth increases from 500 to 800 fs. This result is reasonable because the

effective driving pulse increases its pulsewidth as the delay-time increases, as a result, the mode-locking generates longer optical pulses.

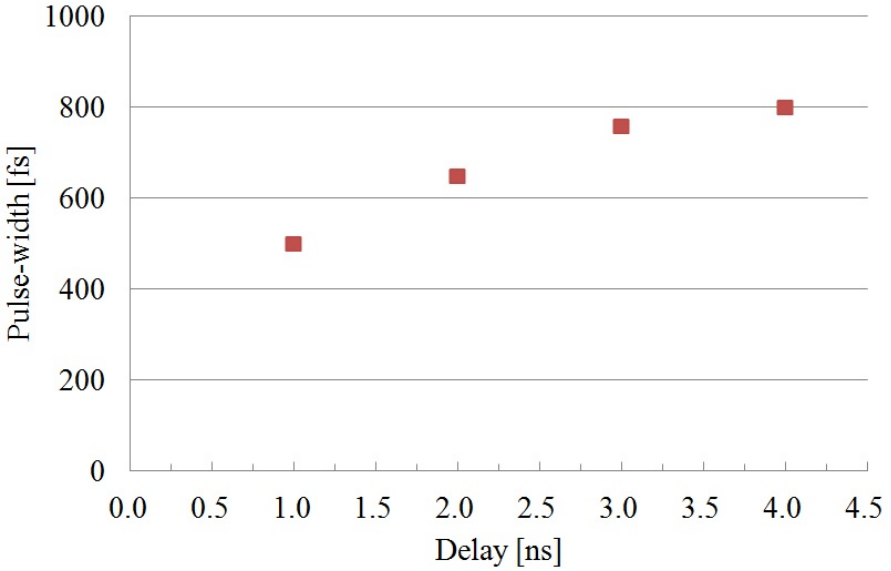

FIGURE 5.9: Relationship between the delay-time and pulsewidth of the output optical pulses

5.3 300-Femtosecond Pulse Generation

From the above experiment, if electrical driving impulses are shorter with sharp rise-time and fall-time, the active mode-locking with impulse modulation might generate shorter optical pulses. At the same time, the shorter delay-time between the two electrodes of the intensity modulator could also bring about faster impulse modulation. From those assessments, a faster electrical impulse generator and a shorter variable delay are needed to generate shorter optical pulses.

In order to obtain a train of sharp driving pulses at the fundamental frequency of the laser cavity, an electrical impulse generator (EIG) is designed and fabricated instead of using a commercial pulse generator. The design of such EIG is described in the following subsection.

5.3.1 Electrical impulse generator

To realize very fast impulse modulation, we fabricated an electrical impulse generation circuit, which could generate picosecond electrical pulses for driving a dual-electrode

Mach-Zehnder intensity modulator placed inside the fiber ring cavity. This impulse generator is based on a broadband bipolar transistor and a nonlinear transmission line comb generator. The transistor works in fast switch-on mode and emits impulses with steep leading edges, which are further compressed by the comb generator

An ultra-wideband (UWB) impulse generator is one of the key components of many transceiver UWB systems. A common impulse generator is based on an edge sharpener, which, with fast switching characteristics, sharpens and accelerates a slow edge of a driving waveform [79].

Semiconductor devices with different physics of fast switching, such as tunnel diodes [79], step recovery diodes (SRD) [80], bipolar transistors [81], and avalanche transistors [82, 83] are commonly used as pulse sharpeners. Avalanche transistors can generate high power, but the pulse repetition rate is limited in the kHz range only. Tunnel diodes have a maximum switch speed at low power. Compared with conventional impulse generators based on SRD, the use of bipolar transistors as key components in impulse generators offers a new and more cost-effective way of generating short impulses [81]. Furthermore, the transistor-based circuit provides a variety of configurations so that its properties can be applied to the field of applications relatively easily.

The UWB impulse generators have also been widely used in laser technologies such as for driving injection lasers [83] and driving actively mode-locked fiber lasers to generate ultrashort optical pulses. In actively mode-locked fiber lasers, fast modulation is required to shorten output optical pulses. Therefore, short impulses with fast leading edges are needed to drive the intensity modulator inside the fiber cavity.

5.3.1.1 Setup

The block diagram of the proposed fast fall-time impulse generator and signal waveforms at each stage are shown in Fig. 5.10. The impulse generator consists of an edge sharpener circuit and a nonlinear transmission line (NLTL) comb generator. The edge sharpener circuit is a common emitter circuit of a broadband npn-bipolar transistor (BFG35). Unlike the bipolar transistor circuit used in [81] which worked in amplifier-mode and emitted output signal with steep switch-off side, our circuit works in switch-on mode and emits output impulses with steep switch-on leading edges.

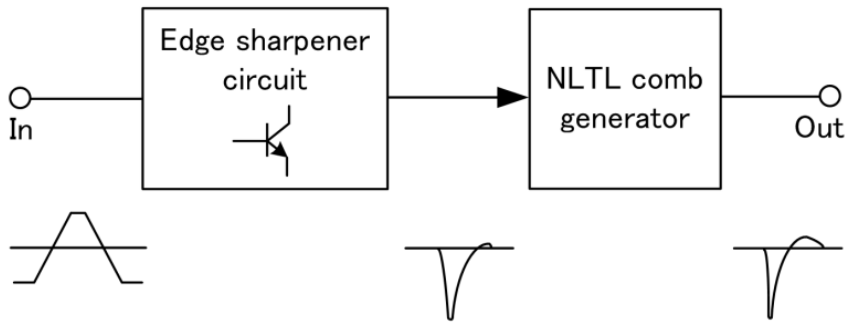

FIGURE 5.10: Block diagram of the EIG with signal waveforms at corresponding stages

The input signal is well-defined arbitrary pulses with repetition rate of 10 MHz, duration of 8 ns (FWHM), and rise-time of 5 ns generated by a conventional function generator (Agilent 33250A). With the leading edge of the input trigger pulse, the transistor switches on and works in the saturation mode. Fig. 5.11 shows the diagram of the edge sharpener circuit. The output coupling capacitor of the circuit is 10 pF and the output matching impedance is 50 Ω, so the RC time constant equals 500 ps. Therefore, when the input pulse is well-defined amplitude and smooth rise-time, the circuit can emit the output impulse with fast switch-on leading edge of around 500 ps. Then, the output impulse of the edge sharpener circuit is going to the input of the NLTL comb generator.

The next element in the signal path is the NLTL comb generator (LPN 7102) which has the function of further compressing the output impulse of the transistor network. The operation of the NLTL comb generator is based on voltage-dependent propagation velocity of a signal propagating on a synthetic transmission line made with varactors [84]. An impulse with peak power of about 1 W at 50 Ω and transition from high to low voltage will be compressed in time as the initial high voltage portion of the leading edge propagates slower than the later low voltage portion of the edge. As a result, the edge of the input impulse will be compressed to a sharper one.

5.3.1.2 experimental results

The experimental output pulses were measured by an Agilent 86100C sampling oscilloscope. Fig. 5.12 shows the measured input signal (dashed line) and the output impulse (solid line) of the edge sharpener transistor circuit. It can be seen that as a result of

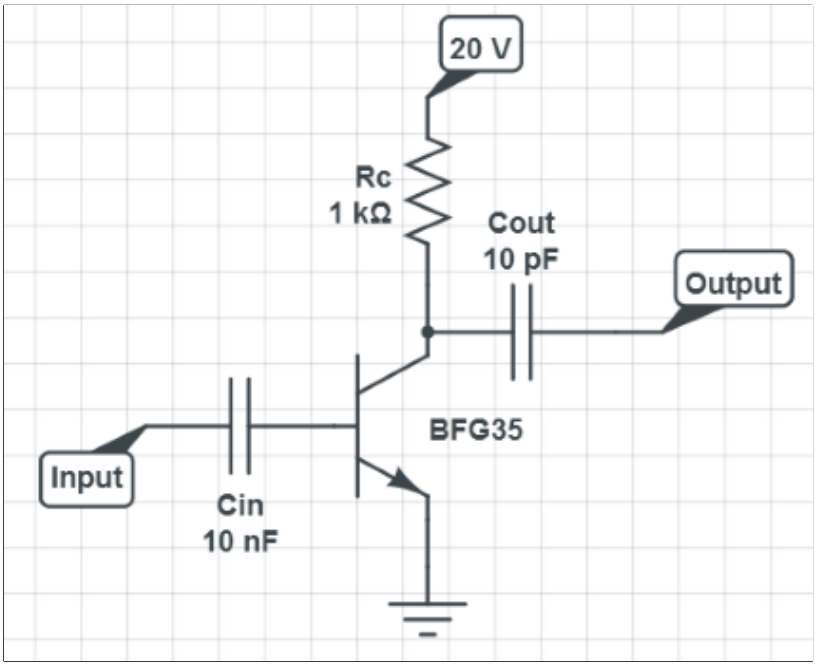

FIGURE 5.11: Diagram of the edge sharpener circuit

the common emitter circuit, the output impulse is inverted with peak amplitude of -7.5 V at 50 Ω (equivalent to a peak power of about 1.1 W). As expected, the generated impulse had a pulsewidth of 1.3 ns (FWHM) and a leading edge fall-time of 518 ps that was close to 500 ps RC time constant of the output coupling circuit calculated above. Compared with the input signal, the output impulse is shorter by a factor of about 6.1 and the leading edge time is faster by a factor of about 9.6.

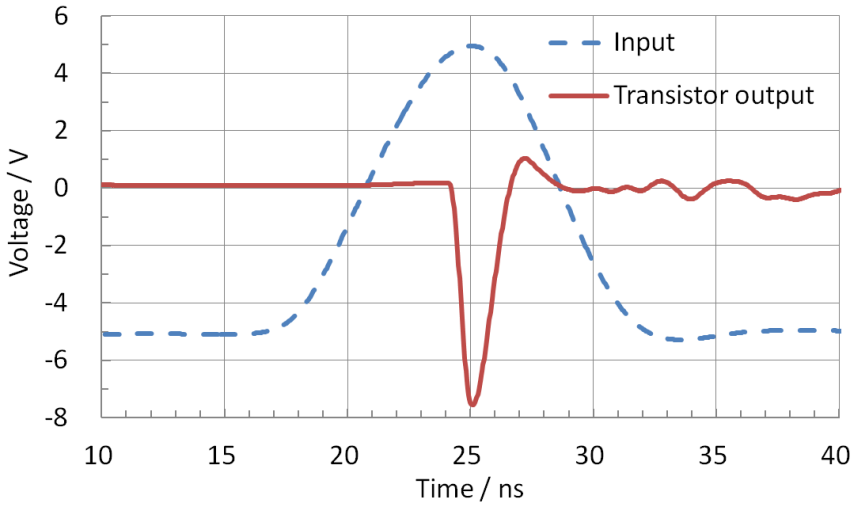

FIGURE 5.12: Measured results of the input (dashed line) and output (solid line) of the edge sharpener circuit

The output from the edge sharpener circuit is fed into the input of the NLTL comb generator to be further compressed. Fig. 5.13 shows the experimental results of the input (solid line) and the output (dashed line) of the NLTL comb generator. It can be observed that the leading edge fall-time of the input impulse is further compressed by a factor of 2.9 to 180 ps. The final output impulse had duration of 725 ps (FWHM) and peak amplitude of -7 V at 50 Ω (equivalent to a peak power of about 1 W). If compared with the initial input signal, the final output impulse is sharper by a factor of about 11 and the leading edge time is faster by a factor of about 27.8. The trailing positive slow ringing is caused by the ringing of the trailing edge of the input signal.

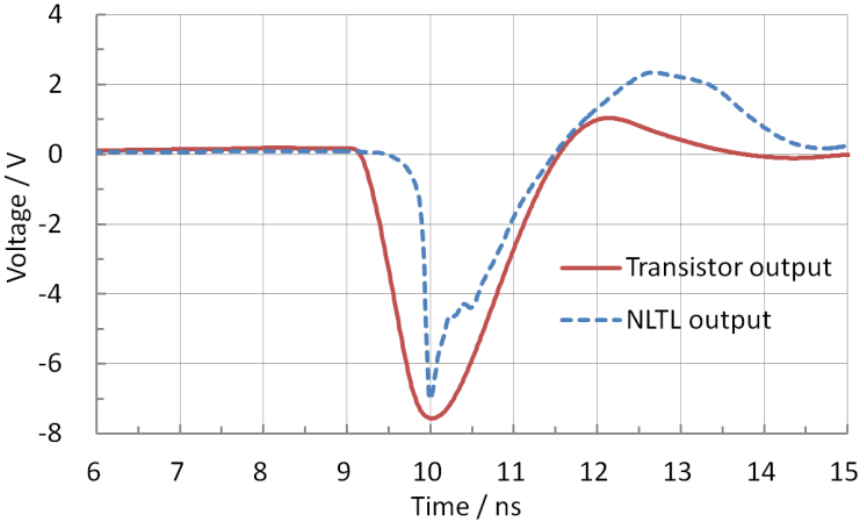

FIGURE 5.13: Measured results of the input (solid line) and the output of the NLTL comb generator (dashed line)

Furthermore, the tunable operation frequency range of the proposed impulse generator is experimentally studied. This impulse generator can work well at any input frequency around 1 to 15 MHz. Fig. 5.14 displays the experimental results of the final output impulses at operation frequencies of 1, 5, 10, and 15 MHz. It can be recognized that the lower frequency, the slightly higher amplitude. This is attributed to the recovery time of the RC-circuit of the collector resistance and the output coupling capacitor. When frequency is higher the period is shorter so that the output coupling capacitor has shorter time for recovery. Consequently, the output amplitude is lower. Therefore, by adjusting the values of the collector resistance and the output coupling capacitor, we can broaden the working frequency range. In addition, the fabricated impulse generator was checked by HP 8593E RF spectrum analyzer with generated high-order harmonic up to 10 GHz.

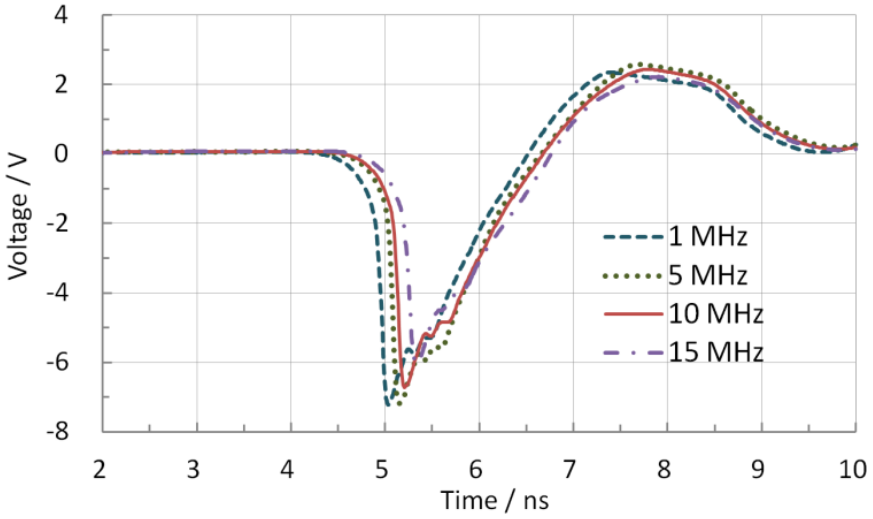

FIGURE 5.14: Experimental results of tuning the operation frequency

5.3.2 Experimental setup

The schematic diagram of the actively mode-locked fiber laser is displayed in Fig. 5.15. The fiber cavity consists of an erbium-doped fiber amplifier (EDFA), a polarization controller (PC), a fiber coupler, and a dual-electrode Mach-Zehnder intensity modulator. The EDFA (see Appendix C), which includes 8 m erbium-doped fiber (EDF) and total 8 m single mode fiber (SMF-28) for the input and the output, provides the gain medium up to 25 dB inside the fiber ring cavity. Its gain bandwidth is 1530-1560 nm. The EDFA also have two optical isolators mounted at the input and the output to guarantee unidirectional operation. Therefore, it is no need to use any external isolator in the cavity. The PC (Newport F-POL-APC) ensures optimal polarized light enters the modulator. The 10/90 fiber coupler extracts 90% power as laser output and provides 10% power feedback to the cavity. Finally, the 20 Gbit/s LN intensity modulator (see Appendix B) is used as the active element of active mode-locking; it has operating wavelength in 1550 nm band, 3 dB down optical bandwidth $\geq$ 18 GHz, insertion loss $\leq$ 6 dB, on/off extinction ratio $\geq$ 20 dB, polarization extinction ratio $\geq$ 20 dB, and optical return loss $\geq$ 30 dB. The input and output optical fibers of the modulator are both polarization maintaining (PM) fiber with length of 1.5 m each. Those PM fibers ensure that the modulator operates stably. Two electrodes D_1 and D_2 of the modulator are driven by the fabricated EIG (described just above). The phase difference of driving signals between the two electrodes is controlled by a line stretcher connected with electrode D_2. This line stretcher can make delay-time as short as 250 ps between the two electrodes.

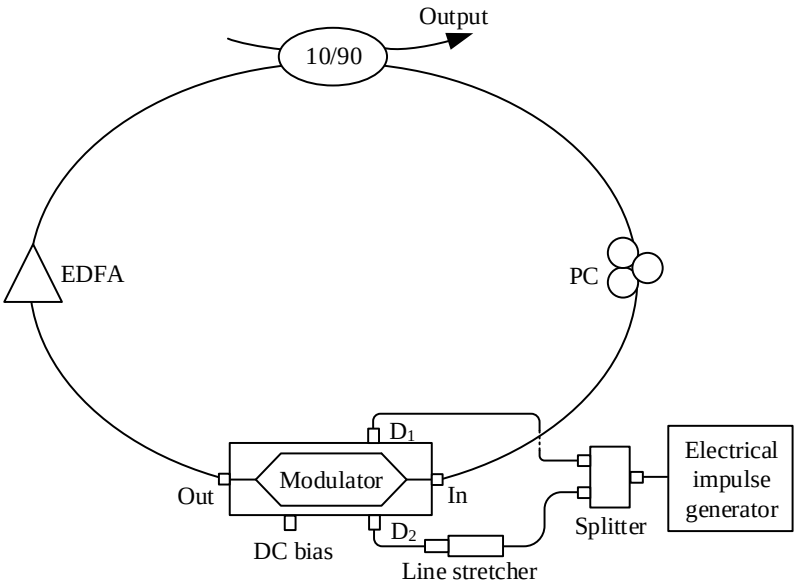

FIGURE 5.15: Schematic of the actively mode-locked fiber laser with a dual-electrode Mach-Zehnder intensity modulator, an erbium-doped fiber amplifier (EDFA), a polarization controller (PC), an output coupler, and an fabricated EIG

5.3.3 Impulse modulation and mode-locking

Fig. 5.16 (a) displays the measured results of two driving voltages on two electrodes D_1 and D_2 of the modulator. The line stretcher made a delay of about 250 ps in the time domain between two driving voltages. According to the operation characteristics of the dual-electrode Mach-Zehnder intensity modulator, two driving voltages applied to the two electrodes can be modeled as an effective driving voltage applied to the transmission factor of the modulator. The effective driving voltage is the difference of the two driving voltages applied to the two electrodes as shown in Fig. 5.16 (b). That was an impulse with 230 ps pulsewidth and a very sharp peak. Such the sharp impulse would make fast and large modulation of the optical field inside the ring cavity. This modulation is called impulse modulation.

Fig. 5.17 (a) shows the measured transmission factor of the modulator as a function of applied DC bias; the effective driving voltage is applied to modulate the transmitted optical field. The modulator has a half-wave voltage (V_π) of about 5 V. Due to the impulse modulation, an ultrashort optical pulse would be generated after the modulator.

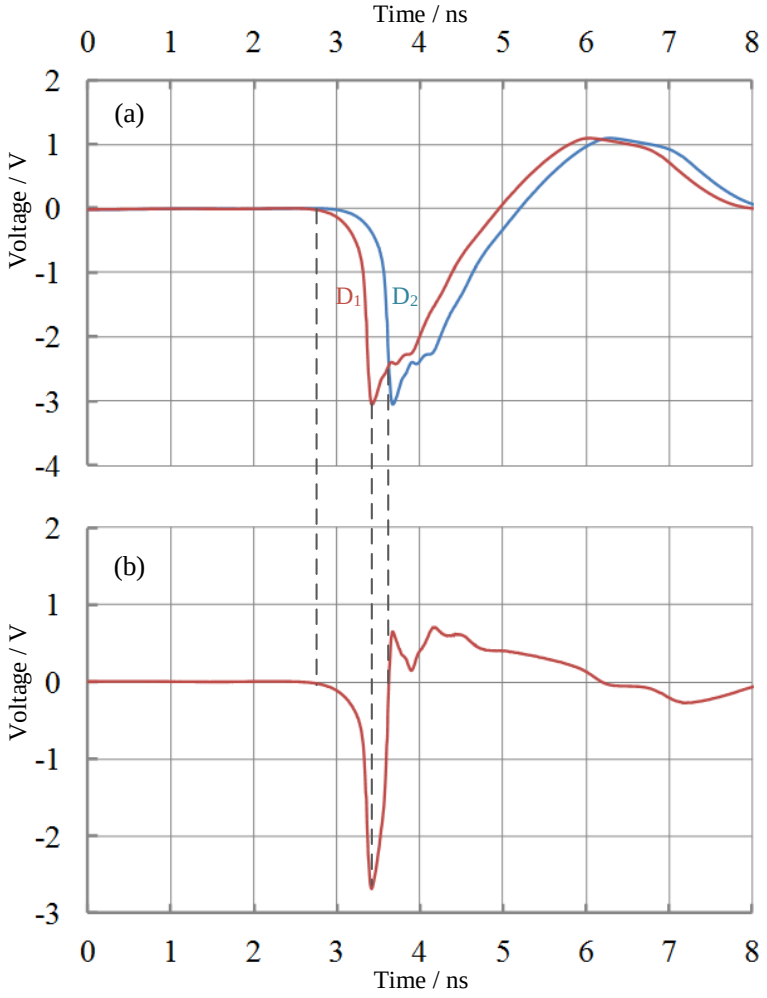

FIGURE 5.16: (a) Measured result of two driving voltages fed into the two electrodes of the modulator. (b) Effective driving voltage

If the frequency of the impulse modulation is the same as the fundamental frequency of the laser cavity, then active mode-locking will happen and just a single optical pulse will oscillate in the cavity. The single pulse will contain almost entire energy of the cavity. The active mode-locking inside the laser cavity by the impulse modulation can be illustrated in the time domain as shown in Fig. 5.17 (b). The cavity losses are modulated by the effective driving voltage. A perfectly timed optical pulse could be generated and passed by the modulator at the exact moments during every round-trip, where the losses are modulated at a minimum. The pulse encounters higher attenuation in its wings, compared with its peak. Therefore, the modulator temporally shortens the pulse after each round-trip. However, this shortening effect is not infinite as it is balanced

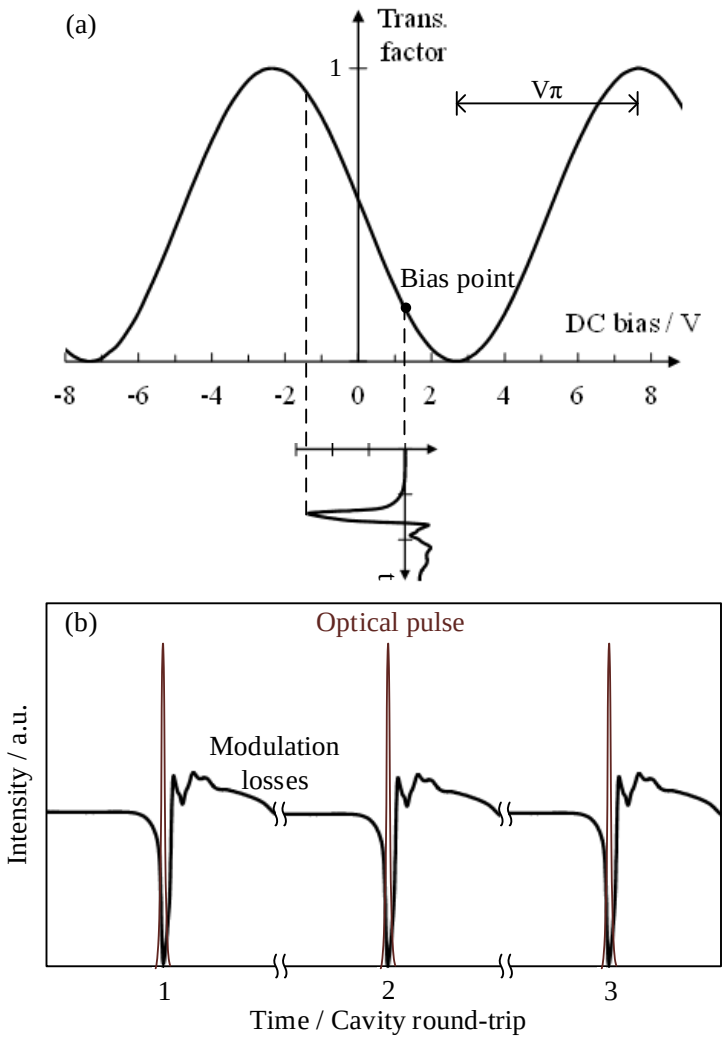

FIGURE 5.17: (a) Transmission factor of the modulator versus applied DC bias; the effective driving voltage modulates the transmitted optical field. (b) Time domain illustration of the active mode-locking using the impulse modulation (the ratio of pulse duration to pulse period is much smaller in reality)

by pulse-broadening effects (chromatic dispersion or the limited gain bandwidth) [85]. If compared with the conventional sinusoidal modulation operating at a high frequency (in the GHz range), the impulse modulation though operating at the fundamental frequency (in the MHz range) could bring about similar shortening effect to the optical pulse, thanks to the sharp peak of the effective driving voltage.

5.3.4 Results and discussion

We carried out the experiment with experimental setup in Fig. 5.15. The round-trip frequency of the fiber ring cavity was $f_m = 9.188$ MHz. The impulse modulation was also carried out at this fundamental frequency to realize active mode-locking. Active mode-locking was observed when the output power of the EDFA exceeded 12 mW and the PC was properly set. Femtosecond pulses were generated as the output power of the EDFA was about 20 mW. Without driving voltages applied to the modulator, no optical pulses were observed at the output.

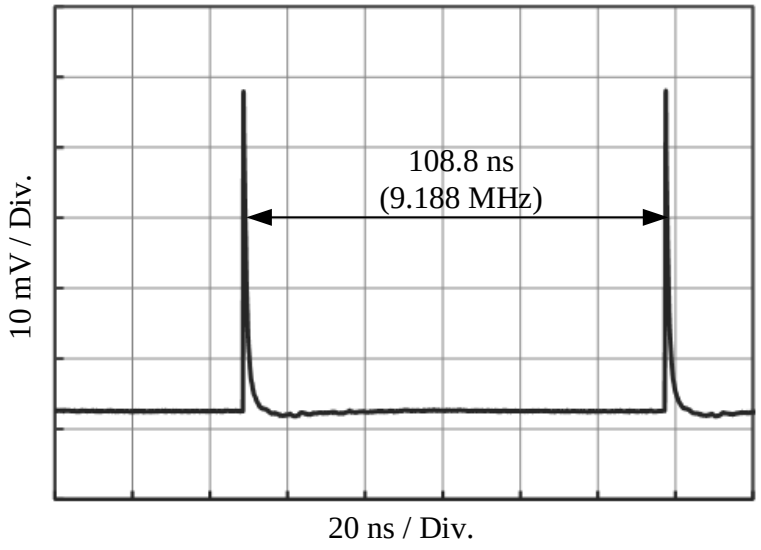

FIGURE 5.18: Output pulse train of the actively mode-locked fiber laser

All measurements were made with 20 mW EDFA output power. The laser output was first characterized by a broadband photodetector (Focus 1454) connected to a 20 GHz oscilloscope (Agilent 86100C). The output pulse train is shown in Fig. 5.18. It can be seen that the actively mode-locked fiber laser generated output optical pulses with a repetition rate of 9.188 MHz (108.8 ns), the same as the fundamental frequency of the laser cavity. This result confirms that the laser cavity was actively mode-locked by the impulse modulation and a single optical pulse was generated after each cavity round-trip.

The output optical pulses were measured by an autocorrelator (Alnair Labs HAC-150). A typical nomalized autocorrelation trace (dotted line) and its corresponding Lorentzian

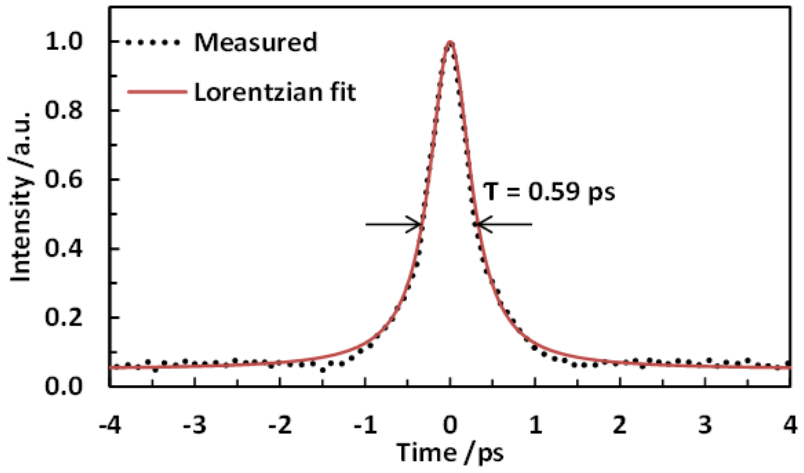

FIGURE 5.19: Typical normalized autocorrelation trace (dotted line) and corresponding Lorentzian fit (solid line). Autocorrelation trace width was 590 fs

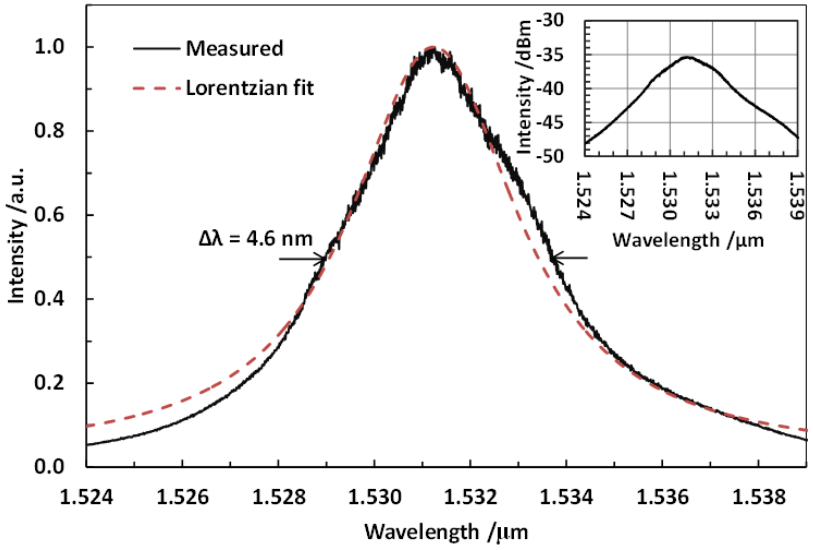

FIGURE 5.20: Normalized optical spectrum (solid line) and corresponding Lorentzian fit (dotted line). The inset displays such spectrum in logarithmic scale.

fit (solid line) are shown in Fig. 5.19. The experimental data was fitted with Gaussian, sech^2, and Lorentzian profiles, and these pulses are most similar to the Lorentzian shape. The full width at half-maximum (FWHM) autocorrelation trace width was 590 fs, corresponding to 295 fs deconvoluted FWHM optical pulsewidth (assuming a Lorentzian pulse shape). An optical spectrum analyzer (Advantest Q8384) was used to measure the optical spectrum of the actively mode-locked fiber laser. The normalized optical spectrum (solid line) and its corresponding Lorentzian fit are displayed in Fig. 5.20.

The 3 dB spectral bandwidth was 4.6 nm (0.6 THz). The inset of Fig. 5.20 shows such spectrum in logarithmic scale.

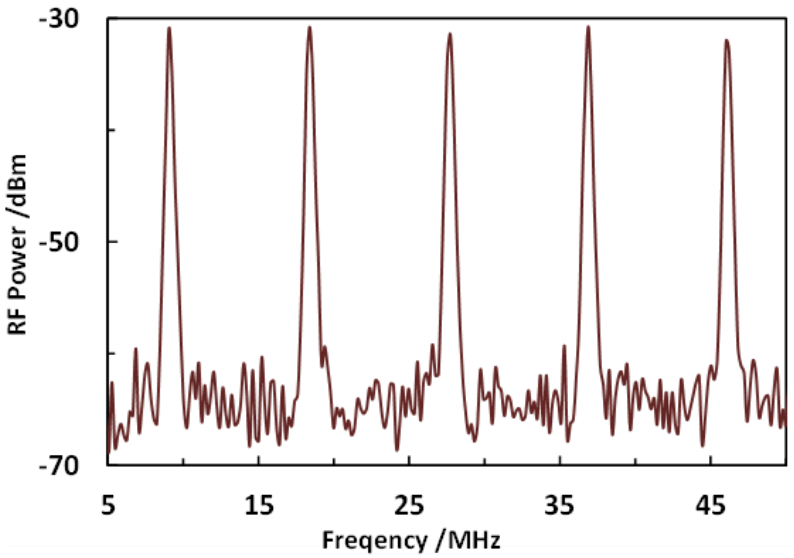

FIGURE 5.21: RF spectrum of the laser output

Fig. 5.21 shows the the RF spectrum of the laser output, which was measured with the photodetector (Focus 1454) and a 3-GHz RF spectrum analyzer (Advantest R3131A) with 199 kHz resolution. The RF spectrum shows a frequency comb of harmonics, which obviously corresponds to the repetition frequency of 9.188 MHz. There is no sideband observed, which suggests that stable mode-locked operation was obtained. The supermode suppression was about 32 dB. From the above values, a time-bandwidth product is 0.177, close to the expected transform-limited value of 0.142 for the Lorentzian pulse profile. Finally, the average output power was measured with a power meter. The maximum average power was about 1 mW, corresponding to the estimated peak power of about 250 W for the 9.188 MHz pulse repetition rate. The output power can be easily increased by using an external EDFA.

In short, with the introduction of the impulse modulation inside the fiber laser cavity, the shortening effect is more effective compared with the conventional sinusoidal modulation operating at the same frequency. As a result, 295 fs pulses can be generated by the actively mode-locked fiber laser at the fundamental frequency of 9.188 MHz. Our findings suggest that femtosecond optical pulses could be generated by the proposed actively mode-locked fiber laser.

Chapter 6

Conclusions

6.1 Conclusions

In this thesis, I worked on developing new technologies for generation and manipulation of ultrashort optical pulses using fiber lasers. For this purpose, a picosecond FM fiber laser and an actively mode-locked femtosecond fiber laser have been developed.

First, I have utilized the idea of using an external dispersive single-mode fiber to compress the constant output of a conventional FM fiber ring laser to picosecond pulse chain output. The issue has been studied theoretically through computer simulation and then experimentally through in-lab experiments. In our experiments, FM fiber laser operation was realized by using a fiber ring cavity with an internal phase modulator and an erbium-doped fiber amplifier. However, the pulse chain output contains a significant background, which is a drawback. To remove this background, we introduced the use of external intensity modulation. The background ratio of the generated pulse chain was calculated and compared with the experimental results. The experimental results showed that a background-free pulse chain at 10 GHz repetition rate was obtained. By the proposed technique, the FM laser could generate optical pulses with pulse width as short as 1.77 ps and a flat spectral bandwidth of 0.5 THz. With short pulse width, wide and flat bandwidth, and high repetition rate, this laser can be used for many applications, such as optical communication.

Second, I have introduced the use of impulse modulation inside an actively mode-locked erbium-doped fiber ring laser to generate femtosecond pulses at the wavelength

band of 1.5 μm. To realize impulse modulation, we fabricated an electrical impulse generation circuit, which could generate picosecond electrical pulses for driving a dual-electrode Mach-Zehnder intensity modulator placed inside a fiber ring cavity. As the operating frequency of the modulator is synchronized with the fundamental round-trip frequency of the ring cavity, active mode-locking will take place. Although the impulse modulation operates in the MHz region, it produces the gating window as fast as that of the conventional sinusoidal modulation operating in the GHz region. With fast and lange modulation characteristics, the impulse modulation creates an ultrashort pulse inside the laser cavity that is amplified and further compressed after each round-trip to the femtosecond range. So far, the proposed actively mode-locked fiber laser could directly generate stable optical pulses with duration of 300 fs at the fundamental repetition rate of 9.188 MHz. Average output power was 2 mW and it could easily be increased up to 100 mW level by using an external fiber amplifier. This femtosecond fiber laser is promising for applications in biology such as cell fusion and cell killing.

6.2 Future Research Suggestions

In this section, I would like to discuss and suggest some future research related to the contents.

It has been theoretically demonstrated that subpicosecond pulses can be obtained by using FM laser with the chirping compression technique using dispersive fiber [77]. To achieve subpicosecond optical pulses, this method would require high modulation frequency ($>$ 20 GHz) and high FM modulation index. In this thesis, the pulse width output of the FM laser is limited by the use of 10 GHz modulation frequency. Therefore, by developing a system using a faster phase modulator, subpicosecond pulse generation might be obtained.

About the actively mode-locked femtosecond fiber laser, the cavity was made out of devices with normal optical fibers. Therefore, there might be a possibility that nonlinear polarization rotation mode-locking could have happened inside the laser cavity. This issue is difficult to address with the current setup. Future works should have the cavity with all-PM fiber to make sure the cavity is purely actively mode-locked or is hybridly

mode-locked with both active mode-locking and nonlinear polarization rotation mode-locking. Theoretical analysis of the active mode-locking with impulse modulation is also important to understand the advantages of this mechanism.

The femtosecond pulses generated by the proposed actively mode-locked fiber laser are promising for applications in biology such as cell manipulation and cell fusion; thanks to its stable and flexible characteristics. I am now working on developing a biological cell fusion system using this femtosecond laser.

Appendix A

Specifications of Phase Modulator

In this thesis, we used a 10 Gbit/s $LiNbO_3$ single electrode phase modulator produced by Sumitomo Osaka Cement Co.,Ltd. [86]. The specifications of this modulator is shown in the following Table A.1.

TABLE A.1: Specifications of the used phase modulator

Model	**T·PM 1.5 - 10 - Y - Z**
Modulation speed	10 Gbit/s
Operating wavelength	1.55 μm
Insertion loss	$\leq$5 dB
Drive voltage (V_π)	$\leq$6 V
Optical bandwidth*1	$\geq$8 GHz
Polarization extinction ratio	$\geq$20 dB
Optical return loss	$\geq$30 dB
Maximum input power	$\leq$10 mW
Electrode impedance	$\approx$ 50 Ω
Input RF connector	K connector (SMA)
Optical fiber input	0.9 mm ϕ PMF
Optical fiber output	0.9 mm ϕ PMF
Fiber lead length	$\geq$0.7 m
Operating temperature	10 $\sim$ 40^{o}C
Polarizer	Included (output side)

*1: 3dB down(130 MHz reference)

Appendix B

Specifications of Intensity Modulator

In this thesis, we used a 20 Gbit/s $LiNbO_3$ dual electrode intensity modulator produced by Sumitomo Osaka Cement Co.,Ltd. [86]. The specifications of this modulator is shown in the following Table B.1.

TABLE B.1: Specifications of the used intensity modulator

Model	**T·DEH 1.5 - 20 - ADC - Y - Z**
Modulation speed	20 Gbit/s
Operating wavelength	1.55 μm
Insertion loss	$\leq$6 dB
Drive voltage (V_π)	$\leq$6.5 V_{p-p}
Optical bandwidth*1	$\geq$18 GHz
ON/OFF extinction ratio	$\geq$20 dB
Polarization extinction ratio	$\geq$20 dB
Optical return loss	$\geq$30 dB
Maximum input power	$\leq$10 mW
Electrode impedance	$\approx$ 50 Ω
Input RF connector	K connector (SMA)
Optical fiber input	0.9 mm ϕ PMF
Optical fiber output	0.9 mm ϕ PMF
Fiber lead length	$\geq$0.7 m
Operating temperature	0 $\sim$ 60^{o}C

*1: 3dB down(1 GHz reference)

Appendix C

Specifications of Erbium-Doped Fiber Amplifier

In this thesis, we used a commercial erbium-doped fiber amplifier (EDFA) produced by Fiber Labs Inc. [87]. The standard specifications of this EDFA is shown in the following Table C.1.

TABLE C.1: Standard specifications of the used EDFA

Model	**AMP-FL8013-CB-13**
Applications	Pre and in-line amplifier
Signal wavelength	1.53 $\sim$ 1.56 μm
Maximum output power*1	$>$ +13 dBm ($>$ 20mW)
Gain*1	$>$ 25 dB
Noise figure*1	$<$ 5 dB
Amplifier control	ACC/ALC
Input/Output fibers	SMF
Optical connectors	FC/PC
Operating temperature	0 $\sim$ 40^{o}C
Storage Temperature	-10 $\sim$ 60^{o}C
Power consumption	$<$ 30 W
Power supply	AC 100 $\sim$ 240 V (50/60 Hz)

*1: Input power: $>$ 0 dBm @1.55 μm

Bibliography

[1] R. Paschotta. Erbium-doped gain media. *RP Photonics Encyclopedia*, . URL `http://www.rp-photonics.com/erbium_doped_gain_media.html`.

[2] S. Honkanen, T. Ohtsuki, S. Jiang, S. I. Najafi, and N. Peyghambarian. High er concentration phosphate glasses for planar waveguide amplifiers. *Proc. SPIE 2996*, pages 32–40, 1997.

[3] R. Paschotta. Ytterbium-doped gain media. *RP Photonics Encyclopedia*, . URL `http://www.rp-photonics.com/ytterbium_doped_gain_media.html`.

[4] Samuli Kivisto. *Short pulse lasers using advanced fiber technology and saturable absorbers*. PhD thesis, Tampere University of Technology, 2010.

[5] Y. Tang and J. Xu. *Frontiers in Guided Wave Optics and Optoelectronics*, chapter Chapter 20: High Power Tunable Tm3+-fiber Lasers and Its Application in Pumping Cr2+:ZnSe Lasers, page 4. Bishnu Pal, 2010.

[6] S. D. Agger and J. H. Povlsen. Emission and absorption cross section of thulium doped silica fibers. *Optics Express*, 14:50–57, 2005.

[7] Samuli Kivisto. *Short pulse lasers using advanced fiber technology and saturable absorbers*. PhD thesis, Tampere University of Technology, 2010.

[8] X. T. Yang, B. Q. Yao, Y. Ding, X. Li, G. Aka, L. Zheng, and J. Xu. Spectral properties and laser performance of ho: Sc2sio5 crystal at room temperature. *Optics express*, 21:32566–32571, 2013. URL `http://dx.doi.org/10.1364/OE.21.032566`.

[9] R. Paschotta. Fiber lasers. *RP Photonics Encyclopedia*, . URL `http://www.rp-photonics.com/fiber_lasers.html`.

[10] I. N. Duling. All-fiber ring soliton laser mode locked with a nonlinear mirror. *Optics Letters*, 16(8):539–541, April 1991. URL `http://dx.doi.org/10.1364/OL.16.000539`.

[11] Shchatsinin Ihar. *Free clusters and free molecules in strong, shaped laser fields*. PhD thesis, Freie Universitat Berlin, 2009.

[12] R. Paschotta. Mode locking, . URL `http://www.rp-photonics.com/mode_locking.html`.

[13] S. W. Harun and Hamzah Arof (Ed.). *Current Developments in Optical Fiber Technology*, chapter 17. InTech, 2013. URL `http://www.intechopen.com/books/current-developments-in-optical-fiber-technology/multi-wavelength-fiber-lasers`.

[14] Anthony E. Siegman. *LASERS*, chapter 27, page 1041. University Science Books, 1986.

[15] Anthony E. Siegman. *LASERS*, chapter 27, page 1047. University Science Books, 1986.

[16] Anthony E. Siegman. *LASERS*, chapter 27, pages 1049–1057. University Science Books, 1986.

[17] R. Paschotta. Active mode locking. *RP Photonics Encyclopedia*, . URL `http://www.rp-photonics.com/active_mode_locking.html`.

[18] R. Paschotta. Passive mode locking. *RP Photonics Encyclopedia*, . URL `http://www.rp-photonics.com/passive_mode_locking.html`.

[19] Anthony E. Siegman. *LASERS*, chapter 27, pages 1104–1127. University Science Books, 1986.

[20] Niels Meiser. *Mode Locking: Chapters 27 and 28 and bonus levels*. Lecture. Laser-Physics, KTH.

[21] Anthony E. Siegman. *LASERS*, chapter 27, pages 1095–1101. University Science Books, 1986.

[22] R. Paschotta. Rare-earth-doped fibers. *RP Photonics Encyclopedia*, . URL `http://www.rp-photonics.com/rare_earth_doped_fibers.html`.

[23] J. C. Diels and W. Rudolph. *Ultrafast Laser Pulse Phenomena*. Elsevier, second ed. edition, 2006.

[24] Andrew M. Weiner. *Ultrafast Optics*, chapter Introduction and Review, pages 1–31. Pure and Applied Optics. John Wiley & Sons, 2009.

[25] T. H. Maiman. Stimulated optical radiation in ruby. *Nature*, 187:493–494, August 1960. URL `http://www.nature.com/nature/journal/v187/n4736/abs/187493a0.html`.

[26] M. Hirano, R. Yotsutani, and A. Morimoto. Generation of flat optical frequency comb based on fm laser operation of fiber ring laser. *IEICE Transactions on Electronics*, E94-C(1):132–133, January 2011. URL `http://search.ieice.org/bin/summary.php?id=e94-c_1_132`.

[27] M. Hirano and A. Morimoto. Generation of flat optical frequency comb by fiber loop modulation. *Optical Review*, 18(1):13–18, January 2011. URL `http://link.springer.com/article/10.1007/s10043-011-0009-z`.

[28] D. Panasenko, P. Polynkin, A. Polynkin, M. Mansuripur J. V. Moloney, and N. Peyghambarian. Er-yb femtosecond ring fiber oscillator with 1.1-w average power and ghz repetition rates. *Photonics Technology Letters, IEEE*, 18(7):853–855, April 2006. URL `http://ieeexplore.ieee.org/xpls/abs_all.jsp?arnumber=1608184&tag=1`.

[29] S. Masuda, S. Niki, and M. Nakazawa. Environmentally stable, simple passively mode-locked fiber ring laser using a four-port circulator. *Optics Express*, 17(8): 6613–6622, April 2009. URL `http://dx.doi.org/10.1364/OE.17.006613`.

[30] K. Tamura, E. P. Ippen, H. A. Haus, and L. E. Nelson. 77-fs pulse generation from a stretched-pulse mode-locked all-fiber ring laser. *Optics Letters*, 18(13):1080–1082, July 1993. URL `http://dx.doi.org/10.1364/OL.18.001080`.

[31] S. E. Harris and R. Targ. Fm oscillation of the he-ne laser. *Applied Physics Letters*, 5(10):202–204, September 1964. URL `http://dx.doi.org/10.1063/1.1723588`.

[32] K. S. Abedin, N. Onodera, and M. Hyodo. Widely-chirped high-repetition-rate continuous wave fm laser oscillation in erbium fiber ring laser. *Japanese journal of*

applied physics, 37:649–652, June 1998. URL http://jjap.jsap.jp/link?JJAP/37/L649/.

[33] K. S. Abedin, N. Onodera, and M. Hyodo. High-repetition-rate fm oscillation in an erbium fiber ring laser and its application for picosecond pulse generation by external chirp compensation. *Optics Communications*, 158(1):77–83, December 1998. URL http://dx.doi.org/10.1016/S0030-4018(98)00559-8.

[34] J. S. Wey, J. Goldhar, D. W. Rush, M. W. Chbat, G. M. Carter, and G. L. Burdge. Performance characterization of a harmonically mode-locked erbium fiber ring laser. *Photonics Technology Letters, IEEE*, 7(2):152–154, February 1995. URL http://dx.doi.org/10.1109/68.345906.

[35] M. Nakazawa, E. Yoshida, and K. Tamura. 10 ghz, 2ps regeneratively and harmonically fm mode-locked erbium fibre ring laser. *Electronics Letters*, 32(14):1285–1287, July 1996. URL http://ieeexplore.ieee.org/xpls/abs_all.jsp?arnumber=503627&tag=1.

[36] M. Nakazawa and E. Yoshida. A 40-ghz 850-fs regeneratively fm mode-locked polarization-maintaining erbium fiber ring laser. *Photonics Technology Letters, IEEE*, 12(12):1613–1615, December 2000. URL http://dx.doi.org/10.1109/68.896324.

[37] D. S. Kim, Y. Matsuda, A. Morimoto, and T. Kobayashi. Electrooptic femtosecond pulse generation using a dispersive optical fiber. *Japanese journal of applied physics*, 36:5125–5129, June 1997. URL http://jjap.jsap.jp/link?JJAP/36/5125/.

[38] E. B. Treacy. Optical pulse compression with diffraction gratings. *Quantum Electronics, IEEE*, 5(9):454–458, September 1969. URL http://dx.doi.org/10.1109/JQE.1969.1076303.

[39] K. Koizumi, T. Hirooka M. Yoshida, and M. Nakazawa. 10 ghz, 1.1 ps optical pulse generation from a regeneratively mode-locked yb fiber laser in the 1.1 m band. *Optics Express*, 19(25):25426–25432, December 2011. URL http://dx.doi.org/10.1364/OE.19.025426.

[40] K. Zoiros, T. Stathopoulos, K. Vlachos, T. Houbavlis A. Hatziefremidis, T. Papakyriakopoulos, and H. Avramopoulos. Experimental and theoretical studies of a

high repetition rate fiber laser, mode-locked by external optical modulation. *Optics Communications*, 180(4):301–315, June 2000. URL http://dx.doi.org/10.1016/S0030-4018(00)00708-2.

[41] H. Feng, W. Zhao, S. Yan, and X. P. Xie. Generation of 10-ghz ultra-short pulses with low time jitter in an actively mode-locked fiber lase. *Laser Physics*, 21(2): 404–409, February 2011. URL http://link.springer.com/article/10.1134/S1054660X11030017.

[42] Z. Li, Y. Gao C. Lou, and K. T. Chan. A dual-wavelength and dual-repetition-rate actively mode-locked fiber ring laser. *Optics Communications*, 185(4):381–385, November 2000. URL http://dx.doi.org/10.1016/S0030-4018(00)00998-6.

[43] M. Malmstrom, W. Margulis, O. Tarasenko, V. Pasiskevicius, and F. Laurell. Soliton generation from an actively mode-locked fiber laser incorporating an electro-optic fiber modulator. *Optics Express*, 20(3):2905–2910, January 2012. URL http://dx.doi.org/10.1364/OE.20.002905.

[44] S. B. Poole, D. N. Payne, and M. E. Fermann. Fabrication of low-loss optical fibres containing rare-earth ions. *Electron Lett.*, 21:737–738, 1985.

[45] R. J. Mears, L. Reekie, I. M. Jauncey, and D. N. Payne. Low-noise erbium-doped fibre amplifier operating at 1.54 μm. *Electron Lett.*, 23:1026–1028, 1987.

[46] R. J. Mears, L. Reekie, I. M. Jauncey, and D. N. Payne. Diode-laser-pumped operation of an er-doped single-mode fibre laser. *Electron Lett.*, 23:1076–1078, 1987.

[47] O. G. Okhotnikov, V. V. Kuzmin, and J. R. Salcedo. General intracavity method for laser transition characterization by relaxation oscillations spectral analysis. *IEEE Photon. Technol. Lett.*, 6:362–364, 1994.

[48] H. W. Etzel, H. W. Gandy, and R. J. Ginther. Stimulated emission of infrared radiation from ytterbium activated silicate glass. *Appl. Opt.*, 1:534–536, 1962.

[49] D. C. Hanna, R. M. Percival, R. G. Smart, P. J. Suni, J. E. Townsend, and A. C. Tropper. Continuous-wave oscillation of a monomode ytterbium-doped fibre laser. *Electron. Lett.*, 21:1111–1113, 1988.

[50] R. Paschotta, J. Nilsson, P. R. Barber, J. E. Caplen, A. C. Tropper, and D. C. Hanna. Lifetime quenching in yb doped fibers. *Opt. Commun.*, 136:375–378, 1997. URL `http://dx.doi.org/10.1016/S0030-4018(96)00720-1`.

[51] J .J. Koponen, M. J. Soderlund, H. J. Hoffman, and S. K. T. Tammela. Measuring photodarkening from single-mode ytterbium doped silica fibers. *Opt. Express*, 14: 11539–11544, 2006.

[52] S. W. Henderson, P. J. M. Suni, C. P. Hale, S. M. Hannon, J. R. Magee, D. L. Bruns, and E. H. Yuen. Coherent laser radar at 2 μ using solid-state lasers. *IEEE Transact. Geoscience and remote sensing*, 31:4–15, 1993.

[53] R. Godard. Infrared (2-12 μ) solid-state laser sources: a review. *C. R. Physique*, 8: 1100–1128, 2007.

[54] D. C. Hanna, I. M. Jauncey, R. M. Percival, I. R. Perry, R. G. Smart, P. J. Suni, J. E. Townsend, and A. C. Tropper. Continuous-wave oscillation of a monomode thulium-doped fibre laser. *Electron. Lett.*, 24:1222–1223, 1988.

[55] R. Paschotta, N. Moore, W. A. Clarkson, A. C. Tropper, D. C. Hanna, and G. Maz'e. 230 mw of blue light from a thulium-doped upconversion fiber laser. *IEEE J. Quantum Electron.*, 3:1100–1102, 1997.

[56] L. Wetenkamp. Efficient cw-operation of a 2.9 μ ho-doped fluorozirconate fibre laser pumped at 640 nm. *Electron. Lett.*, 26:883–884, 1990.

[57] E. Snitzer. Optical maser action of nd3+ in a barium crown glass. *Phys. Rev. Lett.*, 7:444–446, 1961.

[58] C. J. Koester and E. Snitzer. Amplification in a fiber laser. *Appl. Opt.*, 3:1182–1186, 1964.

[59] J. Stone and C. A. Burrus. Neodymium-doped silica lasers in end-pumped fiber geometry. *Appl. Phys. Lett.*, 23:388–389, 1973.

[60] A. J. Mears, L. Reekie, S. B. Poole, and D. N. Payne. Neodymium-doped silica single-mode fibre lasers. *Appl. Phys. Lett.*, 21:388–389, 1985.

[61] S. B. Poole, D. N. payne, R. J. Mears, M. E. Fermann, and R. I. Laming. Fabrication and characterization of low-loss optical fibers containing rare-earth ions. *IEEE J. Lightwave Tech.*, 4:870–876, 1986.

[62] I. P. Alcock, A. C. Tropper, A. I. Ferguson, and D. C. Hanna. Q-switched operation of a neodymium-doped monomode fibre laser. *Electron. Lett.*, 22:84–84, 1986.

[63] I. P. Alcock, A. I. Ferguson, D. C. Hanna, and A. C. Tropper. Mode-locking of a neodymium-doped monomode fibre laser. *Electron. Lett.*, 22:268–269, 1986.

[64] J. D. Kafka, T. Baer, and D. W. Hall. Mode-locked erbium-doped fiber laser with soliton pulse shaping. *Opt. Lett.*, 14:1269–1271, 1989.

[65] M. E. Fermann, M. Hofer, F. Haberl, and S. P. Craig-Ryan. Femtosecond fiber laser. *Electron. Lett.*, 26:1737–1738, 1990.

[66] M. E. Fermann, M. Hofer, F. Haberl, A. J. Schmidt, and L. Turi. Additive-pulse-compression mode locking of a neodymium fiber laser. *Opt. Lett.*, 16:244–246, 1991.

[67] I. N. Duling III. Sup-picosecond all-fiber erbium laser. *Electron. Lett.*, 27:544–545, 1991.

[68] X. Zhou, Y. D. Yoshitomi, S. Tani, and K. Torizuka. Generation of sub-30 fs pulses from a mode-locked yetterbium fiber laser oscillator with phase compensation. *in Proc. of CLEO*, pages 1–2, 2008.

[69] R. Paschotta, R. Haring, E. Gini, H. Melchior, and U. Keller. Passively q-switched 0.1 mj fiber laser system at 1.53 um. *Opt. Lett.*, 24:388–390, 1999.

[70] T. Hakulinen and O. G. Okhotnikov. 8 ns fiber laser q-switched by the resonant saturable absorber mirror. *Opt. Lett.*, 32:2677–2679, 2007.

[71] E. Snitzer, H. Po, F. Hakimi, R. Tuminelli, and B. C. McCollum. Double clad, offset core nd fiber laser. *in Optical Fiber Sensors*, 2:533–537, 1989.

[72] R. Paschotta. Fiber lasers versus bulk lasers. *RP Photonics Encyclopedia*, . URL `http://www.rp-photonics.com/fiber_lasers_versus_bulk_lasers.html`.

[73] C. Rulliere (Ed.). *Femtosecond Laser Pulses: Principles and Experiments*, chapter 2, pages 25–52. Springer, 1998.

[74] W. E. Lamb Jr. Theory of an optical laser. *Phys. Rev*, 134:A1429, 1964.

[75] C. Rulliere (Ed.). *Femtosecond Laser Pulses: Principles and Experiments*, chapter 3, pages 53–82. Springer, 1998.

[76] Anthony E. Siegman. *LASERS*, chapter 27, pages 1062–1067. University Science Books, 1986.

[77] T. Kobayashi, H. Yao, K. Amano, Y. Fukushima, A. Morimoto, and T. Sueta. Optical pulse compression using high-frequency electrooptic phase modulation. *IEEE Journal of Quantum Electronics*, 24(2):382–387, Feb. 1988. URL `http://dx.doi.org/10.1109/3.135`.

[78] Amnon Yariv and Pochi Yeh. *Photonics: Optical Electronics in Modern Communication*, chapter 6, page 275. Electrical and Computer Engineering. Oxford University Press, New York, 2007, 6 Ed.

[79] M. Greitans, V. Aristov, and E. Hermanis. The study of ultra-wide-band pulse sharpers. *Auto. Control Comp. Scien.*, 44(6):330–336, 2010.

[80] P. Protiva, J. Mrkvica, and J. Machac. A compact step recovery diode subnanosecond pulse generator. *Microwave Opt. Technol. Lett.*, 52(2):438–440, 2010.

[81] M. Gerding, B. Schiek, and T. Musch. Electric pulse generator and method for generating short electric pulses. *US Patent 2005/0093601 A1*, 2005.

[82] L. Jinyuan, S. Bing, and C. Zenghu. High voltage fast ramp pulse generation using avalanche transistor. *Review Scientific Instru.*, 69(8):3066–3067, 1998.

[83] J. P. Hansen and W. A. Schmidt. A fast risetime avalanche transistor pulse generator for driving injection lasers. *Proceedings of the IEEE*, 55(2):216–217, 1967.

[84] Picosecond Pulse Labs. A new breed of comb generators featuring low phase noise and low input power. *Microw. Journal*, 2006. URL `http://www.microwavejournal.com`.

[85] R. Paschotta. *Field Guide to Laser Pulse Generation*, chapter Laser Pulse Generation, pages 34–35. SPIE Press, Washington, 2008.

[86] Sumitomo Osaka Cement Co. Ltd. Ln modulator. URL `http://www.socnb.com/product/hproduct_e/ln.html`.

[87] Fiber Labs Inc. C-band optical amplifier (edfa). URL `http://www.fiberlabs-inc.com/c-band-bt-amp.htm`.